Honey authentication: effect of irradiation and ageing on near-infrared (NIR) spectroscopy classification models

by

Alexandra Elizabeth Rust

Thesis presented in partial fulfilment of the requirements for the degree of Master of Science (Food Science) in the Faculty of AgriSciences at Stellenbosch University

Supervisor: Prof Marena Manley
Co-supervisor: Dr Paul James Williams
Co-supervisor: Mr Mike Allsopp

March 2020

Declaration

By submitting this thesis electronically, I declare that the entirety of the work contained therein is my own, original work, that I am the sole author thereof (save to the extent explicitly otherwise stated), that reproduction and publication thereof by Stellenbosch University will not infringe any third party rights and that I have not previously in its entirety or in part submitted it for obtaining any qualification.

Date: March 2020

Abstract

Near-infrared (NIR) spectroscopy was used to investigate the effects of syrup dilution, ageing, storage temperature and irradiation treatment on the NIR spectra of honey. Additionally, NIR spectroscopy and partial least squares discriminant analysis (PLS-DA) were employed to develop a classification model for the rapid screening of high-fructose corn syrup (HFCS) and invert cane sugar syrup (ICSS) diluted honey. Detection of irradiation treatment was also investigated, to assess NIR spectroscopy-based models as a potential screening tool for detecting mislabelled honey.

Unfiltered and unheated honey samples (n = 17) obtained from South African beekeepers were uniformly strained and subjected to treatment combinations of 10 kGy gamma irradiation and dilution with 0, 10 or 20% (w/w) ICSS or HFCS to create sub-samples (n = 174) which were stored at 25°C. Another three undiluted subsets were stored at 4°C, 40°C and in uncontrolled ambient conditions (n = 51). A benchtop BÜCHI Fourier transform-near infrared (FT-NIR) spectrometer and a portable MicroNIR NIR spectrometer, with ranges of 1000–2500 nm and 908-1676 nm respectively, were used to acquire triplicate spectral measurements, over a period of 9 months.

ANOVA-simultaneous component analysis (ASCA) indicated that honey type, diluent type, storage temperature and age had significant ($p > 0.05$) effects on the spectral dataset, while diluent level and irradiation treatment did not. Despite this, irradiation treatment was found to reduce the validation accuracy and efficacy of authentication models, by 5.82% and 7.19% respectively, when PLS-DA models based on only irradiated and only non-irradiated spectral data were compared, suggesting that authentication may be impeded by irradiation treatment to some degree. However, a PLS-DA model discriminating on the basis of irradiation treatment obtained an unsuccessful validation classification of 59.7%, suggesting that there is little or no utilisable effect of irradiation on the spectral data.

The best-performing authentication solutions were individual two-class PLS-DA models for detecting ICSS (75.95% accuracy, 86.31% sensitivity) and HFCS (73.95% accuracy, 82.14% sensitivity) dilution, which demonstrated predictive power adequate for screening purposes. PLS-DA models based on spectral data acquired with the benchtop BÜCHI instrument performed best when compared with the portable MicroNIR instrument and its two sample presentation formats. Despite this, the MicroNIR with Teflon cup sample presentation was shown to be a feasible and cost-effective alternative, demonstrating similar accuracies (70.0-75.47%) and efficiencies (68.22-74.51%).

In addition, quantification of the level of diluent with partial least squares regression (PLSR) was poor for both ICSS (R^2_{Pred} = 0.118, RMSEP = 6.795%) and HFCS (R^2_{Pred} = 0.147, RMSEP = 6.596%) dilutions. This was attributed to an inadequate range of dilution levels in the reference data, as well as the insignificant effect ($p < 0.05$) of diluent level on the overall variation in the spectral data.

The findings of this study highlighted the potential shortcomings of NIR spectroscopy models in providing definite authentication, while demonstrating the capabilities of this technique for authenticity screening.

Uittreksel

Naby-infrarooi (NIR) spekroskopie is gebruik om die effekte van stroop verdunning, veroudering, stoortemperatuur en bestraling behandeling op heuning se NIR spektra te ondersoek. NIR spekroskopie, gekombineer met parsiële kleinste kwadrate diskriminantanalise (PLS-DA), is ook aangewend om ’n klassifikasie model te ontwikkel wat kan onderskei tussen outentieke heuning en heuning wat met hoë-fruktose mieliestroop (HFCS) of omgekeerde suikerriet stroop (ICSS) verdun is. Bepaling van vorige bestraling behandeling is ook ondersoek, om NIR spekroskopie-gebasseerde modelle te assesseer as ‘n moontlike hulpmiddel vir die identifisering van bedrieglik-geetiketteerde heuning.

Rou, ongefiltreerde heuningmonsters (n = 17) verkry van Suid-Afrikaanse byeboere is eenvormig gesyg en met behandelingskombinasies van 10 kGy bestraling en verdunning met 0, 10 en 20% (w/w) ICSS en HFCS onderverdeel (n = 174). Nog drie outentiek en onverdunde deelversamelings is by 4°C, 40°C en in onbeheerde omringende toestande gebêre (n = 51). ’n Laboratorium BÜCHI Fourier-transformasie naby-infrarooi (FT-NIR) spekrofotometer en ‘n draagbare MicroNIR NIR spekrofotometer, met golflengte reekse van 1000–2500 nm en 908-1676 nm, onderskeidelik, is gebruik om spektra in triplikaat te versamel, oor ’n tydperk van 9 maande.

ANOVA-gelyktydige komponentanalise (ASCA) het aangedui dat heuningtipe, verdunningsmiddeltipe, stoortemperatuur en ouderdom beduidende ($p > 0.05$) effekte op die spektrale datastel het, terwyl verdunningsvlak en bestraling geen beduidende effek het nie. Ten spyte hiervan, is bestraling verantwoordelik vir ‘n 5.82% en 7.19% vermindering van validasie akkuraatheid en doeltreffenheid, onderskeidelik, wanneer PLS-DA modelle wat op bestraalde en onbestraalde spektrale data gebou is, vergelyk is. Dit dui daaraan dat bestraling behandeling, heuning egtheid verifikasie tot ’n mate kan belemmer. Egter kon PLS-DA onderskeiding van bestraling behandeling ’n onsuksesvolle validasie akkuraatheid van slegs 59.7% behaal. Dié resultaat stel voor dat bestraling geen bruikbare effek op die spektrale data het nie.

Afsonderlike twee-klas PLS-DA modelle vir ICSS (75.95% akkuraatheid, 86.31% sensitiwiteit) en HFCS (73.95% akkuraatheid, 82.14% sensitiwiteit) verdunningbepaling is as die mees effektiewe verifikasie-oplossing bevind, en het voldoende voorspellingskrag vir keuring gedemonstreer. PLS-DA modelle wat op die BÜCHI laboratorium spekrofotometer data gebou is, het beter opgetree as dié wat op die draagbare MicroNIR spekrofotometer, en albei die MicroNIR se monsterhouers, gebaseer is. Ten spyte hiervan, bied die MicroNIR, met die Teflonhouer, soortgelyke akkuraatheid (70.0-75.47%) en doeltreffenheid (68.22-74.51%) aan, en is dus bewys as ’n haalbare en koste-effektiewe alternatief.

Kwantifisering van verdunningsvlak met parsiële kleinste kwadrate regressie (PLSR) het swak vertoning gewys vir beide ICSS (R^2_{Pred} = 0.118, RMSEP = 6.795%) en HFCS (R^2_{Pred} = 0.147, RMSEP = 6.596%) verdunnings. Hierdie resultaat is toegeskryf aan die onvoldoende verskeidenheid van verdunningsvlakke in

die verwysingsdata, asook die onbeduidende ($p < 0.05$) effek van verdunningsvlak op die algehele variasie van die spektrale data.

Die resultate van hierdie studie beklemtoon NIR spekroskopie se moontlike tekortkominge vir die doeleindes van heuning egtheid verifikasie, maar demonstreer ook die geskiktheid van hierdie tegniek vir heuning egtheid keuring.

This thesis is dedicated to Robert, Anna and Melissa Rust,
Chad Fourie, Megan Higgo, Kyra Mihalopoulos and Tim Köhler,
whose journey this was, as much as it was mine.

Acknowledgements

I wish to express my sincere gratitude and appreciation to the following persons and institutions:

Professor Marena Manley, Professor Federico Marini, and Dr Paul Williams, for their academic advice and reassurances throughout this project;

Mike Allsopp of the ARC PPRI Vredenburg, for his invaluable help in contacting and procuring honey samples from local beekeepers, as well as his advice, academic and otherwise, book recommendations and for guiding our first forays in beekeeping;

The ARC PPRI Vredenburg, for the use of their vehicle and beekeeping equipment;

All honey sample donors, Peel's Honey, Dad's Honey, Hurter's Honey, *Ubusi* Honey, Overberg Honey and Q-Bee Honey - without their contributions this project would not have been possible;

Cape Food Ingredients, Cargill and Tate + Lyle South Africa for providing syrup samples;

BÜCHI Labortechnik GmbH (Flawil, Switzerland) for the loan of their NIRFlex-500 FT-NIR instrument;

VIAVI Solutions Inc. (San Jose, CA, USA) for the loan of their VIAVI MicroNIR OnSite1700 instrument;

Technical staff at the Department of Food Science, Stellenbosch University for their willing assistance; and

My fellow postgraduate students at the Department of Food Science, whose company and camaraderie made this journey endurable.

This thesis is presented in the format prescribed by the Department of Food Science at Stellenbosch University. The language, style and referencing format used are in accordance with the requirements of the *International Journal of Food Science and Technology*.

Table of Contents

List of Figures

List of Tables

List of Abbreviations

ϑ	Spectral contrast angle
2-D	Two-dimensional
3-D	Three-dimensional
AACC	American Association Cereal Chemists
airPLS	Adaptive iteratively reweighted penalized least squares algorithm
A. m.	*Apis mellifera*
ANN	Artificial neural networks
ANOVA	Analysis of variance
AOAC	Association of Official Agricultural Chemists
ASCA	ANOVA-simultaneous component analysis
ATR	Attenuated total reflectance
ATR-FTIR	Attenuated total reflectance Fourier transform near infrared
AUC	Area under the curve
BP-ANN	Back propagation artificial neural networks
CAC	Codex Alimentarius Commission
CARS	Competitive adaptive reweighted sampling
CEM	Expectation maximization (hard updating)
CV	Cross-validation
CV	Coefficient of variation
CVA	Canonical variate analysis
d	Diameter
DA	Discriminant analysis
db	Dry basis
DEFT	Direct epifluorescent filter technique
DN	Diastase number
EDA	Exploratory data analysis
EM	Expectation maximization (soft updating)
FAOSTAT	FAO Statistical Database
FN	False negatives
FP	False positives
FT-IR	Fourier transform infrared
FT-NIR	Fourier transform near-infrared
GC	Gas chromatography
h	Height
HCA	Hierarchical Cluster Analysis
HFCS	High-fructose corn syrup
HF-diluted	High-fructose corn syrup diluted
HF-dilution	High-fructose corn syrup dilution
HMF	5-hydroxymethylfurfural
HPLC	High-performance liquid chromatography
ICSS	Inverted cane sugar syrup
IN	Invertase number
InGaAs	Indium Gallium Arsenide
IR	Infrared
IS-diluted	Invert cane sugar syrup diluted
IS-dilution	Invert cane sugar syrup dilution
kGy	Kilogray

kNN	*K*-nearest neighbours
LDA	Linear discriminant analysis
LC-PAD	Liquid chromatography with pulsed amperometric detection
LMW	Low molecular weight
LOD	Limit of detection
LOD_{max}	Maximum limit of detection
LS-SVM	Least Squares Support Vector Machines
LV	Latent variable
LVs	Latent variables
LVF	Linear Variable Filter
MA	Moving average
MAFF	Ministry of Fisheries and Food (UK)
MANOVA	Multivariate analysis of variance
MC	Mean centring
MDA	Multivariate data analysis
MIR	Mid-infrared
mPLS	Modified partial least squares
MS	Maltose syrup
MSC	Multiplicative scatter correction
NIPALS	Nonlinear iterative partial least squares
NIR	Near-infrared
NIRS	Near-infrared spectroscopy
NMR	Nuclear magnetic resonance
PC	Principal component
PCs	Principal components
PCA	Principal component analysis
PCA-CVA	Principal component analysis canonical variate analysis
PCR	Principal component regression
P.D.O.	Protected designation of origin
PLS	Partial least squares
PLS-CVA	Partial least squares canonical variate analysis
PLS-DA	Partial least squares discriminant analysis
PLS-LDA	Partial least squares linear discriminant analysis
PLSR	Partial least squares regression
r	Class-representing vector
r	Coefficient of correlation
R^2	Coefficient of determination
R^2_{Cal}	Coefficient of determination of calibration
R^2_{CV}	Coefficient of determination of cross-validation
R^2_{Pred}	Coefficient of determination of prediction
R	Diffuse reflectance value
RMSEC	Root mean square error of calibration
RMSECV	Root mean square error of cross-validation
RMSEP	Root mean square error of prediction
ROC	Receiver operating characteristic
RPD	Ratio of prediction deviation
RSD_R	Relative standard deviation of reproducibility
SCA	Spectral Contrast Angle
SCIRA	Stable carbon isotope ratio analysis

SD	Standard deviation
SEC	Standard error of calibration
SECV	Standard error of cross-validation
SEP	Standard error of prediction
SET	Standard error of a single test
SI	Similarity Index
SIMCA	Soft Independent Modelling of Class Analogy
SG	Savitzky-Golay
SNV	Standard normal variate
SVM	Support Vector Machines
TN	True negatives
TP	True positives
TSS	Total soluble solids
URP	Unique Radiolytic Product
USD	United States Dollars
UV-vis	Ultraviolet and visible
VIP	Variable importance in projection
Vis-NIR	Visible and near-infrared
w/w	Weight per weight

Chapter 1 Introduction

The keeping of honeybees has been intertwined with agriculture for millennia, and still plays a vital role in modern crop production. Provision of pollination services and the production of honey are two facets of beekeeping and both may be sources of income for today's professional beekeepers. Honey, the most widely available unrefined sweetener globally, has enjoyed consistent popularity across the ages and is also valued for its pharmacological uses in traditional and modern medicine.

During the past few decades, global demand and consumption of honey have increased substantially, in part due to honey's perceived health benefits and nutritional properties (Ulberth, 2016; Wu *et al.*, 2017). In South Africa, honey production does not meet local demand: in 2013, honey production stood at just over 1000 tonnes whilst a further 2000 tonnes were imported for the South African market (FAOSTAT, 2013). It is cheaper to import honey than to produce it locally, and as a result, a cost discrepancy exists between local honey and imported honey at retail level (M. Allsopp, 2018, Researcher, Agricultural Research Council Vredenburg, Stellenbosch, South Africa, personal communication, 28 February). In a 2008 report by the South African Bee Industry Organisation, cheap imports and profit-taking by imported honey were two of the top five reasons listed for South Africa's shift towards becoming a net honey importer, a position which has only deepened in the decade since the report's release.

As a high-value commodity, often reliant on the convoluted food chains of the 21st century to reach consumers, the potential for honey adulteration and unfair economic gain does exist. Honey was identified as one of the top 10 at-risk products for adulteration by the EU Commission in 2009 (de Lange, 2009). The Food Ingredient Fraud Database of the Food Chemicals Codex listed sixteen reports of widescale honey adulteration between 1995 – 2012, implicating water, sugar cane syrup, corn syrup, high fructose corn syrup, sugar beet syrup, maple syrup, invert sugar, chloramphenicol antibiotic residues and honey of a different, undeclared geographical origin as known adulterants and contaminants (The United States Pharmacopeial Convention, 2014). It is believed that the high demand and low supply of honey worldwide, and in South Africa, creates opportunities for the adulteration of honey and fraudulent financial gain. It has been speculated that adulterated honey is present on supermarket shelves around the world, but despite allegations in recent media reports, it remains to be proven whether South Africa is similarly affected and to what extent (Business Insider SA, 2018).

Honey adulteration has the potential to reduce consumer confidence in South Africa's honey industry and is likely to have unwanted consequences for South African beekeepers, as honey sales are an important component of successful beekeeping operations. These beekeeping operations play a vital role in commercial agriculture and are critical to agricultural job creation and food security, as bees are responsible for pollinating the majority of agricultural crops that do not self-pollinate (Hutton-Squire, 2014), equating to approximately 35% of crops worldwide (Melin *et al.*, 2014). South Africa's high-revenue horticultural

industries require extensive use of pollination services (SABIO, 2008; Melin *et al.*, 2014). The deciduous fruit industry, in particular, relies heavily on managed bee pollination and generates in excess of R12 bn in turnover per annum (HortGro, 2017).

In many ways, the state of South Africa's honey market is also an indication of the financial security of its beekeeping and pollination services, adding greater importance to the issue of honey fraud. Honey product sales make up a significant source of income for pollination service providers, who in turn contribute to national food and agricultural job security. Honey that is cheaply imported competes with authentic local products, with the oversupply of cheap products driving honey prices down, while adulterated honey defrauds the consumer and reduces public confidence in honey products (APIMONDIA Working Group, 2019). Without a favourable market for honey, the job of the disincentivised beekeeper and pollinator is made significantly less financially viable.

Currently recommended analytical authentication methods for honey are not widely available in the developing world and come with great start-up and operational costs, as both expensive instruments and skilled personnel are required. In South Africa, adulteration detection analyses are outsourced to European laboratories infrequently and at a substantial cost. It is therefore of great importance to South Africa's honey industry and regulatory bodies to develop capacity to perform these analyses or screen for authenticity independently.

The proposition of using near-infrared (NIR) spectroscopy to determine honey authenticity is not new; classification models based on NIRS and multivariate data analysis have demonstrated relatively high accuracy in differentiating between adulterated or unadulterated honey samples (Paradkar and Irudayaraj, 2002; Sivakesava and Irudayaraj, 2001a,b, 2002; Paradkar and Irudayaraj, 2001; Irudayaraj *et al.*, 2003; Kelly *et al.*, 2004; Tewari and Irudayaraj, 2005; Toher, 2007; Zhu *et al.*, 2010; Chen *et al.*, 2011; Rios-Corripio *et al.*, 2012; Mouazen and Al-Walaan, 2014; Kumaravelu and Gopal, 2015; Bázár *et al.*, 2016; Guelpa *et al.*, 2017; Li *et al.*, 2017; Ferreiro-González *et al.*, 2018).

One critique of a large proportion of studies available is their treatment of honey as a generic commodity, and that they suffer from a lack of standardization of sample treatment. Methodological inconsistencies have also arisen when samples are not uniformly strained or filtered. In addition, several studies did not contain an adequate number of samples nor did they not contain sufficient seasonal, geographical or botanical variation to be considered a representative reference library (Oliveri and Downey, 2012).

The focus of this project is to further explore the analytical capabilities offered by portable and benchtop NIRS in detecting irradiated and intentionally adulterated honey, taking into account the natural chemical progression that honey undergoes as it ages and after postharvest treatments. The foundations of a NIR spectroscopy screening method for suspected adulterated samples can only be laid once factors that are

thought to affect the spectral fingerprints of honey - and that may interfere in age- and treatment-insensitive classification models that have been proposed in previous studies - have been investigated. It is hoped that in doing this, a clearer understanding will be gained of how these factors affect honey composition and spectra, and ultimately, whether the variation caused by irradiation and sugar adulteration can be separated and individually identified by a combination of statistical techniques.

To complete the study, a classification model that would assist in differentiating between authentic, non-irradiated South African honey samples and those that have been irradiated or intentionally adulterated with other sugars is to be constructed by combining NIRS and suitable multivariate data analysis techniques. The potential industry applications of this would include detection of a variety of adulterations: cheap sugar syrups used to extend honey; and adulterations in which cheaper imported, and therefore irradiated, honey is used as a substitute or diluent for non-irradiated South African produced honey. Scientific literature on the relationship between irradiation and honey composition is limited and, to date, the effect of irradiation on the entire chemical composition of honey has not been studied comprehensively and has never been reported as having been examined with NIRS in scientific literature, making one of the main objectives and the potential findings of this study novel. It remains to be seen whether the products of these reactions are detectable with NIR techniques, and whether their presence can be seen as a reliable indicator of whether irradiation has occurred.

The intended impact of this study is to lay the foundations for developing a rapid, robust and non-destructive analytical method that can grant legitimacy to, and promote fair competition between, honest South African honey producers and, in future, offer some protection from the unfair competition created by honey fraudsters and adulterators.

In summary, the aims of this study are to investigate the effects of ageing, storage temperature and irradiation on NIR spectra of honey, and to develop a classification model for the rapid screening of syrup-diluted honey with NIR spectroscopy and multivariate data analysis techniques, irrespective of irradiation treatment. In addition, the ability to detect irradiated honey samples by means of a simple test would be a potentially valuable addition for honey screening. Attention will be given to standardization of the filtration and postharvest thermal history of honey samples before investigation, to minimize these often-neglected sources of sample variation. The objectives of this study include:

1. monitoring the spectral changes in honey samples, held at four storage temperatures and conditions, over 9 months;
2. comparing spectral changes in honey samples,
    a) before and after irradiation treatment,
    b) before and after dilution with commercially available bulk liquid sweeteners; and

3. creating classification models for detection of irradiated and intentionally diluted honeys.

As a whole, the outputs of this project will contribute to the body of knowledge of honey authentication, honey ageing and irradiation.

1.1. REFERENCES

APIMONDIA Working Group. (2019). *APIMONDIA STATEMENT ON HONEY FRAUD*. Rome.

Bázár, G., Romvári, R., Szabó, A., Somogyi, T., Éles, V. & Tsenkova, R. (2016). NIR detection of honey adulteration reveals differences in water spectral pattern. *Food Chemistry*, **194**, 873–880.

Business Insider SA. (2018). South Africans are probably eating Chinese honey that has been mixed with syrup, warns Wandile Sihlobo [Internet document] . *Business Insider South Africa* URL https://www.businessinsider.co.za/Business/sa-eats-honey-mixed-with-syrup-2018-2. Accessed 04/06/2018.

Chen, L., Xue, X., Ye, Z., Zhou, J., Chen, F. & Zhao, J. (2011). Determination of Chinese honey adulterated with high fructose corn syrup by near infrared spectroscopy. *Food Chemistry*, **128**, 1110–1114.

Ferreiro-González, M., Espada-Bellido, E., Guillén-Cueto, L., Palma, M., Barroso, C.G. & Barbero, G.F. (2018). Rapid quantification of honey adulteration by visible-near infrared spectroscopy combined with chemometrics. *Talanta*, **188**, 288–292.

Guelpa, A., Marini, F., Plessis, A. du, Slabbert, R. & Manley, M. (2017). Verification of authenticity and fraud detection in South African honey using NIR spectroscopy. *Food Control*, **73**, 1388–1396.

HortGro. (2017). *Key Deciduous Fruit Statistics 2017*. Paarl.

Hutton-Squire, J.P. (2014). *Historical relationship of the honeybee (Apis mellifera) and its forage; and the current state of beekeeping within South Africa*.

Irudayaraj, J., Xu, R. & Tewari, J. (2003). Rapid determination of invert cane sugar adulteration in honey using FTIR spectroscopy and multivariate analysis. *Journal of Food Science*, **68**, 2040–2045.

Kelly, J.F.D., Downey, G. & Fouratier, V. (2004). Initial Study of Honey Adulteration by Sugar Solutions Using Midinfrared (MIR) Spectroscopy and Chemometrics. *Journal of Agricultural and Food Chemistry*, **52**, 33–39.

Kumaravelu, C. & Gopal, A. (2015). Detection and quantification of adulteration in honey through near-infrared spectroscopy. *International Journal of Food Properties*, **18**, 1930–1935.

Lange, E. de. (2009). *Report on the food crisis, fraud in the food chain and the control thereof*. Brussels.

Li, S., Zhang, X., Shan, Y., Su, D., Ma, Q., Wen, R. & Li, J. (2017). Qualitative and quantitative detection of honey adulterated with high-fructose corn syrup and maltose syrup by using near-infrared spectroscopy. *Food Chemistry*, **218**, 231–236.

Melin, A., Rouget, M., Midgley, J.J. & Donaldson, J.S. (2014). Pollination ecosystem services in South African agricultural systems. *South African Journal of Science*, **110**, 1–9.

Mouazen, A.M. & Al-Walaan, N. (2014). Glucose adulteration in Saudi honey with visible and near infrared spectroscopy. *International Journal of Food Properties*, **17**, 2263–2274.

Paradkar, M.M. & Irudayaraj, J. (2001). Discrimination and classification of beet and cane inverts in honey by FT-Raman spectroscopy. *Food Chemistry*, **2001**, 231–239.

Paradkar, M.M. & Irudayaraj, J. (2002). Discrimination and classification of beet and cane inverts in honey by FT-Raman spectroscopy. *Food Chemistry*, **76**, 231–239.

Rios-Corripio, M.A., Rojas-López, M. & Delgado-Macuil, R. (2012). Analysis of adulteration in honey with standard sugar solutions and syrups using attenuated total reflectance-Fourier transform infrared spectroscopy and multivariate methods. *CYTA - Journal of Food*, **10**, 119–122.

SABIO. (2008). *The South African Beekeeping Industry: A section 7 committee investigation*.

Sivakesava, S. & Irudayaraj, J. (2001a). Prediction of Inverted Cane Sugar Adulteration of Honey by Fourier Transform Infrared Spectroscopy. *Journal of Food Science*, **66**, 972–978.

Sivakesava, S. & Irudayaraj, J. (2001b). A rapid spectroscopic technique for determining honey adulteration with corn syrup. *Journal of Food Science*, **66**, 787–792.

Sivakesava, S. & Irudayaraj, J. (2002). Classification of simple and complex sugar adulterants in honey by mid-infrared spectroscopy. *International Journal of Food Science and Technology*, **37**, 351–360.

Tewari, J.C. & Irudayaraj, J.M.K. (2005). Floral Classification of Honey Using Mid-Infrared Spectroscopy and Surface Acoustic Wave Based z-Nose Sensor. *Journal of Agricultural and Food Chemistry*, **53**, 6955–6966.

The United States Pharmacopeial Convention. (2014). Food Chemicals Codex (9th Edition) [Internet document] . *The United States Pharmacopeial Convention*URL https://app.knovel.com/hotlink/toc/id:kpFCCE0021/food-chemicals-codex/food-chemicals-codex. Accessed 24/10/2018.

Toher, D. (2007). *A comparison of model-based and regression classification techniques applied to near infrared spectroscopic data in food authentication studies*.

Ulberth, F. (2016). Advances in Testing for Adulteration in Honey. In: *Advances in Food Authenticity Testing* (edited by G. Downey). Pp. 729–753. London: Elsevier.

Wu, L., Du, B., Heyden, Y. Vander, Chen, L., Zhao, L., Wang, M. & Xue, X. (2017). Recent advancements in detecting sugar-based adulterants in honey – A challenge. *TrAC - Trends in Analytical Chemistry*, **86**, 25–38.

Zhu, X., Li, S., Shan, Y., Zhang, Z., Li, G., Su, D. & Liu, F. (2010). Detection of adulterants such as sweeteners materials in honey using near-infrared spectroscopy and chemometrics. *Journal of Food Engineering*, **101**, 92–97.

Chapter 2 Literature Review

The South African honey industry currently faces two complex issues: saturation with cheaper imported products, and the threat of potentially adulterated honey. During the past three decades, South Africa has transitioned from being a self-sufficient honey producer to a net importer, now importing twice as much honey as it produces (FAOSTAT, 2013). Local honey is more expensive to produce than foreign honey is to import but is also more highly valued in South Africa due to consumer perceptions of authenticity, safety and medicinal value. Additionally, honey is a high-value commodity, making an attractive target for adulteration. This, and the price discrepancy between local and imported honey, is considered an opportunity for fraud. Methods of determining various honey quality parameters are frequently used in combination for the authentication of honey, but due to their targeted nature they do not provide unequivocal authenticity determinations alone and can result in wasted time and resources. Meanwhile, currently available methods specific to adulteration detection are costly, highly specialized and not widely available in the developing world.

Non-targeted methods of food analysis have shown great potential in providing reliable, accurate and rapid results to address food quality or authentication issues (Esslinger *et al.*, 2014). Near-infrared spectroscopy is one such method, with a history of successful analytical applications in food. NIRS, in combination with multivariate data analysis, has been used in numerous honey authentication feasibility studies to date. While many of the proposed classification models have achieved excellent classification rates, they have not been extensively implemented in the honey industry yet. There are unaddressed issues of sample standardization and variation introduced by compositional changes, and existing modelling approaches require refinement.

This review covers relevant literature on honey composition, production and processing; chemical and physical characteristics, compositional changes in honey due to ageing and processing; honey legislation, honey production and regulation landscape of South Africa; modes of honey adulteration, verification of honey authenticity and the detection of adulteration and fraud; near-infrared spectroscopy, multivariate data analysis, NIRS and MDA classification as a method for honey authentication.

2.1 HONEY

2.1.1 Botanical description

Honey is the natural, sweet, carbohydrate-rich product predominantly produced by honeybees, *Apis mellifera* or *Apis ceranae*. Honeybees collect blossom nectar or honeydew produced by other organisms, which are mixed with secretions of their own and stored in honeycombs to mature (Codex Alimentarius, 1981; Wu *et al.*, 2017). Honey's success as a durable, long-life source of nutrition for bees can be attributed

to the super-saturation of sugars, low water activity and low pH, which make spoilage by fermentation unlikely to occur (APIMONDIA Working Group, 2019).

The species of honeybee, geographical origin, botanical origin of forage and climatic conditions largely contribute to the composition, aroma and flavour of honey (Cozzolino *et al.*, 2011; Da Silva *et al.*, 2016). A variety of other factors that may play a role in honey quality are the weather conditions, processing conditions, method of packaging and length of storage period. Blossom honeys, and *Apis mellifera* produced honeys form, by far, the majority of farmed honey produced worldwide, and in Southern Africa (M. Allsopp, 2018, Researcher, Agricultural Research Council Vredenburg, Stellenbosch, South Africa, personal communication, 2 November).

2.1.2 Production

Foraging worker bees collect blossom nectar, honeydew or less conventional sugar-containing liquids and store them in a specialized honey sac within the bee's oesophagus, where they are mixed with saliva and enzymes produced by the bee (Maurizio, 1976; APIMONDIA Working Group, 2019). It is in this storage sac that enzyme-induced acid production begins within the diluted nectar, reducing its pH. On returning to the hive, forager bees transfer the dilute nectar to house worker bees for further processing.

Maturation describes the process of concentrating sugars, reducing moisture content and lowering the pH of nectar to form the shelf-stable final product that is honey (APIMONDIA Working Group, 2019). Immature honey is actively and passively ripened by house worker bees in the hive in two stages (Maurizio, 1976). Worker bees manipulate the honey with their mouthparts by repeatedly expelling then sucking the mixture back into their honey sacs, before passing it on to another bee for the process to be repeated. During each regurgitation or handling of the honey, salivary secretions containing enzymes are added (APIMONDIA Working Group, 2019). After the regurgitation process has been repeated a number of times, the half-ripened honey is deposited in open cells in the comb to continue maturing passively.

Evaporation of the remaining excess moisture is a passive process caused by a combination of climatic factors and by ventilation of the hive by the fanning of bees (APIMONDIA Working Group, 2019). Honey may also be moved to different cells around the hive during this period, aiding dehydration. Mature honey is sealed off by capping the honeycomb: cells are capped with a thin wax layer once honey has reached approximately 20% moisture content. This layer prevents moisture uptake, as mature honey becomes increasingly hygroscopic as it dehydrates. Mature honey is a source of nutrition for the hive with a long shelf life and low spoilage potential. Surplus honey will be removed from the hive by the beekeeper. The beekeeper removes frames from the honey super once they are approximately three quarters capped, indicating that the nectar has completely ripened, and the honey has reached maturity (M. Allsopp, 2018, Researcher, Agricultural Research Council Vredenburg, Stellenbosch, South Africa, personal communication, 26 July).

2.1.3 Processing

Once harvested from the hive, honey is extracted from the comb. Capped cells are uncapped by running an uncapping fork over the comb surface and placed into an extractor to spin the honey out. A variety of techniques may be used on the extracted honey to produce a homogenous, stable product. These processing methods may also affect the overall chemistry of honey.

Extracted honey is typically subjected to several processes to improve the quality and shelf life of the final product and meet consumer expectations of a uniform and liquid product. Honey accumulates beeswax, pollen, micro-organisms and other impurities from the natural environment while maturing in the comb (Subramanian *et al.*, 2007). For this reason, honey typically undergoes two processing steps before it is packaged, namely separation and heating.

Separation techniques include straining, done through mesh of 200 to 600 microns and under the weight of the honey itself, and or pressure filtration, in which pressure is used to pass the honey through filtering screens with openings smaller than 200 microns, often around 100 microns or less. Straining may be done on honey as is, or with gentle heating up to 40°C to reduce its viscosity, while honey that is filtered is preheated up to at least 55°C to ensure that honey will easily pass through the filter while beeswax will remain solid and stay behind (Subramanian *et al.*, 2007). The removal of small particles by filtration assists in keeping the honey liquid, as fewer nucleation sites will be present to promote crystal formation. Ultra-filtration processing makes use of a membrane with a specific molecular weight permeability, which allows for the removal of certain microorganisms and high molecular weight proteins, including enzymes (Subramanian *et al.*, 2007). In order to maintain the identity and desirable properties of honey it is recommended by the Codex Alimentarius (1981) that “no pollen or constituent particular to honey may be removed except where this is unavoidable in the removal of foreign inorganic or organic matter”. National legislation and international guidelines, however, do not stipulate a minimum allowable filter size for honey filtration.

Heating eliminates pathogens as well as osmophilic yeasts that pose the risk of initiating fermentation, and also liquefies the honey (Migdal *et al.*, 2000). Fermentation will occur if these osmophilic yeasts are present and if the moisture content and storage temperature of honey are both sufficiently high (Subramanian *et al.*, 2007). A pasteurization treatment of 60 to 65°C for 25 to 30 min is considered sufficient to inactivate the yeasts responsible for spoilage in honey, but time-temperature combinations of 80°C for 90 s are equally effective and may increase throughput while allowing the processor to work with low viscosity honey.

Heat treatment provides the additional benefit of reducing or preventing recrystallization, as crystals that act as sites of crystal nucleation, including those invisible to the naked eye, can be dissolved (Subramanian *et al.*, 2007). Heating of honey may reduce its moisture content, but using heat treatment for

the purpose of further dehydrating honey goes against the recommendations made by the *Codex Alimentarius* (Codex Alimentarius, 1981; Subramanian *et al.*, 2007). High heat treatment may also result in a distinct and detectable loss of enzymes, such as proline and invertase, as well as an increase in 5-hydroxymethylfurfural formation and colour development (Bogdanov, 2009). Only honey that has undergone minimal processing and is unheated and unfiltered may be labelled for sale as 'raw honey' (Department of Agriculture, 2000). Honey that has been heated to 40°C for straining may still be considered raw honey, as it has not undergone pasteurization.

Irradiation is a food processing application that reduces microbiological, biological and some chemical hazards and unwanted effects in food products (Fan, 2013). Honey may be given irradiation treatment to reduce its microbial load, which both prolongs the shelf life of the honey and renders it safe for medical use (Migdal *et al.*, 2000). In accordance with the Agricultural Pest Act of 1983 (Act No. 36 of 1983), honey and other bee products that are imported into South Africa are required to undergo irradiation to remove any potentially hazardous biological agents, such as *Paenibacillus larvae* and *Nosema ceranae*. An exception to this is Zambian honey, which is exempt from mandatory irradiation due to an agreement made in 2015 between the South African and Zambian governments, after Zambian honey was found to meet South African phytosanitary requirements (Shabolyo, 2015). Imported and radurised products are required by the Foodstuffs, Cosmetics and Disinfectants Act, 1972 (Act 54 of 1972) to state their country of origin and indicate that they have been irradiated.

Radiation energy can be applied from any of the three types of ionizing radiation commonly used for food applications. These are gamma rays produced by cobalt-60 and cesium-137 decaying radio-isotopes, electron beams and x-rays. When matter is exposed to ionizing radiation, electrons are knocked out of their previous orbital locations and form charged or ionized molecules, also referred to as ions or free radicals (Fan, 2013). Free radicals have a short lifespan of approximately 10^{-3} seconds but may induce chemical breakdown in food components during this brief period. Primary radicals may themselves decompose, or may induce and propagate ionization in neighbouring molecules, creating secondary radicals which may then decompose (Fan, 2013). Radicals are capable of breaking the covalent bonds in the DNA backbone, effectively killing vegetative bacteria and bacterial spores at 0.5 to 1.0 kGy and 1.0 to 5.0 kGy respectively (Coultate, 2009).

2.2 CHARACTERISTICS OF HONEY

2.2.1 Chemical composition

Honey is essentially a supersaturated sugar solution but contains a vast number of macro and micro-components. Compositionally, honey generally contains comparable ratios (%w/w) of macro-components: a maximum of 20% water, 37 to 39% fructose, 30 to 32% glucose, 0.5 to 2% sucrose and 0.2% ash (Ulberth, 2016). The components that occur in lower concentrations have higher variability and include proteins,

enzymes, free organic acids, phenolic compounds, vitamins and minerals (Wu *et al.*, 2017). These components are largely dependent on the botanical species and geographical area from which nectar is foraged, and therefore are not consistent markers of honey's authenticity or lack thereof (Ulberth, 2016).

Sugars

Of the dry matter within honey, between 95 and 99% consists of sugars. Honey reaches a final sugar content of approximately 80% from an initial content of between 4 and 60% in flower nectar due to the dehydrating activities of bees (Graham, 1993). Nectar contains a mixture of sugars in varying proportions, but chiefly consists of sucrose, fructose and glucose. In mature honey, reducing monosaccharides fructose and glucose make up the majority of the sugar content, although there are small amounts of non-reducing disaccharide sucrose, and an estimated 25 additional oligosaccharides that may be present in honeys (Gallego-Picó *et al.*, 2013). The distribution of sugars determines physical and chemical behaviour of the honey, including the rate of crystallization, viscosity, density and hygroscopicity or sorption behaviour (Gallego-Picó *et al.*, 2013). In particular, the ratio of fructose to glucose has a significant effect on the rate of crystallization of the honey.

Glucose exists in a supersaturated state within honey matrices (Doner, 1977). The glucose content is increased during the ripening process by the action of invertases introduced in the honey sac of bees on sucrose present in nectar (Eyer *et al.*, 2016). It is the least soluble of the predominant honey sugars and exists as either an anhydrous form in solution or as a crystalline monohydrate form. The ratio of fructose to glucose is approximately 1.2:1.0, but may vary (Anklam, 1998). Glucose crystallization occurs at a faster rate than fructose or sucrose crystallization, therefore honeys with higher glucose ratios will form glucose crystals that precipitate out of the supersaturated honey matrix earlier than in fructose-rich honeys (Ulberth, 2016). The addition of glucose to honey therefore has an undesirable effect on the physical properties of the resulting product. In addition, the removal of glucose from solution during crystallization results in an apparent increase in water concentration in the honey matrix and overall, the formation of a heterogenous solution with an increased likelihood of fermentation (Bhandari *et al.*, 1999).

Sucrose, the only significant disaccharide that is consistently present in honey, is found in abundance in the nectar of many plant species but is reduced during honey production due to the activity of invertase enzymes (White, 1976). Sucrose content may be used as a criterion for botanical origin determination (Ruoff *et al.*, 2007). As stipulated in the Codex Alimentarius guidelines for honey, the upper limit for sucrose content in honey is 5% (w/w) for most blossom honeys and 10% (w/w) for honeydew honey and a selection of blossom honeys in which high sucrose content naturally occurs (Garciá-Alvarez *et al.*, 2002). Sucrose determinations by gas chromatography (GC), high-performance liquid chromatography (HPLC) or liquid chromatography with pulsed amperometric detection (LC-PAD) form a standard part of honey quality control and authenticity estimations set out by the International Honey Commission (Bogdanov, 2002, 2009).

Moisture

Honey reaches a final moisture content of approximately 20% from an initial moisture content of between 40 and 96% in flower nectar due to the action of bees (Maurizio, 1976). Moisture present in flower nectar is significantly reduced during honey ripening or maturation to produce honey that is resistant to spoilage. The final moisture content as well as the rate at which it is reached is determined by the initial nectar moisture content and by the conditions of the ripening process, in particular the temperature, air movement and humidity within the hive as well as the size of the colony (Gallego-Picó *et al.*, 2013; Eyer *et al.*, 2016). The moisture content of honey affects many physical parameters: density, viscosity, crystallization rate; biological parameters: microbiological load, shelf-life; and sensory parameters: appearance and flavour (Thamasopinkul *et al.*, 2017). Moisture content should be below 18% to prevent unwanted fermentation from occurring by osmophilic and osmotolerant yeasts (Bogdanov and Martin, 2002). The incidence of microbiological growth and fermentation is also likely to increase in crystallised honeys that have more available water in solution (Bhandari *et al.*, 1999).

Protein

The total protein content of honey, which includes enzymes and other N-containing compounds of both plant and honeybee origin, is typically less than 0.5% and closer to 0.2% on average (Anklam, 1998). Plant proteins are found in the form of pollen, which are unique to the botanical sources from which bees of the hive foraged. Pollen is collected by foraging bees to fulfil the dietary protein requirements of the colony (Eyer *et al.*, 2016). Collected pollen is deposited and stored separately from the honeycomb within the hive but will be present in the honey in small amounts due to inadvertent contamination by airborne pollen and the bodies of bees.

Enzymes

Honey is known to contain a number of enzymes, introduced by bee saliva during the repeated regurgitation of plant nectars during honey formation (Anklam, 1998). Enzymes may occur in variable quantities and commonly found examples include catalase, diastase, glucose oxidase and invertase, of which invertase and diastase are considered important markers of a honey's thermal history or authenticity, as levels of both are reduced by overheating and prolonged storage (Anklam, 1998; Bogdanov *et al.*, 1999). Some botanical varieties of honey do naturally contain low levels of enzymes and provision for these types have been made in *Codex Alimentarius* honey standards (Bogdanov *et al.*, 1999).

Diastase and Invertase are found in their highest quantities in fresh honey. Both the diastase and invertase activities, indicated by the diastase number (DN) and invertase number (IN) respectively, are reduced by overheating and prolonged storage and are therefore regarded as freshness indicators (Bogdanov *et al.*, 1999). The most recent review of the International Honey Commission harmonised methods revealed

that invertase measurements show lower relative standard deviation of reproducibility (RSD_R) values than diastase measurements (Bogdanov, 2009). The IN is therefore generally regarded as a more accurate indicator for honey freshness or age. However, IN values are still not included in the *Codex* standard alongside DN values and are regarded as a supplementary measure.

Amino acids

Proline is an amino acid introduced during the handling of nectar by honeybees and is considered an indicator of maturity or ripeness. Honey adulterated with substantial proportions of other sugars will not have as much proline present. A proline content below 180 mg/kg is considered a strong indicator that a honey sample may have been adulterated with other sugars or has not been allowed to reach maturation (Bogdanov and Martin, 2002; Ruoff *et al.*, 2007; Bogdanov, 2009). Proline content determinations are not specifically recommended by the *Codex Alimentarius* Standard for Honey but are being used by some countries as a supplementary quality measure (Bogdanov and Martin, 2002).

Organic acids

The organic acid content of honey is indicated by the free acidity content and is regarded as an indicator of fermentation in honey (Ruoff *et al.*, 2007). Fermentation occurs more readily when honey has a moisture content above 18%, which may be due to climatic conditions, or as a result of either premature harvesting or adulteration by dilution with water (Bogdanov and Martin, 2002). Quantities of organic acids such as citric acid, fumaric acid, gluconic acid, malic acid, pyruvic acid and succinic acid are also found to occur naturally in honey and are largely dependent on the plant origin (Anklam, 1998). Exceptions have been made in *Codex Alimentarius* and *Codex*-based honey standards for certain varietals of honey that have naturally occurring high organic acid contents (Bogdanov *et al.*, 1999). Free acidity is conventionally determined by titrimetric methods, but interlaboratory evaluations have shown the results obtained by these methods yielded high RSD_R values and therefore poor reproducibility (Bogdanov, 2002).

Other micro-components

Mineral content in honey may range from 0.04 to 0.2% in honeys and is largely dependent on the soil type present in the forage areas (Anklam, 1998). Honeys with higher mineral contents are darker in colour than low mineral content honeys.

Hydroxymethylfurfural (HMF) is a product of Maillard (non-enzymatic browning) reactions that naturally occur when fructose or glucose dehydrates within the acidic environment of honey, the product of which will therefore accumulate with prolonged storage (Da Silva *et al.*, 2016) (Gallego-Picó *et al.*, 2013). However, these Maillard reactions are also accelerated by high temperatures, resulting in increased formation of HMF following pasteurization or other heat treatments. Fresh honey is expected to have a low HMF content, which is increased over storage time and as a result of heat treatments. An increased HMF content may correlate with a darkening of honey colour (Ruoff *et al.*, 2007). It is considered a marker compound for determining

whether honey has been subjected to undeclared heat treatments during processing (Gallego-Picó *et al.*, 2013). HMF may be quantified in a sample with the officially recognised UV-vis spectrophotometry-based method, AOAC 980.23 (AOAC, 1990).

The limit for HMF content permitted by the Codex Alimentarius (1981) is given in Table 2. It is of interest that the recommended limit for HMF in honey produced in tropical regions is twice that of temperate regions, as warm climatic conditions accelerate its formation and make the 40 mg/kg target unreasonable.

Microbiological

Osmophilic and osmotolerant yeast species *Saccharomyces*, *Schizosaccaromyces* and *Torula* account for the majority of the microbiological populations found in honey. *Bacillus* and *Clostridium* bacteria and spores may also be present (Migdal *et al.*, 2000).

Other

A number of smaller components have been identified in adulterated honey products that are of relevance when considering honey authenticity. Mannose is an epimer of glucose that does not naturally occur in honey but has been observed in purified syrups and in honeys treated with ion-exchange technology to remove pollen, pesticides and antibiotics, which is common practice for honeys exported by China (Missler *et al.*, 2016). Difructose anhydrides are products found in heated high-fructose sugar syrups that do not naturally occur in honey, and may be used to detect adulterations (Wu *et al.*, 2017). The compound 2-acetylfuran-3-glucopyranoside has also been identified as an indicator for rice syrup adulterations (Ulberth, 2016).

While knowledge and detection of such markers is valuable, there is no guarantee that these products will always be present at detectable limits and they are only indicative of one of many modes of adulteration to be found. When looked at in isolation, it is unlikely that any single component could give a convincing indication of authenticity, particularly in low level adulterations that do not push the sample out of the acceptable legal ranges. But the effect of adulteration on all of these parameters together may provide a more conclusive answer to the question of authenticity.

2.2.2 Physical properties

The crystallization tendency of honey depends on not only the monosaccharide ratio, but also the thermal history, the amount of nucleation site crystals present and the temperature at which the honey has been stored (Ruoff *et al.*, 2007). Under typical conditions, honey stored in the comb will not crystallize. Once honey is exposed to foreign particles, moisture and moisture loss factors, crystallization becomes possible and increasingly likely (Bhandari *et al.*, 1999). Foreign particulate matter, dust, pollen, beeswax, air bubbles, moisture, container walls and contamination by older crystallized honey can all induce crystal nucleation in honey. Heat treatment may prevent recrystallization by dissolving sugar crystals and crystal nuclei in the honey (Subramanian *et al.*, 2007). An investigation into the effect of crystallization of honey on NIR spectral

data by Bakier (2009) found that crystallization affected the peak area of absorption between 1876 -2014 nm and showed a strong correlation to changes in water activity induced by crystallization.

Honey displays optical rotation of polarized light properties, based on the proportions of sugars that exhibit rotatory behaviour present. The observed, or total, optical rotation is affected primarily by the presence of glucose (+) and fructose (-), and to a lesser extent by melezitose or erlose, which also contribute to a net positive optical rotation (Garciá-Alvarez *et al.*, 2002).

Lastly, electrical conductivity is a property correlated to the acid and ash content of honey, both of which are determined by the botanical sources of forage. As a result it is considered an important physicochemical property for indicating honey origin and is recommended as a routine testing parameter (Bogdanov, 2009).

2.2.3 Stability

Compositional changes

The chemical changes that occur in honey after harvesting and during storage are complex and have been comprehensively reviewed by Da Silva *et al.* (2016). During storage, chemical reactions such as oxidation, fermentation and Maillard reactions result in changes to the composition of honey. Sucrose and other non-monosaccharides decrease in concentration with storage time, while glucose and fructose increase. For this reason, any comparative analyses performed on honey samples should ideally have a similar age and thermal history to eliminate interference introduced by these chemical changes.

The volatile profiles of two varieties of Brazilian honey, cashew and *marmeleiro*, were monitored for 6 months under elevated temperature and acidic conditions in a study by Moreira *et al.* (2010) that aimed to model 'tropical' storage conditions in honey samples (n = 4). It was found that volatile compounds detected in fresh honey samples were reduced to between 37.9 and 50% after 6 months of storage at elevated temperatures of between 35 and 40°C.

During prolonged storage, sugars decompose into furan and furfural (Moreira *et al.*, 2010). Furan and furfural formation from sugars also occurs under acidic or reducing conditions and as a result of Maillard browning and caramelization reactions. In temperature-aged honey types, HMF was observed to increase significantly ($p < 0.05$), although under acidic ageing conditions differences in HMF formation between the honey types were observed (Moreira *et al.*, 2010). The observation that HMF precursor concentrations differ between honey varieties and determine which reactions are favoured, suggest that HMF formation rates cannot be expected to be universal for honeys of all botanical varieties and under all storage conditions.

Irradiation

The propagation or decomposition reactions of radicals induced by irradiation are responsible for many of the biological and chemical changes that may be observed in irradiated foods. Physically, no changes in honey have been observed (Sabato, 2004). Biologically, irradiation is capable of breaking the covalent bonds

in the DNA backbone, which results in killing vegetative bacteria and bacterial spores at 0.5 to 1.0 kGy and 1.0 to 5.0 kGy respectively (Coultate, 2009). Chemically, irradiation results in the formation of low molecular weight (LMW) compounds, which are thought to form as a result of cleavage of intermolecular glycosidic bonds (Fan, 2013). The resulting carbohydrate fragmentation forms LMW products such as glyoxal and formaldehyde (Coultate, 2009).

The chemical effect of irradiation on carbohydrates has been described as similar to heating carbohydrates in an alkaline environment (Coultate, 2009). The mechanism of these carbohydrate reactions is more clearly explained by the influence of irradiation on water. Water, associated closely in solution with carbohydrates, forms a number of radicals which can abstract H atoms from carbohydrate structures, yielding an α-hydroxyl molecule which may go further to catalyse organic acid formation (Fan, 2013). For this reason, the pH of carbohydrate solutions is observed to decrease as a result of irradiation treatment. Other products of irradiated sugars include CO_2, H_2, furans and a variety of carbonyls including formaldehyde, acetaldehyde and malonaldehyde.

Unique Radiolytic Products (URPs) are LMW compounds that have a strong and exclusive relationship to the radiation reaction of interest and may act as valuable markers (Coultate, 2009). A linear relationship exists between the radiation dose and the level of malonaldehyde in carbohydrate solutions, with high radiation doses being capable of causing a build-up of malonaldehyde products (Fan, 2013). Furans may be formed as a result of the irradiation of sugars, fatty acids and ascorbic acid. Mono- and disaccharides such as glucose, fructose and sucrose – the three most abundant carbohydrates in honey, are included in this group of furan precursors (Fan, 2013). Fan *et al*. (2005) found that furan production in irradiated sugar solutions is negatively correlated to an increase in pH, meaning that furans are more readily formed at pH 3 than pH 8. The precise mechanism remains unelucidated. These radicals are unstable and may decompose into more stable aldotetrose molecules. Furan formation has not been studied, and therefore never observed, in irradiated honey, but a study on fresh grape and pineapple fruit, which have similar low pH and high sugar contents, showed that small amounts of furan were formed upon irradiation (Fan, 2005).

Irradiation also induces decomposition of disaccharides and polysaccharides by a mechanism that remains unclear, but is thought to occur by cleavage of the intermolecular glycosidic bonds (Fan, 2013). Overall the amount of breakdown in carbohydrate solution is small at dose levels up to 10 kGy, and the decomposition mechanisms and products not dissimilar to those induced by heating carbohydrates in alkaline solution (Coultate, 2009).

In a limited study by Migdal *et al.* (2000) on the microbial reduction and changes in organoleptic and physicochemical properties of honey samples (n = 7) achieved with irradiation, honey was irradiated at 10 kGy. Irradiation was found to reduce the total microbiological load by 99% in seven honey samples and increase the antibiotic inhibition value of the honey from 1.67 to 2.67 in all three of the honey samples that were tested for inhibition. However, no significant effect on the moisture content, acidity, sucrose, diastase

and HMF values was observed, when tested with standard methods, although slight decreases in diastase and HMF values were observed. No change in the organoleptic properties of the honey was observed either, when evaluated by a sensory panel. While this study has value as a pioneering study within the overlapping fields of radiation chemistry and honey, the sample size limits the reliability.

In another study on the effect of irradiation on honey parameters used in quality control, honey samples (n = 7) were irradiated at 10 KGy and their total soluble solids (TSS), pH, moisture, HMF, sucrose, reducing sugars, ash and free acidity content were measured (Bera *et al.*, 2009). The TSS, pH and moisture did not change significantly during irradiation, while a small number of irradiated samples were observed having statistically lower reducing sugar and sucrose averages ($p \leq 0.05$). This decrease in sucrose content is expected, as gamma radiation is known to cause cleavage of glycosidic bonds. The HMF content differed significantly between irradiated and non-irradiated samples, with irradiation observed to reduce the HMF content in all seven samples. Overall, all samples were within the limits stipulated by Brazilian regulations. As with the aforementioned Migdal *et al.* (2000) paper, the number of samples limits the reliability of the study.

2.3 HONEY INDUSTRY

South African honey production is dominated by farmed *Apis mellifera* spp. that predominantly forage on blossom nectar. Common alternatives of honey from other bee species and honey produced from honeydew secretions of aphids constitute an insignificant proportion of the local market. Two subspecies of *A. mellifera* are found in South Africa: Cape bees, *A. mellifera capensis*, whose natural habitat is comprised of the Western, Eastern and lower regions of the Northern Cape; and the African bee, *A. mellifera scutellata*, which is found in the remaining geographical areas within South Africa's borders. The overlap of these subspecies is naturally maintained by bee species themselves, but also controlled by the Department of Agriculture to limit the destructive effects of 'social parasitism' of *A. m. capensis* on *A. m. scutellata* (Hutton-Squire, 2014; Melin *et al.*, 2014). The honey produced by the two subspecies is thought to be chemically similar but has never been experimentally investigated due to the difficulties of allowing *A. m. capensis* to co-exist with other *Apis mellifera* sub-species in a shared geographical location, owing to their parasitic tendency (M. Allsopp, 2018, Researcher, Agricultural Research Council Vredenburg, Stellenbosch, South Africa, personal communication, 2 November).

In beekeeping and honey production, honey can be classified as either multifloral or monofloral in origin. Monofloral honeys do not occur naturally in most natural habitats as honeybees are generalist foragers by nature and will travel long distances from their hive in search of pollen and nectar. For a honey to be classified monofloral, at least 45% of the pollen counted within a sample must originate from a single botanical source. Melissopalynology, the study of identification and quantification of pollen within honey, and the only true way to determine monoflorality, is a painstaking and seldomly performed process. In the context of this body

of research, the term 'presumed monoflorals' is used to describe the origin of a honey, as perceived by the beekeeper, but is not necessarily proven by melissopalynological methods. Presumed monofloral honey varieties also typically exhibit the characteristics of a known, true monofloral honey type. Masehela (2017) made a survey of the exotic and indigenous botanical foraging sources of importance to beekeepers in South Africa, by province. A few of the most commonly produced and commercially available South African 'presumed monofloral' honeys include sunflower, canola, aloe, citrus blossom, macadamia, litchi, a diversity of Eucalypts, as well as distinct regional floral groupings such as *Protea*, *Strandveld* and *Sandveld fynbos*.

2.3.1 Supply and demand

Since 2013, reported South African honey production has stood constant at just over 1000 tonnes (FAOSTAT, 2013). The almost-identical production quantities, reported over five years of extreme weather fluctuations and documented low honey yielding seasons, suggests these figures are loosely estimated and that accurate production data is simply not available. Further tonnage is imported for the South African market, which has shown a sharp increase in 2016 (**Table 2.1**). Chinese honey products constitute the majority of imports by far but are also the cheapest when compared to other significant imports (**Figure 2.1** and **2.2**). South Africa does export a small volume of honey itself, which has accounted for between 20 and 34% of the estimated total South African production in recent years.

Table 2.1 Honey production, import and export quantities and values for South Africa, 2013 - 2017 (FAOSTAT, 2017)

Year	Production Quantity (t)	Import Quantity (t)	Import Value (USD)	Export Quantity (t)	Export Value (USD)
2013	1086	2373	3804	290	688
2014	1087	2306	3701	361	1109
2015	1087	2300	3708	222	869
2016	1087	3986	5327	372	1590
2017	1088	4206	5682	503	2319

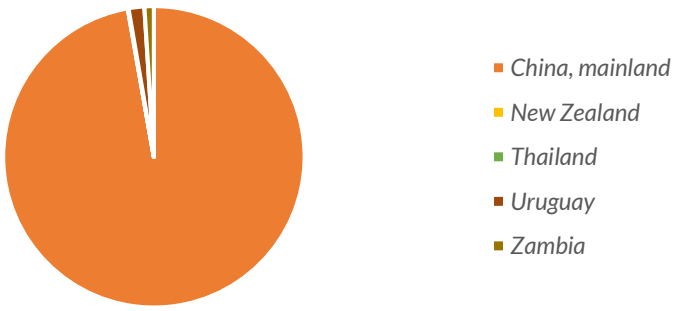

Figure 2.1 Honey import quantities into South Africa by country (FAOSTAT, 2013).

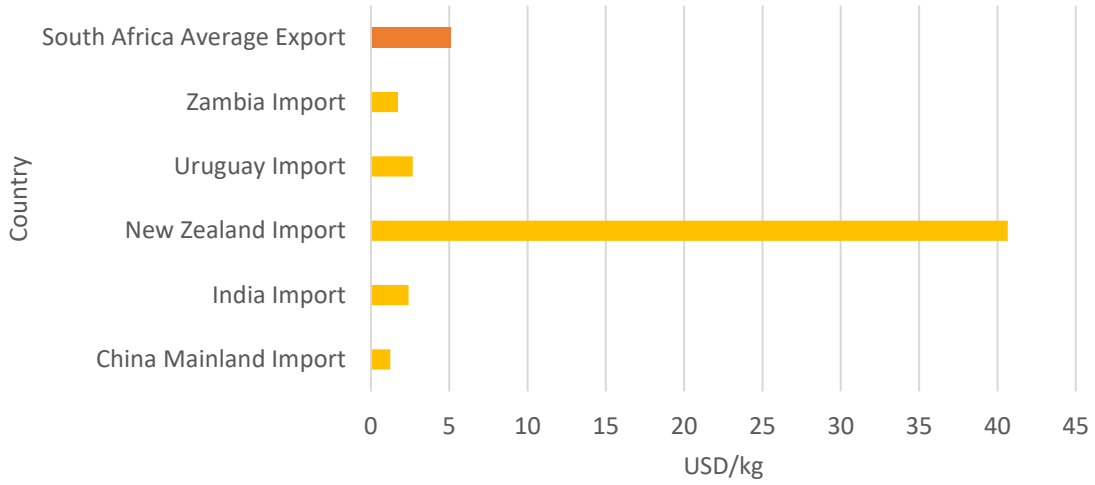

Figure 2.2 Honey import and export values by country (FAOSTAT, 2017).

2.3.2 Regulation

As a natural product, the composition of raw honey has considerable variation, but efforts have been made to formalize these requirements into a universal specification with compositional limits (Codex Alimentarius, 1981) (**Table 2.2**).

Regulations and guidelines applicable to the sale of South African honey do not permit the addition of substances other than honey. South African legislation stipulates that all honey and mixtures of bee products for sale should be free from impurities, additives and adulterants (Department of Agriculture, 2000), while guidelines provided by the Codex Alimentarius Standard for Honey (1981), state that honey should not "have added to it any food ingredient, including food additives, nor shall any other additions be made other than honey," nor should it have any of its original components removed, unless unavoidable during the removal of other foreign matter, neither should honey be "heated or processed to such an extent that its essential composition is changed and/or its quality impaired."

In this statement it is also implied that the conversion of nectar to honey is to be done entirely by bees and should neither require nor include human involvement (APIMONDIA Working Group, 2019). This is intended to address the use of vacuum drying to artificially dehydrate honey instead of relying on the natural maturation process.

Table 2.2 Composition and quality parameters of blossom honey adapted from Codex Alimentarius (1981)

Parameter	Official Method of Analysis	Limits
Essential composition and quality factors		
Moisture content	AOAC 969.38B / J. Assoc. Public Analysts (1992) **28** (4) 183-187 / MAFF Validated method V21 for moisture in honey.	Most honeys ≤ 20% Heather honey ≤ 23%
Sugar contents	AOAC 977.20 for sugar profile	-
Total fructose and glucose	*Not available*	Most honeys ≥ 60 g/100 g Honeydew honey ≥ 45 g/100 g
Sucrose	*Not available*	Most honeys ≤ 5 g/100 g Alfalfa, Citrus, False Acacia, French Honeysuckle, Menzies Banksia, Red gum, Leatherwood and *Eucryphia milligani* honeys ≤ 10 g/100 g Lavender and Borage honeys ≤ 5 g/100 g
Water insoluble solids	J. Assoc. Public Analysts (1992) **28** (4) 189-193/ MAFF Validated method V22 for water insoluble solids in honey	Most honeys ≤ 0.1 g/100 g Pressed honeys ≤ 0.5 g/100 g
Electrical conductivity	*Not available*	Most honeys ≤ 0.8 mS/cm Honeydew and chestnut honeys ≥ 0.8 mS/cm
Added sugars	AOAC 977.20 for sugar profile AOAC 998.12 for C-4 Plant Sugars in Honey	- -
Additional composition and quality factors		
Free acidity	J. Assoc. Public Analysts (1992) **28** (4) 171-175 / MAFF validated method V19 for acidity in honey	<50 milliequivalents acid per 1000 g

Diastase activity	AOAC 958.09	≥ 8 Schade units or ≥ 3 Schade units in honey with naturally low enzyme contents
HMF content	AOAC 980.23	≤ 40 mg/kg Or ≤ 80 mg/kg from tropical climates
Contaminants		
Heavy metals	*Not available*	CAC maximum levels
Pesticide and Veterinary drug residues	*Not available*	CAC maximum levels

2.3.3 Challenges

Contrary to the messages promulgated by popular media worldwide, which portray a bleak future for the farmed honeybee and other non-managed wild pollinators, South Africa has a relatively healthy, growing honeybee population (Melin *et al.*, 2014). Parasites, mite infestations and American and European Foulbrood diseases, which have caused colony collapse and resulted in bee population and pollination productivity declines across Europe and Northern America, are all present in South Africa but have not threatened honeybee colonies to the extent anticipated (Hutton-Squire, 2014). This is in part due to a precautionary phytosanitary measure, a subsection of the Agricultural Pest Act of 1983 that was instituted, requiring imported honey and bee products to undergo irradiation to prevent the transmission of these disease agents, such as *Paenibacillus larvae* and *Nosema ceranae*, to South African colonies.

South African bees do however, still face the threats of pesticide use, destruction of indigenous and invasive forage sources, and hive theft. It also remains to be assessed whether the current pollination capacity of South Africa's managed bees and beekeepers can meet the increasing demands of pollination-dependent agriculture in South Africa, and whether wild forage can support the nutritional needs of honeybee colonies year-round. Eucalypt species, currently threatened by the Working on Water programme, are of particular importance to honeybee colonies as a source of nutrition during critical times of the year when other forage sources are not in flower (Allsopp and Cherry, 2004).

In addition to the constant low supply and high demand for the product worldwide, honey harvests can vary drastically between seasons due to weather fluctuations, sometimes up to ten-fold (M. Allsopp, 2018, Researcher, Agricultural Research Council Vredenburg, Stellenbosch, South Africa, personal communication, 28 February). The supply deficit caused by sudden shortfalls could create opportunities for adulteration or importation of adulterated products as suppliers struggle to maintain their contractual obligations. South Africa currently imports twice as much honey as it produces (FAOSTAT, 2013), but these imports are not monitored by any governmental department, and it is unknown in what form these imports reach

supermarket shelves (M. Allsopp, 2018, Researcher, Agricultural Research Council Vredenburg, Stellenbosch, South Africa, personal communication, 2 November).

2.4 AUTHENTICATION AND ADULTERATION OF HONEY

Food authentication is the verification that a product adheres to legal requirements as well as the description found on its label (Esslinger *et al.*, 2014; Danezis *et al.*, 2016). This description may encompass any declaration of the origin of the product or the method of production or processing employed to produce it. Origin of a product refers to animal species, genetic modifications or the geographic region in which it was produced. Production methods are the farming practices used in primary production and can include free-range, harvesting method or organic descriptors. The processing methods used during product manufacture might include heating, freezing or radiation treatments (Danezis *et al.*, 2016). Foods that are expensive and experience considerable seasonal and harvest variation as a result of weather fluctuations may be most susceptible to adulteration (Kelly *et al.*, 2004).

Authentication or adulteration detection methods are becoming issues of legal and commercial interest. Lawmakers attempt to create legislation that protects consumers and regional producers, but which is also supported by robust and verified analytical methods, while honest producers seek to prove that their products adhere to these standards. There are obvious benefits to being able to prove provenance of a food product. Labels of authentication allow certified products to stand out and often raises the demand and selling price of the product due to the perception of higher quality (Danezis *et al.*, 2016).

Authentication studies have conventionally relied on chemical composition or physical properties of food products to detect adulteration. The impracticality of targeted, proximate food analyses has indicated potential for further development of non-targeted methods of analysis (Manley and Baeten, 2018). The variation of natural products and the complexity of food matrices makes adulteration detection immensely complicated. Biological variation in food products is determined by a spectrum of factors, which include the genetics of the species, season or year of production, weather patterns, processing method used, geographic origin, among others. This inherent variation makes compositional values considered in isolation unreliable predictors of authenticity. In their most recent statement addressing honey fraud, APIMONDIA, working group of the International Federation of Beekeepers' Associations, stressed the need for regular reviewing by authorities of the officially recommended methods of fraud detection, based on the best available methods, the origin of the product and the history of fraudulent activities relevant to the region.

2.4.1 Honey adulteration and fraud

Honey is a high value commodity due to the labour-intensive nature of beekeeping and honey production. During the past decades, global demand and consumption of honey have increased substantially, in part due to honey's perceived health benefits and nutritional properties (Ulberth, 2016; Wu *et al.*, 2017). This growth in demand has not been echoed by a production increase in the major honey-producing countries worldwide,

with the exception of China (Ulberth, 2016). The high demand and low supply of honey worldwide has created opportunities and commercial interest in the adulteration and fraudulent marketing of honey (Da Silva *et al.*, 2016).

Honey fraud can take a variety of forms, most commonly by dilution of honey with sweeteners of lesser value, or by fraudulent labelling of honey from a specified geographical or botanical origin, which may include dilution of the honey of origin with honey of lesser value or quality (Bogdanov and Martin, 2002; Ulberth, 2016; Wu *et al.*, 2017). Adulteration of honey by other sweeteners can occur in one of two ways; the addition of any sugar or syrup, of refined or naturally-occurring origin, directly to honey after harvesting or indirectly by intensively or exclusively feeding these sugars or syrups to honey-producing colonies as an alternative to naturally-sourced plant nectar (Wu *et al.*, 2017). Less common is the harvesting of unripe or green honey, which may be forcibly dehydrated to reach regulation maximum water content (Ulberth, 2016). Lastly, the recent advancement of ion-exchange technology, in which resins may be used to remove pollen, pesticides, antibiotics and colour particles, has created opportunities for low-quality honeys to be disguised and sold as a higher-quality product (Missler *et al.*, 2016; APIMONDIA Working Group, 2019).

The mislabelling of honey products that claim specific treatment conditions (raw, unpasteurized, organic) or do not declare treatment conditions (irradiation, filtration) may also constitute food fraud (Bogdanov and Martin, 2002).

In summary, honey fraud may fall within any of the following categories (Primrose *et al.*, 2010):

1. extension or dilution of a food with a lesser value substrate – cheap honey or sugar syrups;
2. full substitution of a food with a lesser value substrate – cheap honey or sugar syrups;
3. adulteration of food to increase value or improve appearance – lighter honeys added to darker honeys of origin to improve colour;
4. false declaration of processing conditions – failure to declare pasteurization, filtration or irradiation;
5. masking honey origin or quality - use of ion exchange resins to lighten honey or remove pollen, pesticides or antibiotic residues; and
6. false declaration of origin - botanical origin or country of origin.

The adulteration of honey is an international food fraud issue that has received much public attention and been the topic of numerous studies and review papers (Abdel-Aal *et al.*, 1993; Padovan *et al.*, 2003; Chen *et al.*, 2011; Tosun, 2014; Bázár *et al.*, 2016; Li *et al.*, 2017; Siddiqui *et al.*, 2017), but until recently (Guelpa *et al.*, 2017) has not been extensively studied in South Africa.

In South Africa, all imported honey is irradiated. Consumer perceptions associated with irradiation render the overall demand for imported, irradiated honey less than for local, non-irradiated honey, likely due to public scepticism and negative labelling claims which have cast irradiation in an unfavourable light. And

very importantly, if cheaper imported honey is being used as a substitute or diluent for South African honey, there is no official analytical method implemented for detecting this type of fraud and adulteration.

Choice of adulterants

Adulterants added to honey will affect the chemical and or physical properties of the resulting honey mixture. Simple adulterations involving the addition of commercially obtainable sugars, with unaltered compositions, are easily detected. Glucose is not a favoured adulterant option, as the addition of glucose solutions increase the rate of crystallization of the honey, causing quality deterioration that is unacceptable to the consumer (Ulberth, 2016). Sucrose is also considered a less sophisticated adulterant due to its ease of detection and its naturally low occurrence in honeys (Ruoff *et al*., 2007; Ulberth, 2016). Neither is water addition considered a realistic adulteration method, as the effect on the product's quality and shelf stability is likely to outweigh the lucrative potential of the adulteration (Ulberth, 2016).

High-fructose corn syrup (HFCS) is an ideal addition, due to the compositional similarity of certain HFCS grades to honey and its affordability and abundance in most countries (Ulberth, 2016). Furthermore, it may be undetectable at up to 50% in honey adulterations, as it will not cause the sugar composition to deviate from the limits specified by Codex Alimentarius, making it a viable adulterant. Additionally, it is common for preparations of high fructose corn syrup and cane invert sugar to be manipulated to resemble the glucose and fructose composition of honey (Ulberth, 2016; Manley and Baeten, 2018). Corn syrups, and in particular HFCS, are not produced, nor are they widely available in Southern Africa, as sugar cane dominates local table sugar and sugar syrup production. Inverted cane sugar syrup (ICSS) is the most commonly utilized liquid sweetener in South Africa and is both widely and cheaply available.

The addition of sucrose in the form of acid-hydrolysed invert syrup can be detected as a result of an elevated HMF content caused by the increased acidity of the honey. Invert syrup produced by enzymatic hydrolysis cannot be detected by this method, however.

Rice and sugar beet syrups are other major global sugar sources that have found popularity as honey adulterants (The United States Pharmacopeial Convention, 2014). The major attraction of these two sugars is their ability to elude detection by the official AOAC 998.12 method of sugar adulteration detection, which is limited to detecting C_4 plant derived sugars, such as cane and corn sugar (Ulberth, 2016).

2.4.2 Authentication methods

In the context of this literature study, authentication refers to the process of determining whether a honey product complies with the description given on its label. Information relating to a honey's purity, processing history, irradiation history and botanical and geographical origin all form part of its identity - and its authenticity if coherent with the product's stated description. A variety of traditional chemistry methods as well as several modern, instrumental approaches can be taken in an attempt to determine the authenticity of honey.

The earliest authentication methods for honey relied on the quantification of macro-components, such as moisture, fructose, glucose or sucrose content. Many of these methods still form part of the routine analyses stipulated by national authorities (Department of Agriculture, 2000) and international guidelines, such as Codex Alimentarius and the harmonized methods of the International Honey Commission (Codex Alimentarius, 1981; Bogdanov, 2009). Due to the extent of botanical and geographical variations, however, macro-components are generally regarded as unreliable markers of honey's authenticity and would not be employed to investigate authenticity today. For this reason most modern and more effective traditional analytical approaches focus on identifying the presence and quantity of chemical micro-component by-products removed or introduced during adulteration, such as diastase or HMF as indicators of heat treatment, proline as an indicator of maturity or difructose anhydrides as a marker for added high-fructose syrups (Ulberth, 2016).

The ingenuity and complexity of adulterations found today are challenging existing authentication methods and exploiting their vulnerabilities. Methods that target single parameters cannot screen for the variety of possible adulterations, rendering these methods functionally, though often not legally, obsolete. For each honey component of interest, a separate and specific classical analytical method must be applied, resulting in a time-consuming and waste-generating analysis for each sample under investigation. This limits sample processing capacity and comes with a number of analytical costs (Ruoff *et al.*, 2007). In addition, traditional chemistry methods such as GC and HPLC have fallen out of favour in recent years due to their laborious and destructive nature, as well as the undesirable generation of waste products.

The AOAC 998.12 stable carbon isotope ratio analysis (SCIRA) method is the most common approach currently used to detect sugar adulteration in honey (Anklam, 1998; Bogdanov and Martin, 2002). A form of mass spectrometry paired with GC, stable carbon isotope ratio analysis (SCIRA) makes use of the carbon isotope ratio ($^{13}C/^{12}C$) in a sample to determine whether the fixed atmospheric carbon contained in the sample's carbohydrates originates from a C_3 or C_4 photosynthetic pathway (White and Winters, 1989). This gives an indication of the plant's source of origin as honeybees typically collect nectar from C_3 sugar-producing plants, while cane- and corn-derived sugars, the raw materials of some common adulterants, are from C_4 plants. The $^{13}C/^{12}C$ ratio of the protein fraction of honey remains unchanged after syrup addition, and a comparison of the carbohydrate and protein fraction ratios will indicate deviations. Most pure honey should contain less than 7% C_4 sugars. There are several criticisms of the SCIRA method, as detection is limited to corn or sugar cane adulterations, meaning that C_3 adulterants, such as beet, coconut or rice sugar syrups cannot be detected (Ulberth, 2016). Additionally, the start-up and operational costs for these analyses are expensive and facilities are not widely available in the developing world.

Food profiling is a similar group of analysis methods in which the composition of the entire sample is captured as a unique pattern or fingerprint of the food sample (Esslinger *et al.*, 2014). Profiling with spectroscopy techniques does not identify all metabolites present in a sample, but when paired with

multivariate analysis it may provide an excellent comparative data tool for the classification or differentiation of samples. Influences of composition, geographical region, species of origin and processing conditions may be revealed through the building of appropriate classification models (Esslinger *et al.*, 2014). Spectroscopic methods such as Raman spectroscopy, nuclear magnetic resonance (NMR) spectroscopy, mid-infrared (MIR) spectroscopy and near-infrared (NIR) spectroscopy are popular choices for fingerprinting analyses as they allow for rapid, non-destructive data collection. They allow for non-targeted analysis, which can reveal sample covariation and correlation between classes of samples when paired with chemometric methods. The broad scope of food fingerprinting also allows multiple factors to be captured and compared within a single dataset acquired from a single analytical method, providing a clear advantage over targeted analysis approaches.

Raman, NMR, MIR and NIR spectroscopy are instrumental methods that have all been used in recent honey authenticity studies, to varying degrees of success. Classification models based on this combination of instrumental analytical methods and statistical data analysis have demonstrated high accuracy in differentiating between adulterated or unadulterated honey samples (Chen *et al.*, 2011; Bázár *et al.*, 2016; Guelpa *et al.*, 2017; Li *et al.*, 2017). A full comparison of recent spectroscopic honey adulteration studies may be found in **Table 2.5**.

Irradiation detection

Detection of irradiation is difficult and inexact by nature of the methods available (Coultate, 2009). None of the methods in existence are applicable to all foods. The URPs generated by irradiation are a small fraction compared to the total number of products generated by irradiation, and have only been observed at levels of up to 300 mg kg^{-1} for a 10 kGy dose (Coultate, 2009). URPs also vary between food products, as they are determined by the product's original composition. Many compounds generated by irradiation are not exclusive to irradiated products and may be found at similar levels in heat-treated products. Therefore, the absence of URPs are not a guarantee that a food product has not undergone irradiation, nor do they preclude a food product from having undergone irradiation (Coultate, 2009).

The microbial levels of a food product are a strong indicator of irradiation treatment, as the microbial counts will be low and there should be ample evidence of dead bacteria (Coultate, 2009). The ratio of dead to alive bacterial cells can be detected by direct epifluorescent filter technique (DEFT), as a strong suggestive indicator of irradiation (Coultate, 2009). The detection of DNA fragmentation that occurs as a result of irradiation induced covalent bond breaking.

In addition, the breaking of the covalent bonds in the DNA backbone results in fragmentation, the residues of which can be detected by microelectrophoresis techniques (Coultate, 2009). Yeasts, pollens and sloughed bee cells found in honey would yield these products when irradiated, but the cost and degree of specialization of this technique make this an unfavourable option. Other irradiation detection methods rely

on compositional requirements such as relatively high lipid content, presence of silica or hard biological matrices such as bone or shell (Coultate, 2009).

2.5 NEAR INFRARED SPECTROSCOPY

2.5.1 Working principles

NIR spectroscopy is a non-destructive analytical tool that has shown great potential for non-targeted analysis or fingerprinting of food samples. Near-infrared radiation falls in the 780-2500 nm (13 300 – 4000 cm^{-1}) range of the electromagnetic spectrum, which is composed of energy waves that can penetrate organic matter and excite the molecular bonds present (Abbas *et al.*, 2012; Bázár *et al.*, 2016).

NIR spectroscopy is essentially the measurement of vibrational transitions that occur when molecular bonds, which have an energy gap of a specific magnitude between their ground and fundamental state, are excited with radiation. Intra- and intermolecular bonds become excited and enter this fundamental state due to energy of equivalent magnitude being absorbed from incident radiation (Manley, 2014). Bonds containing hydrogen almost always absorb within the NIR region, making this type of analysis appropriate for organic samples. Bond vibrations of -CH, -NH, -OH and -SH, which are prevalent in organic molecules, are observed in the 800-2500 nm region (Roggo *et al.*, 2007), while more specifically the region of interest for NIR food applications is 1100 – 2500 nm (Norris, 2009). An NIR spectrum is an average spectrum based on the excitation of the whole sample, making it best-suited to the analysis of homogenous samples, such as honey.

Near-infrared region spectra typically contain broad absorption bands instead of sharp and resolved peaks seen originating from the MIR region of 2500-25 000 nm. This is due to the excitation of various overtone bands in the NIR region corresponding to the fundamental vibrations found in the MIR region, which creates a spectrum of crowded and severely overlapping peaks, in contrast to the distinct shifts produced in the MIR region (Cozzolino *et al.*, 2011; Abbas *et al.*, 2012; Manley, 2014).

Spectra of honey

A NIR spectrum of honey typically shows absorption bands relating to O-H deformation and stretching, caused by water molecules, and bands relating to C-H, C-C and C-O bond stretching due to the presence of sugars. Detailed descriptions of band assignments for NIR spectra of honey have been reported in the work of Thamasopinkul *et al.* (2017) and Latorre *et al.* (2013) (**Table 2.3**).

Table 2.3 Band assignments of NIR spectra of Mel de Galicia honey reported by Latorre *et al*., (2013) and of longan honey reported by Thamasopinkul *et al.* (2017)

Wavelength (nm)	Bond assignment	Band type	Reference
1202	C-H	-	Latorre *et al.*, (2013)
1460	H_2O	Stretching modes - combination	Thamasopinkul *et al.* (2017)
1480	O-H	First overtone	Latorre *et al.*, (2013)
1580	O-H	Stretching - first overtone	Latorre *et al.*, (2013)
1770	CH_3 and CH_2	Stretching - first overtone	Thamasopinkul *et al.* (2017)
1935	O-H	Stretching and deformation	Latorre *et al.*, (2013)
1940	H_2O	Stretching and deformation - combination	Thamasopinkul *et al.* (2017)
2100	O-H and C-O	O-H deformation and C-O stretching	Latorre *et al.*, (2013), Thamasopinkul *et al.* (2017)
2280	Sugar	C-H - combination	Thamasopinkul *et al.* (2017)
2321	C-H	-	Latorre *et al.*, (2013)
2330	Sugar	C-H - combination	Thamasopinkul *et al.* (2017)
2460	Starch and sugar	C-C and C-H stretching - combination	Thamasopinkul *et al.* (2017)

2.5.2 Instrumental considerations

The instrumentation and operational principles of NIR spectrophotometry have been reviewed extensively (Abbas *et al.*, 2012; Manley, 2014).

There are several methods of capturing NIR spectra, all of which are based on the transmission or reflection of radiation, or some combination or variation thereof. Transmittance mode is best suited to acquisition of transparent substances, while diffuse transmittance caters for samples that are not transparent and will cause more light scattering (Manley and Baeten, 2018). Diffuse reflectance is typically employed for spectral acquisition of solids that do not permit light transmittance, and due to the extent of light scattering it creates is not as successful as a mode. Transflectance mode, a combination of transmittance and reflectance, makes use of a metallic cover or plate placed behind the sample to diffusely reflect light back through the sample to the detector. It is suited to analysis of liquids of any kind.

Both transmission and reflectance modes may be used in NIRS analysis of honey. Transmittance spectra have been found to have better peak definition and resolution, when compared to reflectance spectra (Qiu *et al.*, 1999). In addition, the performance of transmittance calibration models is estimated to have a 30 to 70% improvement on reflectance spectroscopy when used in modified partial least squares (mPLS) models and evaluated with the standard error of cross-validation (SECV). An optical path length of 1 mm yielded transmission spectra with the least saturation and the lowest SECV between 1300 – 2500 nm, when compared to 2, 4, and 10 mm path length quartz cuvettes (Qiu *et al.*, 1999).

Parameters

A few considerations need to be taken into account for honey analysis with NIRS. NIR spectra are highly influenced by the temperature of the sample and attention to temperature control during capturing NIR spectra of honey was stressed by Downey (2003). High water content samples are particularly susceptible to the influence of temperature, as the energy-holding capacity of water is relatively high (Thamasopinkul *et al.*, 2017). Hydrogen bonds, a commonplace intermolecular bond in aqueous systems, exert weak forces on intramolecular bonds, affecting the resultant IR spectrum. Temperature variation creates a noticeable change in hydrogen bonding, and therefore will also influence the spectra.

A study by Thamasopinkul *et al.* (2017) attempted to address the lack of robust quantitative NIR calibrations for honey caused by inconsistencies in sample temperature during spectral acquisition. A PLSR model, created with standard normal variate (SNV) pre-processing, was proposed that was calibrated with sets of moisture and sugar content data at three temperature intervals from *longan* honey samples (n = 35) and adulterated *longan* honey samples (n = 75), to form a temperature compensating model. The resulting model performed well for predicting the moisture and reducing sugar contents, with R^2 = 0,95 and ratio of prediction deviation (RPD) = 3.8. The spectra of honey samples, even those with up to 25% sugar syrup adulteration, are expected by the authors of the study to follow a similar trend. While this study has a quantitative focus, unlike an authentication study, it demonstrated the effect of considering temperature in model building. Additionally, it was noted in this study that multiplicative scatter correction (MSC) was found to be useful when building PLSR models with datasets captured at different temperatures.

Limits of NIR detection

Knowledge of the limits of detection (LOD) of a NIR method are topical to this study, given the relatively low levels at which certain adulteration or irradiation marker compounds are thought to present in honey. The LOD of NIR calibrations are a field of study in its own right. A number of challenges arise when attempting to use NIR spectroscopy to detect adulterants at trace levels of 1 ppm or less. In order to prove that samples can be differentiated at a specific level or LOD such as 1 ppm or lower, it must be proven that noise likely to be encountered during spectral acquisition does not cause interference sufficient to allow false classifications (Norris, 2009). A number of studies have covered the detection limits of simple single-compound systems,

but research on complex food matrices is lacking. As such, there is much research that demonstrates the feasibility of low concentration determination in simple systems, but little for a variety of realistic food applications.

The LOD is essentially the point at which the spectral signal of an analyte becomes significantly different to the background signal of a blank sample. The LOD_{max} of an analyte in solution is highly dependent on the signal-to-noise ratio, which may be influenced by wavelength range, path length, intensity of incident light and co-adding scan times (Inagaki *et al.*, 2017). The LOD_{max} is also indirectly dependent on the molar absorptivity of the analyte and there is an inverse relationship between detector noise and the square root of the time taken for measurement capture. The sensitivity of a measurement is generally observed to increase linearly as the path length increases, following the Beer-Lambert Law.

In a 2017 study by Inagaki, in which a NIR spectrophotometer with a fibre optic attachment was used in the 6300 – 5800 cm^{-1} (1587 - 1724 nm) region, the lowest LOD for potassium hydrogen phthalate in aqueous solution was approximately 150 ppm when quantified with a partial least square (PLS) calibration. A path length of 5 mm gave the lowest LOD value and the optimal number of scans was 32, with higher numbers resulting in more noise. Increasing the intensity of light with a larger aperture was also found to result in lower instrumental variance and better LOD_{max} values between measurements.

The addition of an adulterant at the 1 ppm level will have no bearing on the scattering captured in the spectra but will contribute to a slight increase in the log(1/*R*) value, where *R* is the diffuse reflectance value (Norris, 2009). In order to detect this increase in absorbance, the instrumental noise level must be less than the magnitude of the increase, and furthermore, in order for it to be measurable the noise level must be one tenth smaller than the increase itself. The spectrophotometer must have great enough resolution to detect the adulterant, should it have a narrow bandwidth.

Sampling noise may further contribute to the difficulty of low level detection, as the sample temperature, environmental humidity, particle size, packing density between samples, as well as movement and distribution of the particles in the beam, which may vary in non-homogenized samples, will all affect the noise of spectrometric measurements (Norris, 2009).

It can then be concluded that irradiation would have to exact a chemical change well over the 150 ppm of Inagaki *et al.* (2017) in order for the differences to be detected by NIR spectroscopy, under the same experimental conditions. For adulterations, this is likely realistic, as dilutions will likely be in excess of 5% in order to be profitable. Undeclared irradiation presents an uncertainty. Even should the chemical change be in excess of this, if the changes caused by irradiation do not cause the chemical content to exceed the acceptable range of chemical variation within honey, then irradiation treatment will remain undetectable by NIR spectroscopy.

2.5.3 Multivariate data analysis

NIR spectroscopy is a secondary method as it requires a reference sample set, with known reference values or identities to correlate with the spectral data (Manley, 2014). In addition, the complex NIR spectra usually comprised of several hundred data points and therefore require appropriate data processing to extract meaningful information about the variables of interest (Abbas *et al.*, 2012; Manley, 2014). The advantage of combining NIR spectroscopy with chemometric techniques, to develop classification models, is that data pertaining to multiple variables can be collected and simultaneously quantified or classified within one rapid, inexpensive measurement, once a model has been developed (Ruoff *et al.*, 2007). Lastly, NIR spectroscopy offers a non-destructive analytical method alternative with a low cost per analysis.

Pre-processing of spectral data

Chemometric techniques include mathematical pre-processing and many categories of univariate and multivariate methods. Pre-processing treatments are used for selecting data of interest, reducing both the dataset size (wavelength selection, principal component analysis) and the effects of unwanted external variation (scatter correction, smoothing, normalization and detrending), and maximizing variation of interest (derivation). Pre-processing techniques have previously been described comprehensively by numerous other authors (Toher, 2007; Rinnan *et al.*, 2009; Oliveri and Simonetti, 2016; Callao and Ruisánchez, 2018; Manley and Baeten, 2018).

Qualitative methods of analysis

Multivariate chemometric techniques are complex pattern recognition methods used for analysis of datasets containing multiple variables. These techniques are generally more effective than univariate methods in food authenticity modelling as they enable the correlations between several measured parameters in a data set to be evaluated (Oliveri and Simonetti, 2016). The intricate nature of food matrices almost guarantees large and complex spectral datasets, necessitating a multi-variable approach.

Multivariate pattern recognition techniques may be either supervised or unsupervised. Unsupervised classification methods, primarily used for data exploration, base their classification solely on data within a set, not on prior knowledge of the samples (Roggo *et al.*, 2007). This is followed by explanation or categorization of the resulting clusters by the operator. The classical unsupervised approach is principal component analysis (PCA), which separates the variation within the dataset into statistically independent, or orthogonal, components (Oliveri and Simonetti, 2016). Principal components are ordered with respect to their contribution to the overall variation, each of which may represent the contribution of an experimental factor (e.g. temperature or species) to the dependent variable set. This allows for reduction of the number of variables within the dataset, and visualization of the data and its features (also referred to as *loadings*), around which clustering of variables may be observed (Roggo *et al.*, 2007; Oliveri and Simonetti, 2016). PCA exploration sets the foundation for complex supervised techniques.

Supervised recognition models can be predictive, with a qualitative or quantitative focus. Qualitative modelling is primarily aimed at classification of samples based on similarity or dissimilarity of their spectra and is reliant on prior categorization of samples within a training set. Qualitative data analysis is typically employed in authentication studies, which require authentic and non-authentic biological samples to be discriminated between (Oliveri and Downey, 2012). Quantitative modelling employs regression techniques to predict a specified parameter or component in unknown samples using values previously determined with accepted reference methods. In this review, the chemometric methods discussed and used will largely be limited to unsupervised data exploration and supervised qualitative modelling.

Qualitative modelling techniques that are popular for food applications include k-Nearest Neighbours (KNN) (Fix and Hodges, 1951), Linear Discriminant Analysis (LDA) (Fisher, 1936; Izenman, 2008), Partial Least Squares Discriminant Analysis (PLS-DA) (Ståhle and Wold, 1987), Soft Independent Modelling of Class Analogy (SIMCA) (Wold and Sjöström, 1977) and Support Vector Machines (SVM) (Izenman, 2013) (**Table 2.4**). While qualitative studies may result in a variety of classification outcomes a binary outcome is required for authenticity studies (Oliveri and Simonetti, 2016).

Within the field of supervised qualitative modelling, methods can be classified on whether they place emphasis on class-similarity or discrimination. Furthermore, methods may be linear or non-linear, as well as parametric or non-parametric, i.e. reliant on assumption of a normal distribution or not. Two major families of methods are class modelling and discriminant techniques. Class modelling, or one-class classification, investigates compliance with an in-or-out strategy: the authenticity of samples are confirmed if they fall within an acceptance region, which has a defined confidence level, for the specific class of interest (Oliveri and Downey, 2012; Rodionova *et al.*, 2016). Only samples that fall within the class under investigation contribute to this model and often additional models must be created if more than one class is to be considered. SIMCA as well as machine-learning based methods, SVM and artificial neural networks (ANN), fall within this category of techniques.

Discriminant, or multi-class classification, creates a decision rule for categorizing samples by defining a delimiter that separates two or more classes within the sample space. Every sample of every class contributes to the delimiter's decision rule. In discriminant models, it is of great importance to have classes that represent all the available variation, both within- and between-classes, as without it, the decision rule and model will be biased. Examples of discriminant methods include LDA, KNN and PLS-DA.

Oliveri and Downey (2012) argue that this is often impractical, as to define the entire sample space of a commodity is to catalogue all possible variation of that commodity, and in the case of an adulteration study, would require all possible adulterations be represented in the model's reference library. The authors recommended the use of class modelling rather than discriminant classification methods for food authenticity, their rationale being that the sources of variation present among out-of-specification samples is likely to be far greater than the variation present among in-specification samples. It is therefore easier to

define an acceptance region based only on in-specification samples, as including out-of-specification samples would require all possible, and often unpredictable, sources of variation to be accounted for and included within the classification model.

Honey is a non-linear food matrix composed of a variety of carbohydrates and other compounds that interact and interfere with other components (Zhu *et al.*, 2010). It has been suggested that as mutual interference exists between the components of honey, that the recognition and predictive abilities of calibration models could be improved if non-linear data analysis methods are used.

Validation

All classification models must be validated by an independent set of authentic samples to evaluate the effectiveness of the model before it can be used to classify unknown samples (Oliveri and Simonetti, 2016). To select a representative sample set that will remain independent of the model, a selection method or algorithm must be used.

The simplest validation methods rely on a single, once-off division of samples. Single set validation selection algorithms select the most representative calibration (often referred to as *training*), testing and validation data-subsets from the measured spectra, of which the most common is the Kennard-Stone (Kennard and Stone, 1969) and DUPLEX (Snee, 1977) algorithms. The Kennard-Stone or CADEX algorithm was designed to select a predetermined proportion of the most uniformly distributed, and therefore representative samples, across the sample set to be excluded from calibration and form the validation set. The DUPLEX algorithm aimed to improve upon the Kennard-Stone by additionally ensuring that the calibration and validation sets both have an equal distribution of the most extreme points within the data set (Snee, 1977).

Cross-validation (CV) is one of the most common validation strategies for evaluating the predictive ability of a model (Oliveri and Simonetti, 2016). All available samples are systematically assigned to a number of groups that are then each alternated as the validation set, while the remaining groups function as the training set. The prediction rate is calculated from the cumulative outcomes of all the resulting permutations. Today, cross-validation is commonly used during calibration to select the optimal number of factors for inclusion in the model.

Table 2.4 Selected classification technique descriptions

Model	Description	Original reference
KNN	A linear, non-parametric discriminant method, that creates classes of a predetermined size based on the lowest Euclidean distances between neighbouring samples (Oliveri and Simonetti, 2016). The creation of these classes forms a complex delimiter that determines further classifications.	Fix and Hodges (1951)
LDA	A linear, parametric, and probabilistic discriminant method that focuses on achieving maximum separation between classes, achieved by creating probability regions that are separated by a linear class delimiter (Oliveri and Simonetti, 2016).	Fisher, (1936)
PLS-DA	A parametric and linear discriminant method based on the Partial Least Squares Regression (PLSR) method that focuses on identifying latent variables that demonstrate maximum covariance with response variables (Oliveri and Simonetti, 2016). Unknown samples are trialled in classes and assigned a predicted class membership dummy value between 0 (non-member) and 1 (member), with a predetermined cut-off threshold drawing distinction between the member and non-member classes (Manley and Baeten, 2018).	Ståhle and Wold (1987)
SIMCA	A linear and parametric class modelling method based on PCA modelling. A one-class classification technique, it emphasizes similarity within classes. Each class is considered in isolation, with a PCA performed separately. Validation objects are trialled in each class and allocated to the class that has the lowest residual (Roggo *et al.,* 2007).	Wold and Sjöström (1977)

Statistical Evaluation

Once calibration and validation have been performed, it is vital to evaluate the usefulness of a model to determine whether a model fulfils its purpose and how well it does so. The accuracy and precision, as well as sensitivity, specificity and effectiveness of a model may be calculated and reported in statistical form.

Statistical estimators that are of use when evaluating NIRS-based models include reliability, sensitivity, specificity, efficiency, standard deviation (SD), the coefficient of variation (CV), coefficient of correlation (r),

coefficient of determination (R^2), standard error of a single test (SET), standard error of prediction (SEP), standard error of calibration (SEC), standard error of cross-validation (SECV) and ratio of prediction deviation (RPD), among others (**Table 3.8**). Excellent explanations of these estimators can be found in many publications, such as Williams (2007), Oliveri and Downey (2012), Westad *et al.* (2013) and Manley and Baeten (2018).

2.5.4 Prediction of honey authentication with NIR spectroscopy

In the context of an authentication study, the region of interest within a spectrum is any wavelength or wavelength range in which distinct changes may be observed that correlate with, and are often proportional to, the addition of adulterants. In a study by Rios-Corripio *et al*. (2012) in which attenuated total reflectance-Fourier transform infrared (ATR-FTIR) spectroscopy was used to detect corn and cane sugar syrup adulterated Mexican honey samples, the region of interest, being the wavelength range that included noticeable changes in adulterated samples, was determined to be between 650 and 4000 cm^{-1} (900 - 1140 nm), which falls within the NIR range of the IR spectrum.

The potential of NIR spectroscopy in determining the composition of honey has been demonstrated in a number of studies (Qiu *et al.*, 1999; Ruoff *et al.*, 2007). In a study on composition determination of honey with NIRS, major components including glucose, fructose and moisture could be accurately predicted (R^2 = 0.91 – 1.0) with PLSR (Qiu *et al.*, 1999). Adequate predictions (R^2 = 0.86 – 0.93) were also obtained for sucrose and maltose content. HMF, pH, free acidity and lactone acidity are parameters that have not been successfully quantified (R^2 < 0.66) with NIRS data models (Qiu *et al.*, 1999).

In another comprehensive study by Ruoff (2007), FT-NIR spectroscopy was used to quantify 24 different chemical components and parameters in 421 different honey samples with varying botanical origins. Standard classical analytical methods were employed to determine reference values for the calibration of the model. Glucose, fructose, total monosaccharide content, water content and sucrose could be accurately predicted (SEP = 1.3, 1.6, 2.6, 0.3, and 0.4 g/100 g, respectively). However, predictions of the HMF, proline, pH-value, electrical conductivity, free acidity and twelve minor sugar contents of the samples had poor accuracy. NIR spectroscopy does not allow for accurate estimations of these physical parameters as they are not dependent on the gross chemical composition and there is only weak correlation between absorption in spectral regions and the reference values (Ruoff *et al.*, 2007).

Classification models based on a combination of NIR spectral data and statistical analysis for differentiating between adulterated or unadulterated honey samples are given in **Table 2.5**, several of which demonstrated very good predictive ability. However, many of the available studies have treated honey as a generic and inalterable commodity, not explicitly considering the age of the honey, its total solids content, its thermal history and the temperature control of samples during storage and spectral acquisition within the methodology. As an example, in many studies all samples were incubated at 55°C, which is well above the

threshold of 40°C at which noticeable chemical changes begin to occur in honey (Bogdanov, 2009). Inconsistencies have also arisen when samples are not uniformly strained or filtered, meaning that greater presence of particulate matter in some may have contributed unevenly to the similarity or differences between samples.

Lastly, almost all studies were purely academic and did not contain adequate sample sizes, with some being limited to less than 100 (Gallego-Picó *et al.*, 2013). A representative reference library of the sample class containing a broad range of seasonal, geographical and botanical variation must be assembled before classification or quantification models can be built and used (Oliveri and Downey, 2012).

Kelly, Downey & Fouratier (2004) conducted one of the first studies on identifying honey samples that had been diluted with cheap sweeteners. D-glucose and D-fructose solutions in similar ratios to those found in honey, were used to dilute genuine honey samples (n = 25) at three concentration levels of 7, 14, and 21%, and then analysed with ATR equipped FT-IR spectroscopy. A satisfactorily large set of 320 samples and sub-samples was used, and samples were incubated overnight at a safe threshold of 40°C prior to spectral acquisition. PLSR was used to quantify the level of adulterant added and kNN applied for classification of the authentic and adulterated samples, both paired with a combination of normalization and Savitzky-Golay (SG) 1st and 2nd derivative pre-processing. Spectral differences at specific absorption bands relating to glucose and fructose allowed for overall accuracy of 92% for authentic vs. adulterated honey. Combining these two models, an 88.4% correct classification of the level of adulterant (SEP = 2.44 – 4.28; R^2 = 0.9513 – 0.8408) was achieved.

FT-IR has also shown some promising outcomes in authentication studies. In a study by Rios-Corripio *et al*. (2012), cane sugar syrup and corn syrup were used to adulterate Mexican honey samples (n = 17) at ratios of 1:10 to 9:10. This sample set is not considered optimal for development of a robust classification model; Gallego-Picó *et al.* (2013) recommends in excess of 200 samples. An FT-IR instrument with ATR accessory were used to capture spectra in the range of 650-4000 cm^{-1}. A PCA plot was constructed which showed clear discrimination between the three classes of authentic honey and honey adulterated with cane sugar or corn sugar syrup. A PLSR model, built with HPLC reference measurements, was used to predict glucose, fructose, sucrose and monosaccharide content of honey, with R^2 of 0.941 and above, however, SEP values for glucose, fructose, sucrose and monosaccharides varied considerably.

Li *et al.* (2017) used NIR spectroscopy to quantify and identify HFCS and maltose syrup added to honey. A sufficient set of 102 samples and 480 subsamples was used, including samples of different botanical origins. However, samples were incubated at 55°C, which is well above the recommended upper threshold of 40°C at which chemical changes begin to occur in honey (Bogdanov, 2009). Norris and 2nd derivative pre-processing was used, competitive adaptive reweighted sampling (CARS) was utilized for wavelength variable selection, followed by PLS compression and LDA (PLS-LDA) for classification and PLSR for the level of adulteration. Classification by PLS-LDA was successful, with classification accuracies of 86.3% and 96.1% for HFCS dilutions

and maltose syrup dilutions, respectively. Quantification of HFCS was not successful, but satisfactory quantification of maltose syrup was possible (R^2_{Pred} = 0.901, RMSEP = 4.041). In a previous study, Raman spectroscopy was used by Li *et al.* (2012) to conduct the same experiment. Raman outperformed NIR for authenticity classifications.

Toher (2007), Chen *et al.* (2011) and Ferreiro-González *et al.* (2018) performed similar work to Li on a number of different adulterants with relatively good accuracies.

In a study by Ferreiro-González *et al.* (2018), Vis-NIR spectroscopy was used with HCA, PCA, LDA and PLS multivariate techniques to develop a rapid screening method for quantification of HFCS adulteration in Granada PDO honey samples (n = 33) taken from one year of harvest (2016). The sample set size is not considered optimal for development of a robust classification model. A HFCS grade containing 81% dry solids and 8.5% fructose was used at addition levels of between 0 and 90%. A spectral range of 400 – 2500 nm was used. Exploratory methods HCA and PCA demonstrated separation of adulteration percentage levels but did not provide conclusive adulterant quantification. A 10-factor PLS model produced a robust model for quantifying HFCS adulteration percentage (RMSEP = 4.71). The repeatability and precision of the model was also evaluated over a three-day window and within the days themselves, demonstrating high repeatability (CV = 3.90%) and good intermediate precision (CV = 3.63%) coefficient of variation values.

A study on detecting the addition of sugars or cheaper honeys to authentic South African honey was conducted by Guelpa *et al.* (2017). The set of 84 samples and subsamples that was used is not considered optimal for development of a robust classification model. Samples were incubated at 55°C, above the temperature of 40°C recommended by the harmonized methods of the International Honey Commission (Bogdanov, 2009). One notable outcome of this study was the demonstration of the classification capabilities and accuracies of both a benchtop spectrophotometer, portable and handheld instruments. These two provided comparable classification accuracies when used with PLS-DA and SNV pre-treatments, despite the portable instrument only covering 908-1680 nm, in contrast to the full 1000-2500 nm range of the benchtop.

Zhu *et al.* (2010) compared the usefulness of several algorithms for classification of authentic versus adulterated honey and found that a least-squares SVM algorithm obtained better classification results than LDA or kNN and that the classification accuracy improved markedly with compression of the data before modelling.

Table 2.5 Applications of spectroscopic techniques in honey adulteration studies

Adulterant investigated	Technique	Wavelength range	Sample number	Sample preparation	Spectral data pre-processing	Multivariate model	Accuracy or Error	Source
CLASSIFICATION								
Corn syrup, HFCS, invert sugar	ATR-FTIR	2500 – 15385 nm	78	-	1st derivative SG smoothing	PLSR, SIMCA	100%	Gallardo-Velázquez *et al.*(2009)
Corn syrup, invert sugar syrup, cane sugar syrup	ATR-FTIR	2500 – 15385 nm	32	Incubation at 35°C, followed by adulteration at different % w/w, then adjustment to 70 °Brix and vigorous stirring	-	PCA, PLSR	SEC: 0.377-0.583% SEP:1.550-3.150%	Rios-Corripio *et al.* (2012)
Fructose, glucose solutions	FT-IR	2500 – 12500 nm	320	Incubation at 40°C	Normalization, 1st and 2nd derivatives	PLS-DA, kNN, PLSR	92.7% (adulterated) 90.9% (unadulterated)	Kelly *et al.* (2004)
Fructose and glucose syrup, inverted beet syrup, HFCS	NIR	400 – 2498 nm	157	Incubation at 40°C overnight, stirring, dilution to 70 °Brix	SG derivatives	DA, PLSR, EM and CEM algorithms	>95%	Toher (2007)
Fructose and glucose	NIR	1000 - 2500 nm	135	Incubation at 55°C overnight, stirring, dilution to 70 °Brix	SNV	LS-SVM, SVM, BP-ANN, LDA, KNN	95.1% (LS-SVM)	Zhu *et al.* (2010)
Fructose, glucose, imported honey	NIR	1000.0-1415.6 nm 908.1-1453.2 nm 861.8-2514.8 nm	84	Incubation at 55°C overnight, equilibration to room temp for 1 h, dilution to 70 °Brix	SNV, 1st and 2nd derivative, mean centring (MC)	PLS-DA	96.9% 93.7% 87.5%	Guelpa *et al.* (2017)
HFCS	FT-NIR	1000 – 2500 nm	144	Storage at room temperature before analysis	Smoothing, MC, multiplicative scattering correction (MSC), first and second derivative.	PLS-DA	97.9% (adulterated) 95.8% (unadulterated)	Chen *et al.* (2011)

HFCS and maltose syrup (MS)		1000 – 2500 nm	205	Incubation at 55°C, stirring, dilution to 65 °Brix	Norris and 2nd derivative, CARS	PLS-LDA	86.3% (HFCS) and 96.1% (MS)	Li *et al.* (2017)
Inverted beet syrup and inverted cane syrup	FT-Raman	6250 - 50000 nm	47	Dilution with syrups followed by stirring, storage at room temperature	Area normalization	LDA, PCA-CVA, PLS-CVA	96%	Paradkar and Irudayaraj (2001)
HFCS and maltose syrup	Raman	3846 - 57143 nm	74	Incubation at 55°C, stirring, dilution to 65 °Brix	airPLS	PLS-LDA	91.1% (HFCS), 97.8% (MS) and 75.6% (in combination)	Li *et al.* (2012)
QUANTIFICATION								
Inverted cane sugar	ATR-FTIR	6667 - 12500 nm	53	Incubation at 50°C for 10 min, stirring, equilibration to room temp	PLS compression	PLS, LDA, CVA	88 – 96.4%	Sivakesava and Irudayaraj (2001a)
Fructose, glucose, sucrose, inverted beet syrup, cane sugar syrup	ATR-FTIR	2500 – 25000 nm	51	Incubation at 50°C until dissolved, stirring, equilibration to room temp	MC, 1st derivative, variance scale	PLS, PCR	-	Sivakesava and Irudayaraj (2001b)
Corn syrup, invert sugar syrup, cane sugar syrup	ATR-FTIR	2500 – 15385 nm	32	Incubation at 35°C, followed by adulteration at different % w/w, then adjustment to 70 °Brix and vigorous stirring	-	PLSR	SEC: 0.377-0.583% SEP:1.550-3.150%	Rios-Corripio *et al.* (2012)
HFCS	NIR	1300 – 1800 nm	40	Dilution with HFCS followed by stirring, storage at room temperature for 24h	Moving average (MA) smoothing, SNV, gap segment method.	PLSR, PCR	RMSECV = 1.48%	Bázár *et al.* (2016)
HFCS and maltose syrup (MS)	FT-NIR	1000 – 2500 nm	180 and 60	Incubation at 55°C, stirring, dilution to 65 °Brix	Norris and 1st derivative	PLSR	R^2_{CV} = 0.018-0.078% (HFCS), RMSECV = 11.951-12.340% (HFCS)	Li *et al.* (2017)

							R^2_{Pred} = 0.901-0.981% (MS), RMSEP = 1.789-4.041% (MS)	
HFCS	Vis-NIR	400 – 2500 nm	33	Room temperature storage in darkness. Adulteration with HFCS, followed by incubation at 30°C for 24 h and manual stirring.	MA smoothing	PCA, HCA, LDA, PLS.	RMSEC = 3.05% RMSEP = 4.71%	Ferreiro-Gonzalez *et al*. (2018).
Inverted beet syrup and inverted cane syrup	FT-Raman	6250 - 50000 nm	47	Dilution with syrups followed by stirring, storage at room temperature	1st derivative	PLS, PCR	SEP = 1.574-2.151% (beet syrup), SEP = 2.059-2.195% (cane invert syrup)	Paradkar and Irudayaraj (2001)

An investigation into detection of honey diluted with jaggery (unrefined cane sugar) syrup, by Kumaravelu and Gopal (2015), used PLSR to quantify the dilution of a set of honey subsamples (n = 16) created by dilution of four unique honey types at three levels. Baseline correction, SNV and Savitzky-Golay smoothing pre-treatments were done, followed by a PLS regression. SEC of the model was 0.00751 and R^2 = 0.9924. With four honey varieties used, the variation in initial honey samples is unlikely to cover a significant proportion of all honey produced and is not sufficient for development of a robust classification model. Sixteen sub-samples, with ten scans of each were included in the model, which are insufficient for an accurate and reliable calibration and resulted in pseudo-replication, respectively. No cross-validation was performed.

Mouazen and Al-Walaan (2014) used vis-NIR spectroscopy to quantify the level of glucose syrup added to imported and local Saudi honey samples (n = 69) used to create a total of 345 adulterated sub-samples at five levels of adulteration. Spectra were pre-treated with averaging, baseline correction, Savitzky-Golay first derivative with second order polynomial and Savitzky-Golay smoothing. PLSR, with leave-one-out cross-validation, obtained 'good' model predictions, with RMSEP = 5.56 g/100 g, RPD = 2.54, and R^2 = 0.78 for the prediction set (30%). In both PCA and PLSR models, lower concentration adulterations of 5% (w/w) were difficult to distinguish from authentic samples, but 12, 19 and 33% (w/w) adulterations could be perfectly separated from authentic samples.

When studying their honey spectra, Mouazen and Al-Walaan (2014), noted that the expected protein reflectance peak at 2180 nm was not detected. It was also noted that clear differences in spectra of authentic honey when compared to adulterations at 5, 12, 19 and 33% (w/w) could be seen in the pre-processed spectra. This is due to syrup lightening the colour of the mixed samples, therefore increasing their reflectance in the visible range. Care was taken in this study to include samples from colonies that had been fed sugar as well as those that had not been fed. Commercial local and imported samples were also used. However, there was no mention of standardization of filter size or Brix content for the samples.

In a novel study by Bázár *et al.* (2016), water spectral patterns studied in aquaphotomics were found to be affected by HFCS adulterations in honey. Aquaphotomics is a field of NIRS based on aqueous hydrogen bonding throughout the sample matrix being reflected in the NIR absorbance at key wavelengths and absorption bands (Tsenkova, 2009). These differences in absorbances have been found to be useful as an indication for the state of the entire sample's chemical composition. Water spectral patterns of 19 Hungarian *Robinia* honeys were found to be affected by HFCS adulterations of 0 to 40% (w/w). Making use of the spectral range of 1300 - 1800 nm yielded the best model accuracy with lowest error of cross-validation (RMSECV = 1.48%). The findings, in the form of aquagrams, showed that the honey samples contained highly organised water molecules, such as trimers, in greater quantities than the HFCS adulterated samples. This suggests that when compared to the more complex matrix of authentic honey, HFCS may contain more unstructured water molecules that partake in less H-bonding. The authors concluded that HFCS adulteration may introduce this less structured mode of bonding to honey mixtures, which may be rapidly described by

aquaphotomic techniques. However, the limitations of aquaphotomics mean that while aquagrams may give a visual indication of non-compliance and may be useful for screening purposes, they are unlikely to yield unequivocal authenticity classifications.

2.6 CONCLUSIONS

Honey is a complex food matrix and an easy target for food adulteration. A number of honey authenticity studies based on instrumental techniques were found demonstrating high accuracy. However, unaddressed sample standardization issues were found in some, including a lack of standardization of TSS content and a lack of consistent filtration or ultrafiltration between classes; incubation at above 40°C, at which point chemical change begins to occur rapidly in honey; use of syrup grades which contained different glucose: fructose ratios than that of honey to simulate adulteration; and irradiation, which is known to cause chemical changes to sugars in solution and may affect the NIR spectral data of honey. Differences between the authentic and syrup-diluted honeys in these studies, which have driven their separation during discriminant analysis, may have been caused by physicochemical differences in the honey as a result of non-standardized sample pre-treatment, not necessarily as a result of each sample's unique chemistry. Upon concluding this study, it is clear that existing literature has some limitations:

- Scientific literature on the relationship between irradiation and honey composition is limited, has never been studied with a sufficient sample size and has never been examined with NIR spectroscopy.
- Parameters that are thought to affect the composition and spectra of honey have not always been considered in authenticity studies, including the natural chemical progression that honey undergoes while ageing and accounting for the filtration, irradiation and thermal history of samples.

This calls into question whether NIR classification of honey is, at best, suited to screening and not for unequivocal predictions of authenticity. Further investigation into and controlling for each of these processing factors may be necessary to investigate the confounding effect of these treatments on dilution detection. Ultimately, to create more realistic – and potentially more informative – authentication tools, classification models should be built upon sample reference libraries of all possible sample treatment combinations in order to broaden their application.

2.7 REFERENCES

Abbas, O., Dardenne, P. & Baeten, V. (2012). Near-Infrared, Mid-Infrared, and Raman Spectroscopy. In: *Chemical Analysis of Food: Techniques and Applications* (edited by Y. Picó). Pp. 59–89. Oxford: Elsevier.

Abdel-Aal, E.S.M., Ziena, H.M. & Youssef, M.M. (1993). Adulteration of honey with high-fructose corn syrup: Detection by different methods. *Food Chemistry*, **48**, 209–212.

Allsopp, M. & Cherry, M. (2004). *An assessment of the impact on the Bee and Agricultural industries in the Western Cape of the clearing of certain Eucalyptus species using questionnaire survey data*. Stellenbosch.

Anklam, E. (1998). A review of the analytical methods to determine the geographical and botanical origin of honey. *Food Chemistry*, **63**, 549–562.

APIMONDIA Working Group. (2019). *APIMONDIA STATEMENT ON HONEY FRAUD*. Rome.

Bakier, S. (2009). Capabilities of near-infrared spectroscopy to analyse changes in water bonding during honey crystallisation process. *International Journal of Food Science & Technology*, **44**, 519–524.

Bázár, G., Romvári, R., Szabó, A., Somogyi, T., Éles, V. & Tsenkova, R. (2016). NIR detection of honey adulteration reveals differences in water spectral pattern. *Food Chemistry*, **194**, 873–880.

Bera, A., Almeida-Muradian, L.B. & Sabato, S.F. (2009). Effect of gamma radiation on honey quality control. *Radiation Physics and Chemistry*, **78**, 583–584.

Bhandari, B., D 'arcy, B. & Kelly, C. (1999). Rheology and Crystallization Kinetics of Honey: Present Status. *International Journal of Food Properties*, **2**, 217–226.

Bogdanov, S. (2002). *Harmonised Methods of the International Honey Commission*. Bern, Switzerland.

Bogdanov, S. (2009). *Harmonised Methods of the International Honey Commission*. *International Honey Commission*. Bern.

Bogdanov, S., Lüllmann, C., Martin, P., Ohe, W. von der, Russmann, H., Vorwohl, G., Oddo, L.P., Sabatini, A.-G., Marcazzan, G.L., Piro, R., Flamini, C., Morlot, M., Lhéritier, J., Borneck, R., Marioleas, P., Tsigouri, A., Kerkvliet, J., Ortiz, A., Ivanov, T., D'Arcy, B., Mossel, B. & Vit, P. (1999). Honey quality and international regulatory standards: review by the International Honey Commission. *Bee World*, **80**, 61–69.

Bogdanov, S. & Martin, P. (2002). Honey authenticity: a review. *Mitt. Lebensm. Hyg*, 1–20.

Callao, M.P. & Ruisánchez, I. (2018). An overview of multivariate qualitative methods for food fraud detection. *Food Control*, **86**, 283–293.

Chen, L., Xue, X., Ye, Z., Zhou, J., Chen, F. & Zhao, J. (2011). Determination of Chinese honey adulterated with high fructose corn syrup by near infrared spectroscopy. *Food Chemistry*, **128**, 1110–1114.

Codex Alimentarius. (1981). Standard for Honey.

Coultate, T.P. (2009). Preservatives. In: *Food: The Chemistry of its Components*. Pp. 359–380. Royal Society of Chemistry.

Cozzolino, D., Corbella, E. & Smyth, H.E. (2011). Quality control of honey using infrared spectroscopy: A review. *Applied Spectroscopy Reviews*, **46**, 523–538.

Danezis, G.P., Tsagkaris, A.S., Camin, F., Brusic, V. & Georgiou, C.A. (2016). Food authentication: Techniques, trends & emerging approaches. *TrAC - Trends in Analytical Chemistry*, **85**, 123–132.

Department of Agriculture. (2000). *Regulations Relating to the Grading, Packing and Marking of Honey and Mixtures of Bee Products Intended for Sale in The Republic of South Africa*. Pretoria: Department of Agriculture.

Doner, L.W. (1977). The sugars of honey—A review. *Journal of the Science of Food and Agriculture*, **28**, 443–456.

Esslinger, S., Riedl, J. & Fauhl-Hassek, C. (2014). Potential and limitations of non-targeted fingerprinting for authentication of food in official control. *Food Research International*, **60**, 189–204.

Eyer, M., Neumann, P. & Dietemann, V. (2016). A Look into the Cell: Honey Storage in Honey Bees, Apis mellifera. *PLoS ONE*, **11**, 1–20.

Fan, X. (2005). Formation of furan from carbohydrates and ascorbic acid following exposure to ionizing radiation and thermal processing. *Journal of Agricultural and Food Chemistry*, **53**, 7826–7831.

Fan, X. (2013). Radiation Chemistry of Food Components. In: *Food Irradiation Research and Technology* (edited by X. Fan & C.H. Sommers). Pp. 75–97. Blackwell Publishing.

FAOSTAT. (2017). Food and agriculture data.

Ferreiro-González, M., Espada-Bellido, E., Guillén-Cueto, L., Palma, M., Barroso, C.G. & Barbero, G.F. (2018). Rapid quantification of honey adulteration by visible-near infrared spectroscopy combined with chemometrics. *Talanta*, **188**, 288–292.

Fisher, R.A. (1936). The use of multiple measurements in taxonomic problems. *Annals of Eugenics*, **7**, 179–188.

Fix, E. & Hodges, J.L. (1951). *analysis, nonparametric discrimination: Consistency properties*. Randolph Field, Texas: USAF School of Aviation Medicine.

Gallardo-Velázquez, T., Osorio-Revilla, G., Loa, M.Z. de & Rivera-Espinoza, Y. (2009). Application of FTIR-HATR spectroscopy and multivariate analysis to the quantification of adulterants in Mexican honeys. *Food Research International*, **42**, 313–318.

Gallego-Picó, A., Garcinuño-Martínez, R.M. & Fernández-Hernando, P. (2013). Honey Authenticity and Traceability. *Comprehensive Analytical Chemistry: Food Protected Designation of Origin: Methodologies and Applications*, **60**, 511–541.

Garciá-Alvarez, M., Ceresuela, S., Huidobro, J.F., Hermida, M. & Rodríguez-Otero, J.L. (2002). Determination of polarimetric parameters of honey by near-infrared transflectance spectroscopy. *Journal of Agricultural and Food Chemistry*, **50**, 419–425.

Graham, J.M. (1993). *The Hive and the Honeybee*. 19th edn. Hamilton, Illinois: Dadant & Sons, Inc.

Guelpa, A., Marini, F., Plessis, A. du, Slabbert, R. & Manley, M. (2017). Verification of authenticity and fraud detection in South African honey using NIR spectroscopy. *Food Control*, **73**, 1388–1396.

Herrero Latorre, C., Peña Crecente, R.M., García Martín, S. & Barciela García, J. (2013). A fast chemometric procedure based on NIR data for authentication of honey with protected geographical indication. *Food Chemistry*, **141**, 3559–3565.

Hutton-Squire, J.P. (2014). *Historical relationship of the honeybee (Apis mellifera) and its forage; and the current state of beekeeping within South Africa*.

Inagaki, T., Watanabe, T. & Tsuchikawa, S. (2017). The effect of path length, light intensity and co-Added time on the detection limit associated with NIR spectroscopy of potassium hydrogen phthalate in aqueous solution. *PLoS ONE*, **12**, 1–14.

Izenman, A.J. (2008). Linear Discriminant Analysis. In: *Modern Multivariate Statistical Techniques*. Pp. 237–280. New York: Springer-Verlag .

Izenman, A.J. (2013). Support Vector Machines. In: *Modern Multivariate Statistical Techniques*. Pp. 369–406. New York: Springer-Verlag.

Kelly, J.F.D., Downey, G. & Fouratier, V. (2004). Initial Study of Honey Adulteration by Sugar Solutions Using Midinfrared (MIR) Spectroscopy and Chemometrics. *Journal of Agricultural and Food Chemistry*, **52**, 33–39.

Kumaravelu, C. & Gopal, A. (2015). Detection and quantification of adulteration in honey through near-infrared spectroscopy. *International Journal of Food Properties*, **18**, 1930–1935.

Li, S., Shan, Y., Zhu, X., Zhang, X. & Ling, G. (2012). Detection of honey adulteration by high fructose corn syrup and maltose syrup using Raman spectroscopy. *Journal of Food Composition and Analysis*, **28**, 69–74.

Li, S., Zhang, X., Shan, Y., Su, D., Ma, Q., Wen, R. & Li, J. (2017). Qualitative and quantitative detection of honey adulterated with high-fructose corn syrup and maltose syrup by using near-infrared spectroscopy. *Food Chemistry*, **218**, 231–236.

Manley, M. (2014). Near-infrared spectroscopy and hyperspectral imaging: non-destructive analysis of biological materials. *Chemical Society Reviews*, **43**, 8200–8214.

Manley, M. & Baeten, V. (2018). Spectroscopic Technique: Near Infrared (NIR) Spectroscopy. In: *Modern Techniques for Food Authentication* (edited by D.W. Sun). Pp. 51–102. London: Elsevier Inc.

Masehela, T.S. (2017). *An assessment of different beekeeping practices in South Africa based on their needs (bee forage use), services (pollination services) and threats (hive theft and vandalism)*.

Maurizio, A. (1976). How Bees Make Honey. In: *Honey: A Comprehensive Survey* (edited by E. Crane). Pp. 77–105. London: William Heinemann Ltd.

Melin, A., Rouget, M., Midgley, J.J. & Donaldson, J.S. (2014). Pollination ecosystem services in South African agricultural systems. *South African Journal of Science*, **110**, 1–9.

Migdal, W., Owczarczyk, H.B., Kędzia, B., Holderna-Kędzia, E. & Madajczyk, D. (2000). Microbiological decontamination of natural honey by irradiation. *Radiation Physics and Chemistry*, **57**, 285–288.

Missler, J., Wiezorek, T. & Beckh, G. (2016). Mannose: a marker for adulteration with syrup or resin treatment of blossom honey. In: *Proceedings of the XIII International Conference on the Applications of Magnetic Resonance in Food Science*. Pp. 17–20. Karlsruhe: IM Publications.

Moreira, R.F.A., Maria, C.A.B. De, Pietroluongo, M. & Trugo, L.C. (2010). Chemical changes in the volatile fractions of Brazilian honeys during storage under tropical conditions. *Food Chemistry*, **121**, 697–704.

Mouazen, A.M. & Al-Walaan, N. (2014). Glucose adulteration in Saudi honey with visible and near infrared spectroscopy. *International Journal of Food Properties*, **17**, 2263–2274.

Norris, K. (2009). Hazards with near infrared spectroscopy in detecting contamination. *Journal of Near Infrared Spectroscopy*, **17**, 165–166.

Oliveri, P. & Downey, G. (2012). Multivariate class modeling for the verification of food-authenticity claims. *Trends in analytical chemistry*, **35**, 74–86.

Oliveri, P. & Simonetti, R. (2016). Chemometrics for Food Authenticity Applications. In: *Advances in Food Authenticity Testing* (edited by G. Downey). Pp. 701–728. London: Elsevier.

Padovan, G.J., Jong, D. De, Rodrigues, L.P. & Marchini, J.S. (2003). Detection of adulteration of commercial honey samples by the13C/12C isotopic ratio. *Food Chemistry*, **82**, 633–636.

Paradkar, M.M. & Irudayaraj, J. (2001). Discrimination and classification of beet and cane inverts in honey by FT-Raman spectroscopy. *Food Chemistry*, **2001**, 231–239.

Primrose, S., Woolfe, M. & Rollinson, S. (2010). Food forensics: Methods for determining the authenticity of foodstuffs. *Trends in Food Science and Technology*, **21**, 582–590.

Qiu, P.Y., Ding, H.B., Tang, Y.K. & Xu, R.J. (1999). Determination of chemical composition of commercial honey by near-infrared spectroscopy. *Journal of Agricultural and Food Chemistry*, **47**, 2760–2765.

Rinnan, Å., Berg, F. van den & Engelsen, S.B. (2009). Review of the most common pre-processing techniques for near-infrared spectra. *Trends in Analytical Chemistry*, **28**, 1201–1222.

Rios-Corripio, M.A., Rojas-López, M. & Delgado-Macuil, R. (2012). Analysis of adulteration in honey with standard

sugar solutions and syrups using attenuated total reflectance-Fourier transform infrared spectroscopy and multivariate methods. *CYTA - Journal of Food*, **10**, 119–122.

Rodionova, O.Y., Oliveri, P. & Pomerantsev, A.L. (2016). Rigorous and compliant approaches to one-class classification. *Chemometrics and Intelligent Laboratory Systems*, **159**, 89–96.

Roggo, Y., Chalus, P., Maurer, L., Lema-martinez, C., Edmond, A. & Jent, N. (2007). A review of near infrared spectroscopy and chemometrics in pharmaceutical technologies. *Journal of Pharmaceutical and Biomedical Analysis*, **44**, 683–700.

Ruoff, K., Luginbühl, W., Bogdanov, S., Bosset, J.O., Estermann, B., Ziolko, T., Kheradmandan, S. & Amadò, R. (2007). Quantitative determination of physical and chemical measurands in honey by near-infrared spectrometry. *European Food Research and Technology*, **225**, 415–423.

Sendin, K., Williams, P.J. & Manley, M. (2018). Near infrared hyperspectral imaging in quality and safety evaluation of cereals. *Critical Reviews in Food Science and Nutrition*, **58**, 575–590.

Shabolyo, N. (2015). South Africa Grants Zambia Permit to Export Pure Honey [Internet document] . *Zambian High Commission in South Africa*URL http://www.zambiapretoria.net/south-africa-grants-zambia-permit-to-export-pure-honey/. Accessed 20/02/2019.

Siddiqui, A.J., Musharraf, S.G., Choudhary, M.I. & Rahman, A. ur. (2017). Application of analytical methods in authentication and adulteration of honey. *Food Chemistry*, **217**, 687–698.

Silva, P.M. Da, Gauche, C., Gonzaga, L.V., Costa, A.C.O. & Fett, R. (2016). Honey: Chemical composition, stability and authenticity. *Food Chemistry*, **196**, 309–323.

Sivakesava, S. & Irudayaraj, J. (2001a). Prediction of Inverted Cane Sugar Adulteration of Honey by Fourier Transform Infrared Spectroscopy. *Journal of Food Science*, **66**, 972–978.

Sivakesava, S. & Irudayaraj, J. (2001b). A rapid spectroscopic technique for determining honey adulteration with corn syrup. *Journal of Food Science*, **66**, 787–792.

Snee, R.D. (1977). Validation of regression models: methods and examples. *Technometrics*, **19**, 415–428.

Ståhle, L. & Wold, S. (1987). Partial least squares analysis with cross-validation for the two-class problem: A Monte Carlo study. *Journal of Chemometrics*, **1**, 185–196.

Subramanian, R., Hebbar, H.U. & Rastogi, N.K. (2007). Processing of honey: A review. *International Journal of Food Properties*, **10**, 127–143.

Thamasopinkul, C., Ritthiruangdej, P., Kasemsumran, S., Suwonsichon, T., Haruthaithanasan, V. & Ozaki, Y. (2017). Temperature compensation for determination of moisture and reducing sugar of longan honey by near infrared spectroscopy. *Journal of Near Infrared Spectroscopy*, **25**, 36–44.

The United States Pharmacopeial Convention. (2014). Food Chemicals Codex (9th Edition) [Internet document] . *The United States Pharmacopeial Convention*URL https://app.knovel.com/hotlink/toc/id:kpFCCE0021/food-chemicals-codex/food-chemicals-codex. Accessed 24/10/2018.

Toher, D. (2007). *A comparison of model-based and regression classification techniques applied to near infrared spectroscopic data in food authentication studies*.

Tosun, M. (2014). Detection of adulteration in honey samples added various sugar syrups with 13C/12C isotope ratio analysis method. *Food Chemistry*, **165**, 555–559.

Tsenkova, R. (2009). Aquaphotomics: Dynamic spectroscopy of aqueous and biological systems describes peculiarities

of water. *Journal of Near Infrared Spectroscopy*, **17**, 303–314.

Ulberth, F. (2016). Advances in Testing for Adulteration in Honey. In: *Advances in Food Authenticity Testing* (edited by G. Downey). Pp. 729–753. London: Elsevier.

Westad, F., Bevilacqua, M. & Marini, F. (2013). Regression. In: *Data Handling in Science and Technology*. Pp. 372–410.

White, J.W. (1976). Composition of Honey. In: *Honey: A Comprehensive Survey* (edited by E. Crane). Pp. 157–206. London: William Heinemann Ltd.

White, J.W. & Winters, K. (1989). Honey protein as internal standard for stable carbon isotope ratio detection of adulteration of honey. *Journal of the Association of Official Analytical Chemists*, **72**, 907–11.

Williams, P. (2007). Near-infrared Technology - Getting the Best Out of Light.

Wold, S. & Sjöström, M. (1977). SIMCA: A Method for Analyzing Chemical Data in Terms of Similarity and Analogy. In: *Chemometrics: Theory and Application*. Pp. 243–282. Washington DC: American Chemical Society.

Wu, L., Du, B., Heyden, Y. Vander, Chen, L., Zhao, L., Wang, M. & Xue, X. (2017). Recent advancements in detecting sugar-based adulterants in honey – A challenge. *TrAC - Trends in Analytical Chemistry*, **86**, 25–38.

Zhu, X., Li, S., Shan, Y., Zhang, Z., Li, G., Su, D. & Liu, F. (2010). Detection of adulterants such as sweeteners materials in honey using near-infrared spectroscopy and chemometrics. *Journal of Food Engineering*, **101**, 92–97.

Chapter 3 Materials and Methods

3.1. RATIONALE OF EXPERIMENTAL DESIGN

To address issues of sample standardization found in previous NIR-based honey authentication studies and avoid misclassification of samples, all irrelevant sources of variation were minimized. To minimize the risk of interference due to sample age, honey samples were obtained from the narrowest possible time window and were stored under identical conditions prior to NIR spectral analysis to prevent changes that could not be accounted for. Care was taken to select diluents that would realistically be used by adulterators and that closely resemble the sugar profile of honey, therefore posing a challenge to detect.

This included standardizing as far as possible the straining or filtration of honey, as well as liquefying samples and adjusting their TSS content prior to scanning. The state or level of processing of a honey sample has been shown to affect its NIR spectrum. Woodcock *et al.* (2007) observed that the NIR spectra of unfiltered honey samples had higher absorbance values overall, than the spectra of filtered honey samples, although the authors did remark these differences could not be solely attributed to the filtration method due to suspected instrumental drift. Bakier (2009) found that the NIR absorption peak area between 1876 - 2014 nm showed a strong correlation to changes in water activity induced by crystallization. Adjustment to 70°Brix has been justified in previous studies as a method of preventing spectral complications due to inherent variation in sugar composition of honey (Downey *et al.*, 2003; Kelly *et al.*, 2006; Toher, 2007). The TSS may be affected by many factors besides sugar addition or botanical origin, such as honey ripeness at harvest or the postharvest storage conditions. It is therefore not considered a reliable indicator to use as a proxy for authenticity or origin, and may lead to misclassification if not standardised (Ulberth, 2016).

3.1.1. Storage Trial

The **Storage Trial** was designed to address the first and second objectives of the study, to 'monitor the spectral changes of honey samples, held at three storage temperatures, over a period of 9 months', as well as 'compare spectral changes in honey samples before and after irradiation'. The 4°C, 25°C and 40°C sample subsets were created to compare spectral changes in honey samples stored at different temperatures, ranging from ideal to well beyond recommended (**Table 3.1**). A 25°C irradiated sample subset was created to compare spectral changes with the 25°C sample subset before and after irradiation over a period of 9 months.

Table 3.1 Storage Trial sample treatments and rationale

Storage	Treatment	Rationale
Controlled	4°C	Treatment to simulate ideal storage temperature at which minimal chemical changes will occur over the storage period
	25°C	Treatment to simulate ideal warehouse storage temperatures
	40°C	Treatment to simulate excessive warehouse storage temperatures
Uncontrolled	Ambient light and temperature ~23°C	Treatment to simulate typical retail storage

3.1.2. Dilution trial

The **Dilution Trial** was designed to complete the second objective of the study, to 'compare spectral changes in honey samples before and after dilution with other sugar syrups.

Two commonly used industrial, bulk sweetener syrups were chosen for use as diluents based on their compositional similarity to honey, HFCS and ICSS. HFCS is an industrial sweetener used in North America and Asia and has been implicated in a number of honey adulteration cases between 1995 and 2012 in the Food Ingredients Fraud Database (The United States Pharmacopeial Convention, 2014). Corn-derived syrups were implicated in the majority of cases in this database. HFCS is an ideal addition, due to its low cost and the compositional similarity of certain corn syrup grades to honey, with some researchers suggesting it may be undetectable at up to 50% in honey when relying on conventional sugar profile determinations, such as AOAC method 977.20 (Ulberth, 2016). HFCS was chosen for inclusion in the trial as an adulterant of international importance and the most likely diluent to be found in imported honey.

ICSS is the most commonly used industrial sweetener in South African food manufacturing. There is no widescale production of corn syrup in South Africa, and the niche it occupies in international food manufacturing is filled by cane-derived syrups in the local market. ICSS was chosen for inclusion in the trial as an adulterant of local importance as it is a diluent possibly found in locally produced honey.

The percentage dilution levels, of 10 and 20%, were chosen based on what were reasoned to be the lowest levels at which lucrative substitution would take place. If detection at these low levels is proved feasible by this screening method, the possibility of detection at higher levels may be assumed.

The 10 and 20% ICSS and 10 and 20% HFCS sample subsets (also referred to by the sample codes IS10, IS20, HF10 and HF20, respectively), stored at 25°C, were created to compare spectral changes in honey

samples before and after dilution. Additionally, the irradiated 10 and 20% ICSS and 10 and 20% HFCS sample subsets, also stored at 25°C, were created to compare spectral changes in honey samples before and after dilution, as well as before and after irradiation.

3.2. SAMPLE ACQUISITION AND PROCESSING

3.2.1. Sample description

Seventeen *Apis mellifera* blossom honeys with distinct botanical origin were collected from trusted beekeepers and honey packers operating in South Africa's Western Cape (n = 10), Kwa-Zulu Natal (n = 2), Mpumalanga (n = 2), Free State (n = 1), North West (n = 1) and Northern Cape (n = 1) provinces. All honey samples were produced by colonies that foraged on blossom nectar, and both *Apis mellifera capensis* (n = 10) and *scutellata* (n = 7) produced honeys were included in the sample set. The bias towards Western Cape honey is partly due to geographical proximity, as well as due to the larger variety of agricultural crops and significant forage sources found within the Western Cape (Masehela, 2017).

In order to maximize variation within the classification model, as much distinct botanical variety as possible was included in the sample set. Honey samples presumed to come predominantly from either indigenous species, exotic species or agricultural crops were collected. The details of each sample in the set are described in **Table 3.3**. Honey samples were obtained from the narrowest possible time window and were stored under identical conditions prior to NIR spectral analysis to prevent changes that could not be accounted for. Samples were required to be < 9 months old (i.e. produced in 2018) at the start of the trial to fit the arbitrarily predefined requirement of 'fresh' honey. All samples were unfiltered, though could have been strained, and raw (no history of heating to above 40°C). Samples were stored at ambient, controlled temperature (20 - 23 degrees) in opaque plastic buckets while the complete sample set was assimilated, and sub-sets created.

Two industrial liquid sweeteners, HFCS (Cargill, Bursa, Turkey) and ICSS (Super Syrups, Durbanville, South Africa) were sourced to be used as adulterants. The properties of the two products are given in **Table 3.2.**

Table 3.2 Properties and source of industrial sugar syrup adulterants

Supplier	Chemical name	Source	°Brix	Fructose (%)
Cargill	Fructose-glucose syrup	Maize	75.5	55%
Super Syrups	Fructose-glucose syrup	Cane sugar	76	50%

Table 3.3 Suppliers and origin information of honey samples acquired for this study

Supplier	Predominant botanical origin	Province	Location	*Scutellata* or *Capensis*
Peel's Honey	Macadamia *Macadamia spp.*	KwaZulu-Natal	Empangeni	*Scutellata*
Peel's Honey	Kidney bean *Phaseolus vulgaris*	Free State	Bethlehem	*Scutellata*
Peel's Honey	Saligna gum *Eucalyptus grandis*	KwaZulu-Natal	Midlands	*Scutellata*
Peel's Honey	Sunflower *Helianthus annuus*	North West Province	Klerksdorp	*Scutellata*
Q Bee	*Strandveld* or South Cape *fynbos*	Western Cape	South Cape	*Capensis*
Q bee	Lucerne *Medicago sativa*	Western Cape	Klein Karoo	*Capensis*
Hurter's Honey	Citrus Blossom *Citrus spp.*	Western Cape	Citrusdal	*Capensis*
Hurter's Honey	*Sandveld* or West Coast *fynbos*	Western Cape	West Coast	*Capensis*
Hurter's Honey	Aloe *Aloe greatheadii* subsp. *davyana*	Mpumalanga	Springbok Flats	*Scutellata*
Hurter's Honey	Litchi *Litchi spp.*	Mpumalanga	Lowveld	*Scutellata*
Ubusi	River Red Gum *Eucalyptus camaldulensis*	Western Cape	Berg River	*Capensis*
Ubusi	Onion *Allium cepa*	Western Cape	Klein Karoo	*Capensis*
Overberg	Pumpkin *Curcurbita sp.*	Western Cape	Overberg	*Capensis*
Overberg	Carrot *Daucus carota*	Western Cape	West Coast	*Capensis*
Overberg	Acacia *Acacia spp.*	Northern Cape	Douglas	*Scutellata*
Dad's Honey	*Protea* or mountain *fynbos*	Western Cape	Helderberg	*Capensis*
Dad's Honey	Canola *Brassica napus* var. *oleifera*	Western Cape	Caledon	*Capensis*
Total				17

3.2.2. Processing

Samples were heated to 40°C overnight in an incubator, before being strained in a standard 500-micron nylon gauge strainer. Sample sub-sets were created by homogenising the honey in each bucket by stirring thoroughly for one minute, then dividing honey into equivalent weight samples in preparation for receiving different treatments. For the storage trial, authentic samples of 300 g were weighed out into dust-free, airtight plastic 300 mL jars. For the dilution trial, samples were weighed out, mixed and stored in dust-free, airtight 50 mL plastic vials. All 10% w/w diluted samples were made up by combining 63 g honey with 7 g diluent, while 20% w/w diluted samples were made up of 56 g honey and 14 g diluent, bringing the total weight of each sample to 70 g. All jars and vials were labelled with their respective sample codes. Sub-sets were ordered as shown in **Figure 3.1.** Two diluent control samples of 300 g were included in the dilution sample sub-set for each diluent; one irradiated and the other not.

Irradiation of samples was done at HEPRO (High Energy Processing (Pty) Ltd., Montague Gardens, Cape Town). The HEPRO facility makes use of gamma radiation provided by decaying Cobalt-60 rods to irradiate products in a batch pallet system. Samples were irradiated at an exposure time typically used to achieve a 10 kGy dose consistent with the Agricultural Products Act (Department of Health, 1986; Department of Agriculture, 2000), but received an actual dose of 22 kGy, registered by a dosimeter attached to the outside of the box of samples.

The Storage Trial sample set consisted of the seventeen bulk honey samples, which were subdivided and stored in controlled and uncontrolled conditions to create authentic non-irradiated (n = 68) and authentic irradiated (n = 17) honey sample classes (**Figure 3.1a**). Ambient light and temperature conditions were simulated for the uncontrolled storage trial by storing honey jars in front of a South-facing window, out of direct sunlight, in a room with an ambient temperature that fluctuated at around 23°C and fluorescent lighting for 9 h, 5 days a week. Jars were rotated by 90° every 1-3 days to ensure even exposure to the ambient light from the window.

The Dilution Trial sample set also consisted of the seventeen bulk honey samples, which were subdivided and treated to create authentic non-irradiated (n = 17), authentic irradiated (n = 17), diluted non-irradiated (n = 68) and diluted irradiated (n = 68) honey sample classes, as well as sugar syrup control samples (n = 4) for a total of 174 sub-samples. (**Figure 3.1a** and **b**).

The schematic of the organisation of sample treatments (**Figure 3.2a**), represents each set of the 17 unique honey samples that has undergone a specific treatment, as shown on the axes, as a block. The data is grouped into Storage (**Figure 3.2b**) and Dilution Trial (**Figure 3.2c**) datasets, which are used and referred to as such. The sets overlap and both contain the irradiated and non- irradiated authentic 25°C samples.

a)

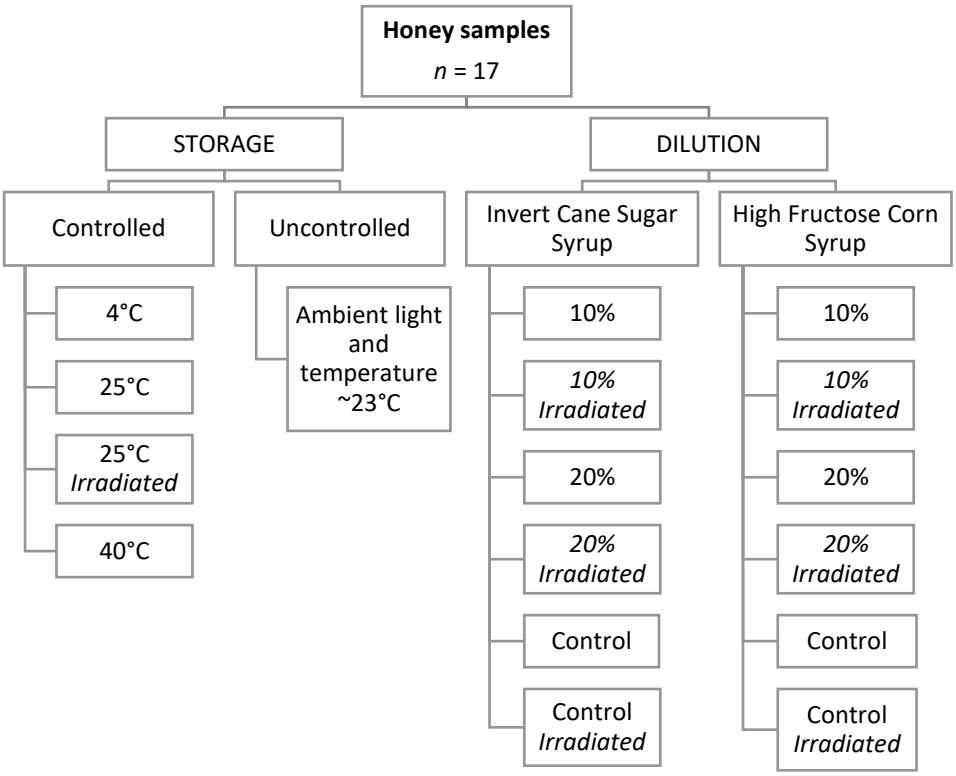

b)

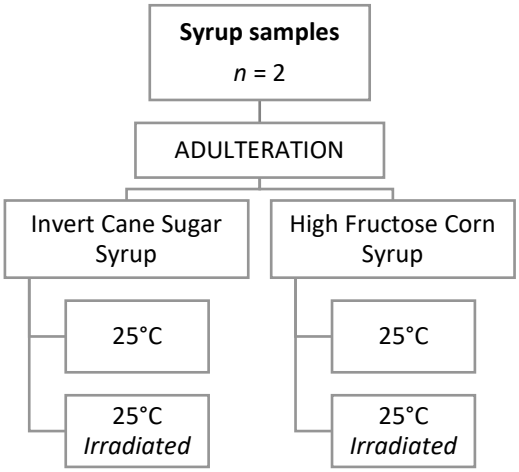

Figure 3.1 Organisation of a) honey and b) diluent syrup sample sets and treatments.

All Storage and Dilution Trial samples were stored for 9 months, where one 'month' was defined as 28 days for the purposes of the investigation. Samples within the Storage Trial sample set were scanned at month 0, then every 28 days for the first six months and 3 months later at the 9-month mark. Triplicate spectra of each of the 85 Storage Trial sub-samples were acquired eight times over a span of 9 months, for a total of 2040 spectra. Samples within the Dilution Trial sample set were scanned every 3 months or 84 days over the entire 9-month period. Triplicate spectra of each of the 174 Dilution Trial sub-samples were acquired four times over a span of 9 months, for a total of 2088 spectra. The datasets were labelled and will be referred to as indicated (**Table 3.4**).

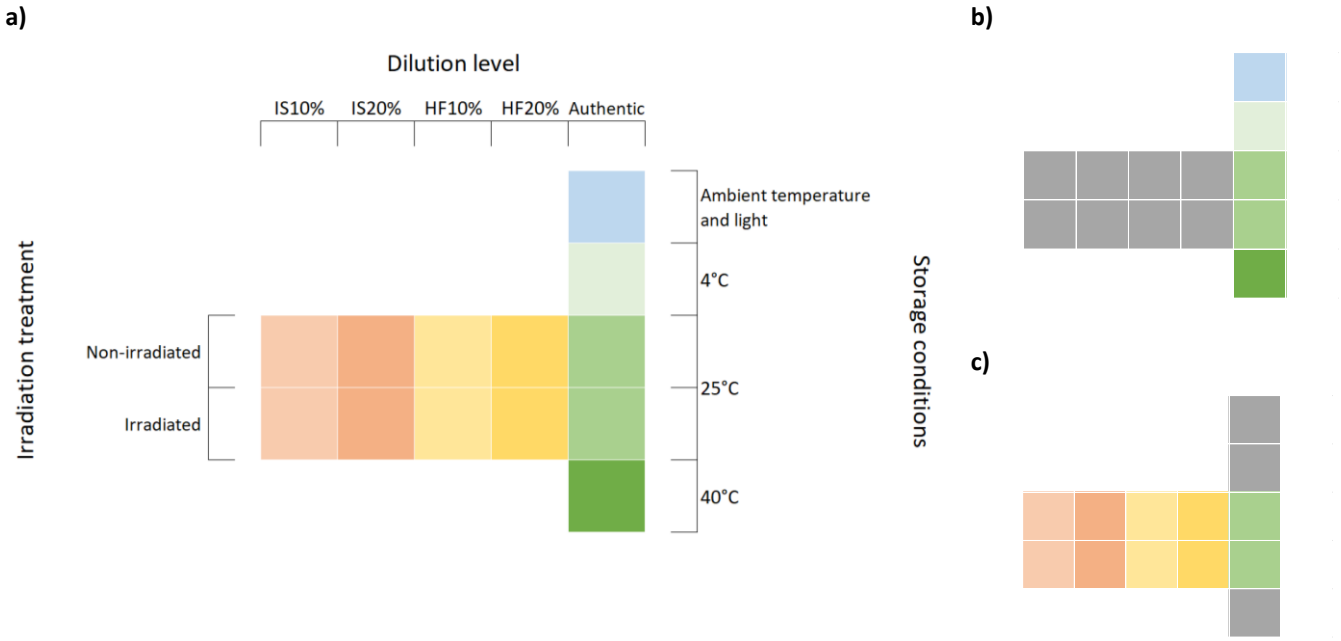

Figure 3.2 a) Organisation of the entire sample treatment space, each coloured block representing a complete set of sub-samples from the seventeen bulk honey samples, treated according to the axes; b) the storage trial subsets and c) the dilution trial subsets.

Table 3.4 Labelling of datasets, where complete dataset for each month contains an authentic and, where applicable, a diluted data subset

Month	Complete dataset	Authentic or Storage dataset	Diluted dataset
0	M_0	A_0	D_0
1	M_1	A_1	
2	M_2	A_2	
3	M_3	A_3	D_3
4	M_4	A_4	
5	M_5	A_5	
6	M_6	A_6	D_6
7			
8			
9	M_9	A_9	D_9
All	M_{All}	A_{All}	D_{All}

3.3. NEAR-INFRARED INSTRUMENTATION AND SPECTRAL ACQUISITION

3.3.1. Near-infrared spectroscopy instrumentation

Two NIR spectrometers were used for spectral acquisition of all samples: the VIAVI MicroNIR OnSite 1700 portable NIR spectrometer (VIAVI Solutions Inc., San Jose, CA, USA) and the BÜCHI NIRFlex-500 FT-NIR spectrometer (BÜCHI Labortechnik GmbH, Flawil, Switzerland). A comparison of the raw spectra obtained

from the two instruments and three sample holders (**Figure 3.3**) of a honey sample, shows the VIAVI MicroNIR covering the second and third overtones, while the BÜCHI NIRFlex-500 covers the second and first overtones, as well as the combination band regions.

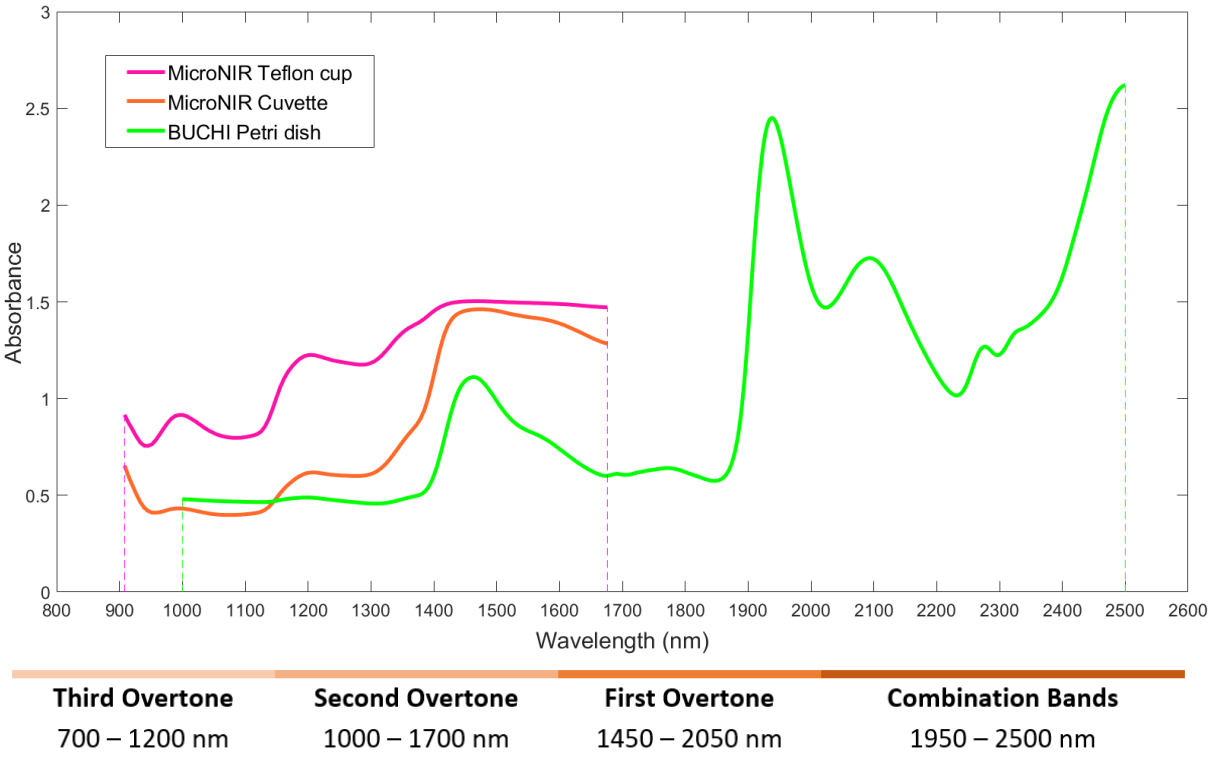

Figure 3.3 Wavelength ranges covered by the VIAVI MicroNIR and BÜCHI NIRFlex-500 spectrometers in the NIR region.

The VIAVI MicroNIR 1700 is a handheld device which is able to capture the spectral range of 908 to 1676 nm and can be operated in diffuse reflectance mode, or transmission mode if coupled with a transmission fixture. It is possible to present a liquid sample to the MicroNIR in at least two ways for acquiring diffuse reflectance spectra: in a sample cell placed directly under the window covering the radiation source and detector, or in a cuvette by means of a cuvette adapter accessory. Both commercially obtained 10 mm diameter glass cuvettes and custom-manufactured white Teflon cells, with diameter and depth of 18 mm and 9 mm respectively, were used to capture spectra in this study. The effects of these two cells on the accuracy and repeatability of spectral acquisition was not known prior.

The BÜCHI NIRFlex-500, a benchtop instrument with a 1000 – 2500 nm range, offers the greatest coverage of the NIR region. The BÜCHI has both Liquid and Solid attachments, offers various options for acquiring liquid and solid spectra, in diffuse reflectance, transmission, diffuse transmission and transflectance modes. For viscous liquid samples, the Solids attachment with a 100 mm glass Petri dish and a 0.5 mm transflectance plate has proven the most convenient and cost-effective option.

Both instruments are coupled to indium, gallium and arsenic (InGaAs) photodiode array detectors, but have different radiation sources and detector attributes (Friedrich *et al.*, 2014; BÜCHI, 2017). A comparison of the performance attributes of both spectrometers is given (**Table 3.5**).

Table 3.5 Performance attributes of the VIAVI MicroNIR and BÜCHI NIRFlex-500 FT-NIR spectrophotometers

Instrument	Detector	Wavelength selection	Illumination source	Spectral Range	Optical Resolution	Geometric Resolution	Signal-to-noise ratio	Integration time
VIAVI MicroNIR OnSite1700	InGaAs photodiode array	Linear Variable Filter (LVF)	Tungsten lamps	908 – 1676 nm	< 12.5 nm	6.25 nm	25 000:1	0.25 – 0.5 s
BÜCHI NIRFlex-500 FT-NIR	InGaAs (extended range)	Polarization interferometer	Tungsten halogen lamps	1000 – 2500 nm	8 - 16 cm^{-1}	0.4 nm	10 000:1	0.25 – 0.5 s

InGaAs - Indium Gallium Arsenide

For this study, spectra were acquired in triplicate and with three sample cell and instrument combinations: the VIAVI MicroNIR, with both a Teflon cup and a glass cuvette with Teflon insert, and with the BÜCHI NIRFlex-500 in a Petri dish paired with a 0.5 mm transflectance plate. Each instrument and sample cell combination resulted in a unique set of spectral acquisition parameters and scanning procedure requirements (**Table 3.6)**. In totality, the spectra of each sample and at each age, was captured three times with each of the three sample cell and instrument combinations, resulting in nine scans of each sample at each age.

Table 3.6 Specifics of spectral acquisition modes with the VIAVI MicroNIR and BÜCHI NIRFlex-500 FT-NIR spectrophotometers

Instrument	Sample cell	Dimensions	Pathlength	Scanning mode	Scanning procedure
VIAVI MicroNIR	Teflon cup	18 mm (*d*) x 9 mm (*h*)	18 mm	Diffuse reflectance	Cell filled, tapped and scraped to remove bubbles. Cell repositioned by rotation to obtain three scans.
VIAVI MicroNIR with vial adapter accessory	Glass cuvette with Teflon pathlength insert	Cuvette: 10 mm (*d*) x 45 mm (*h*) Insert: 8 mm (*d*)	1 mm	Diffuse reflectance	Cuvette filled with 1 – 2 mL of sample, insert placed in centre of cuvette. Cell repositioned by rotation to obtain three scans.

BÜCHI NIRFlex-500 FT-NIR with Solids attachment	Petri dish with transflectance cover	Petri dish: 10 mm (*d*) x 18 mm (*h*) Transflectance cover: 0.5 mm depth	1 mm	Transflectance	Petri dish filled with ~5 of mL sample, tapped to burst bubbles, cover placed over sample ensuring contact with surface of dish, underside of covered dish inspected for bubbles, dish wiped with paper towel before scanning. Three scans, with no repositioning.

Spectra were captured with both instruments and in the case of the MicroNIR, both sample cells, with the intention of comparing the performance of each option. The MicroNIR offers greater operational convenience and portability, but has a shorter wavelength range, which may reduce the suitability of the resulting spectra for authentication. The BÜCHI covers almost the full NIR range and is likely to capture more useable spectral information, but is a more costly instrument with limited portability, therefore confining authentication to in-laboratory analysis.

3.3.2. Sample preparation

Methods

The AACC Official Method 80.51-01 'Solids in Syrups – Refractometer Method' was followed for all TSS determinations, before and after dilution of the honey samples (AACC, 1999a). While there is no officially-recognised AOAC or AACC method available for NIR spectroscopic analysis of honey, the AACC Official Method 39-00.01 Near-Infrared Methods – Guidelines for Model Development and Maintenance which provides guidelines on NIR model development and evaluation of model performance for cereal analysis, was adapted for use in this study (AACC, 1999b).

Samples were prepared and scanned in a different randomized order for each spectral acquisition period. Samples were incubated in their watertight permanent storage containers in a water bath (Scientific Engineering (Pty) Ltd, Johannesburg, South Africa) at 40°C for 2 or 3 h to liquefy the honey. Sample vials (*d* = 28mm) were incubated for 2 h, while sample jars (*d* = 65mm) were incubated for 3 h, to obtain consistent heating results between samples. Prior to scanning, the samples required adjustment to a standardized °Brix value to avoid the misclassification based on their ratio of sugars to moisture or the TSS. At Month 0, the °Brix value of each sample was measured using an analog refractometer (Atago Co., Ltd, Japan). The masses of honey and dH_2O needed to make up a 70 ± 0.5 °Brix solution was calculated based on each sample's original °Brix value. Each jar was stirred with a metal spatula before honey was weighed out into clean, dry glass Petri dishes on a mass balance (Axis, Gdansk, Poland). The required mass of dH_2O was added with a pipette and

the solution was homogenized by stirring with a metal spatula. The adjusted °Brix values were checked using the refractometer and were further adjusted to 70 ± 0.5 °Brix, as required, and recorded.

3.3.3. Spectral acquisition

Between sample preparation and scanning, samples were allowed to equilibrate to room temperature (20-23°C) for approximately 1 h. Each honey sample was stirred again before filling the sample cells. Teflon cells were filled first and tapped against the workbench to allow any air bubbles introduced during homogenisation to rise to the surface. Remaining bubbles were scooped off the surface using a metal spatula.

The lamps of the **VIAVI MicroNIR** were allowed to warm up to 28°C before acquiring spectra. The dark current and reference spectra were taken, according to the manufacturer's specifications every 10 min, and triplicate spectra of each sample were acquired in diffuse reflectance mode. The MicroNIR sample cells were rotated to reposition for each of the three scans. To collect spectra with the cuvette cell, the dark current was captured in the same manner as was done for the Teflon cell. To capture the reference spectra, the MicroNIR vial attachment was coupled to the instrument and the white reference inserted. Thereafter, cuvettes were filled with sample and the 1 mm Teflon pathlength insert and the outside of the cuvette was wiped with soft tissue before scanning and scanned one at a time. The insert was washed and dried with soft tissue between uses. For each measurement an average of 100 scans was taken.

Before spectral acquisition with the **BÜCHI NIRFlex-500 FT-NIR**, samples were stirred again and decanted into the 100 mm soda-lime glass BÜCHI-compatible Petri dishes (Duran Group, Mainz, Czech Republic). The scanning Petri dishes were tapped on the counter to burst any bubbles. The 0.5 mm transflectance reflectance plate was then placed over the sample at an angle and pressed down to ensure contact with surface of dish. The underside of the covered Petri dish was inspected for bubbles and wiped with soft tissue before scanning. Spectra were acquired in transflectance mode using the NIRFlex-500 Solids attachment. The transflectance cover was washed with dH_2O and dried with soft tissue between uses. The internal and external references were collected as per manufacturer specifications every 20 min. A spectral interval of 0.4 nm and resolution of 16 cm^{-1} (half resolution) was used. For each measurement an average of 32 scans was taken. Spectra were converted to pseudo-absorbance using the BÜCHI NIRCal software.

3.4. DATA PROCESSING

Spectral data were imported into Microsoft Excel (Microsoft Corporation, Seattle, WA) and combined with categorical information of each sample in a single spreadsheet. Data were then imported into The Unscrambler® X v10.5 (CAMO Software AS., Oslo, Norway), MATLAB® (R2016b, MathWorks Inc, Natick, MA) and PLS_Toolbox (Eigenvector Research Inc., Wenatchee, WA) for spectral pre-processing and multivariate data analysis (MDA).

In the Unscrambler X, triplicate spectra of each sample were reduced to a single mean spectrum. For spectroscopic characterization and derivation of the initial exploratory data analysis (EDA), the full range of

each dataset was retained. PCA was calculated on wavelength ranges of 1300 – 2450 nm, as most substantial absorption of the honey constituents took place within this region. For multivariate data analysis (MDA), the BÜCHI spectra were used at their full range (1000-2500 nm) as well as reduced to wavelength ranges of 1300 – 2450 nm and 1300-1800 nm to evaluate the performance of models based on different ranges of the NIR region. The MicroNIR spectra were reduced to a wavelength range of 908 – 1651 nm to remove scattering effects present in the spectra above 1651 nm.

3.5. SPECTROSCOPIC CHARACTERIZATION

Prior to data analysis, all spectra within the data set were inspected and characterized within their acquisition month groupings. Raw spectra were plotted and examined to identify differences. Spectra within each month's dilution class (Authentic, HF10, HF20, IS10, IS20) were averaged and the resulting five mean spectra were plotted. Mean spectra of the non-irradiated and irradiated classes of each month were also computed and plotted. At this point, absorption bands were also identified and assigned using the tables of Osborne *et al*. (1993), and the spectra and assigned bands were compared to those described by other researchers of *Apis mellifera* honey.

Difference spectra allow wavebands where the largest differences in absorption lie to be identified for each class relative to the average authentic sample. The averaged irradiated class and average diluted classes were subtracted from the average authentic honey sample to create difference spectra, which were plotted and compared. The average pure diluent spectra were also subtracted from the average authentic sample.

3.6. SPECTRAL PRE-PROCESSING

Pre-processing treatments are used for reducing the effects of unwanted external variation introduced by scatter (normalization, SNV transform, MSC and detrending), and maximizing variation of interest (derivation). Scattering of light by solids or solid particles suspended within solutions introduces a type of systematic variation that is not of interest, and should be reduced with pre-processing techniques (Rinnan, 2014). In a matrix such as honey, which may contain crystals that are invisible to the naked eye even when liquid, this is particularly important.

Seven combinations of pre-processing treatments (**Table 3.7**), based on those used in similar NIR spectroscopy-based honey authentication studies, were applied to the raw spectra in an attempt to find an optimal combination. Mean-centring was automatically applied to all data after pre-processing.

Table 3.7 Pre-processing technique combinations applied in data analysis

Pre-processing combinations	**Abbreviation**
Mean-centring	MC
SNV + detrend (2nd order polynomial) + mean-centring	SNV, DT (2) and MC

MSC + mean-centring	MSC and MC
1st derivative, SG 3rd order polynomial, 11 smoothing points + mean-centring	1st derivative SG (3, 11) and MC
2nd derivative, SG 3rd order polynomial, 11 smoothing points + mean-centring	2nd derivative SG (3, 11) and MC
SNV + 1st derivative SG 3rd order polynomial, 11 smoothing points + mean-centring	SNV, 1st derivative SG (3, 11) and MC
SNV + 2nd derivative SG 3rd order polynomial, 11 smoothing points + mean-centring	SNV, 2nd derivative SG (3, 11) and MC

MC – Mean centring, SNV – Standard Normal Variate, MSC - Multiplicative Scatter Correction, SG – Savitzky-Golay

3.7. EXPLORATORY DATA ANALYSIS

3.7.1. Derivation

Derivation of averaged difference spectra is a useful exploratory tool for NIR data analysis. In particular, second order derivatives adhere to the log(1/R) spectral pattern of the original spectrum but with enhanced resolution (Shenk *et al*., 2001). All peaks that correlate to significant absorption in the original spectrum can be found in the negative region of the derivatized plot, pointing downward, while peaks in the positive region represent 'valleys' in the original spectra and may be disregarded.

The averaged diluted classes (Authentic, HF10, HF20, IS10, IS20) were each subtracted from the averaged authentic class to create difference spectra, which were processed with 2nd derivative with Savitzky-Golay smoothing (3rd order, 11 smoothing points).

3.7.2. Principal Component Analysis

Unsupervised classification methods, primarily used for data exploration, base their classification solely on data within a set, not on prior knowledge of the samples (Roggo *et al.*, 2007). Principal component analysis (PCA) was conducted to explore relationships between the samples, as well as identify potential outliers. PCA separates the variation within the dataset into statistically independent, or orthogonal, components (Oliveri and Simonetti, 2016). Principal components (PCs) are ordered with respect to their contribution to the overall variation and can be visualised by means of a 2- or 3-D bilinear projection. This is followed by explanation or categorization of the resulting clusters by the operator.

The Storage and Dilution Trial datasets were constructed by combining the D_0 – D_9 datasets, and the A_0 – A_9 datasets. PCA models were built for the Storage and Dilution Trials in The Unscrambler X with data treated with SNV, detrend (2nd order polynomial) and mean-centring pre-processing. In addition, 2nd derivative Savitzky-Golay derivative (3nd order polynomial, 15 smoothing points) and mean-centring was also applied to the raw data to evaluate whether the score projections could be improved by the use of derivative pre-processing. PCA models with 7 components were calculated with full cross-validation and 30 000

nonlinear iterative partial least squares (NIPALS) iterations. Potential outliers, identified from the raw spectra and the PCA scores plots, were flagged and the Hotelling's T^2 and Q-residuals influence plot were examined to confirm true outliers. Hotelling's T^2 is a way of applying the t-test to PCA scores and allows a confidence limit to be applied to the samples. The Q-residuals is the sum of squared residuals, the variation of samples that is not explained by the model. Influential spectra, that were not well-modelled by the PCA, were removed if sufficient evidence of spectral errors or non-conformities could be found.

Once outliers had been removed, PCA models were re-calculated and interpreted further. The number of PCs considered for each PCA was determined with the assistance of the X-variance vs. PCs plot or explained variance plot. Score plots, of PCs 1-7 in varying combinations, were visualised in two- and three-dimensions with each of the experimental design factors (i.e. honey type, adulterant class, adulterant level, scanning month, irradiation treatment class) highlighted, in turn, to expose noteworthy clustering. The loadings line and correlation loadings line were used to identify spectral regions that were contributing to the separation between clusters observed in the score plots.

Overall, it was intended for PCA to be used to determine the optimal pre-processing combinations for the spectral data, for further use in qualitative multivariate data analysis.

3.7.3. ANOVA Simultaneous Component Analysis

ANOVA-simultaneous component analysis (ASCA) is an exploratory data analysis method based on analysis of variance (ANOVA) and PCA (Smilde *et al.*, 2005). ASCA is an adapted PCA method that distinguishes between variation induced by different experimental design factors, unlike straightforward PCA and ANOVA methods, which pool all variation together. This allows the contributions and interactions of these treatment or time factors to be interpreted individually. The statistical significance of each design factor can also be determined by a permutation test, where the null hypothesis in each case is that each factor is not significantly contributing to the variation of the designed dataset. ASCA extends the application of ANOVA-based analysis to spectroscopic data, as multivariate-ANOVA (MANOVA) does not generally perform well with spectral datasets, which typically contain more variables than samples (Jansen *et al.*, 2005).

ASCA was conducted using the built-in ASCA function within PLS_Toolbox, as well as an in-house written MATLAB function. The Storage and Dilution Trial datasets were analysed separately, with the syrup control samples omitted from the Dilution Trial dataset to prevent skewing of the results. The spectral data and relevant experimental design factors were entered as separate matrices and pre-processed separately. For both trials, the experimental design matrix was processed with and the spectral data with SNV, detrend (2^{nd} order polynomial) and mean-centering. A t-test at the 0.05 significance level with 100 permutations was performed in order to determine the statistical significance of each factor. The interaction effects within and between (two-way effects) design factors were also compared and the interaction scores were visualised by means of score plots.

3.7.4. Spectral Contrast Angle

The spectral contrast angle (SCA) method is a spectral comparison technique for determining the similarity between two spectra, often employed in mass spectroscopy (Wan *et al.*, 2002). A vector is used to represent the prominent absorbance peaks within each spectrum under consideration, with the angle between vectors of two spectra being calculated as a measure of the similarity of that spectral pair. The SCA method is considered an improvement upon the similarity index (SI) method, an earlier spectral comparison tool.

Substantial absorbance peaks present in two classes of spectra under investigation, A and B, are identified. The absorbance values of the substantial peaks are averaged across replicates within each class, and used to calculate a vector of *N* dimensions, in which the absorbance values of *N* substantial peaks were included, defined as

$$r_a = \sqrt{\sum_i {a_i}^2} \tag{3.1}$$

where *r* is the class-representing vector and *a* the absorbances of the substantial peaks in one averaged class spectrum. The absorbances of classes A and B at corresponding wavelengths are multiplied and summed, which then is divided by the dot product of these vectors. The spectral contrast angle is calculated

$$cos\theta = \frac{\sum_i a_i b_i}{\sqrt{\sum_i {a_i}^2 \cdot \sum_i {b_i}^2}} \tag{3.2}$$

where ϑ is the spectral contrast angle, and *a* and *b* represent the absorbances of the substantial peaks in the two spectra under comparison. A spectral contrast angle close to zero implies a strong degree of similarity between two spectra, while an angle close to 0.5π suggests a large degree of dissimilarity.

Spectral contrast angles were calculated and compared for the authentic, HF10, HF20, IS10 and IS20 classes, respective and irrespective of irradiation, as well as the irradiated and non-irradiated classes, respective and irrespective of dilution. In each case, substantially absorbing peaks were chosen based on the largest 2nd derivative difference peaks revealed in **7.1 Derivation**.

3.8. MULTIVARIATE DATA ANALYSIS

All classification models were built in MATLAB® (R2016b, MathWorks Inc, Natick, MA), using the PLS_Toolbox software package (Eigenvector Research Inc., Wenatchee, WA). A variety of classification techniques were applied to the dilution detection problem. Using the best-performing modelling technique, specific diluent detection and irradiation detection was also attempted, following the same modelling approach and selection criteria.

3.8.1. Validation selection algorithms

Selection of independent calibration and validation sets during classification model building is required to prevent over-optimistic classification results. Single set validation selection algorithms select the most representative calibration and validation data-subsets from the complete dataset. Kennard-Stone or CADEX is one such algorithm, which can be used to select a predetermined proportion of the most uniformly distributed, and therefore representative samples, across the sample set by comparison of Euclidean distances. Samples are alternately added to the calibration and validation sets (Kennard and Stone, 1969).

The DUPLEX algorithm, an improvement on the Kennard-Stone algorithm, additionally ensures that the calibration and validation sets both have an equal distribution of the most extreme points within the data set (Snee, 1977). The DUPLEX algorithm was used to create representative calibration (70%) and validation sets (30%) for all classification models.

3.8.2. SIMCA

SIMCA models were built in PLS_Toolbox with data treated with the seven selected pre-processing combinations. PCA models were constructed as described in **7.2 Principal Component Analysis**. The explained variance plot, of X-variance vs. PCs, was used to determine which components were contributing substantially to each PCA model. The number of components chosen for inclusion were determined by the point at which the cumulative X-variance neared 100%, or where the curve began to plateau, with a preference for the lowest number of principal components. These were minimized to avoid including unnecessary variation and increasing the model complexity.

3.8.3. PLS-DA

PLS-DA models were built in PLS_Toolbox with data treated with the seven selected pre-processing combinations. Venetian blinds, 10-fold cross-validation was used.

The average cross-validation classification error plotted against the number of latent variables was used to determine the optimal number of latent variables for inclusion in each PLS-DA model. The number of latent variables that yielded the lowest cross-validation (CV) error and highest calibration accuracy were selected for each model, with a preference for the lowest number of latent variables possible. The number of latent variables is intentionally minimized, as model complexity in increased with every latent variable added. Higher-numbered components could be accounting for unnecessary variability or non-ideal behaviour in some of the spectra and inclusion of these could reduce the overall robustness of the model.

Models that performed well were recalculated using different numbers of latent variables that still yielded low average CV classification errors, to determine whether increased classification accuracy, sensitivity and specificity could be obtained.

Once PLS-DA has been shown to be the most effective classification technique, three categories of PLS-DA models were developed using the BÜCHI spectral data. In addition to building the intended diluent detection model, two preliminary investigations were conducted into the selection of the most effective wavelength range and the effect of irradiation using generalised dilution detection PLS-DA models. For generalised detection of dilution, or classification of authentic and diluted samples, two-class PLS-DA models were constructed, using authentic and inauthentic as the two classes. The diluted class was defined as all samples diluted with any diluent and at any level. For both investigative models, data were confined to the Dilution Trial set in order to avoid bloating the model with too many sources of variation. Again, for each of the proposed models in these three categories, seven models were actually built using the selected pre-processing combinations and the best-performing model was selected with the same criteria of accuracy, sensitivity and specificity. For the overall diluent detection model, the Storage and Dilution Trial datasets were combined to form a larger reference library containing more realistic variation to simulate a comprehensive database.

Irradiation detection was also attempted, following the same modelling approach and selection criteria as the general dilution detection models.

3.8.4. QUANTIFICATION

Quantification of diluent level was attempted, using partial least squares regression (PLSR) and the optimal pre-processing combinations determined during classification model building. The individual diluent models were chosen for quantification, as they proved to have the best discrimination power between the authentic and diluted honey, and therefore between the 0% and the combined 10, 20 and 100% dilution classes. A wavelength range of 1300-1800 nm was used, and the best-performing pre-processing combination determined during classification were used, although the number of latent variables was reselected for optimisation.

The Duplex algorithm was used to select representative calibration (70%) and validation (30%) sets of the combined month 0-9 Storage and Dilution Trial datasets, excluding all identified and verified outliers. Models were calculated with and without the pure diluent syrup classes, based on the methodology of Bázár *et al.* (2016). Dilution level percentage was selected as the Y-variable or reference data for the calibration. Venetian blinds, 10-fold cross-validation was used to determine the number of latent variables for each model, by selecting the number of components that yielded the lowest error of cross-validation. The coefficients of determination and root mean square errors of calibration and cross-validation were used to evaluate the performance of each regression model. Variable importance in projection (VIP) scores were calculated to indicate the importance of variables and their contribution to the overall variation of the variable space (Westad *et al.*, 2013).

3.8.5. STATISTICAL PERFORMANCE INDICATORS

A full panel of classification performance indicators were generated from the confusion matrix of each pre-processing and modelling technique combination to holistically evaluate the performance of each model (**Table 3.8**). A combination of three measures was used to optimise the performance of classification models: the validation classification accuracy, as well as the validation sensitivity and specificity.

Sensitivity (or recall) is also known as the true positive rate, or proportion of samples correctly accepted by the model, and specificity (or selectivity) as the true negative rate, or the proportion of samples correctly rejected by the model. An authentic vs. diluted honey model that has 100% sensitivity will accept all authentic samples, and a model with 100% specificity will correctly reject all diluted samples. However, while 100% sensitivity and specificity are ideal in a model, in practice it is likely that one parameter will be sacrificed to increase the other.

Another measure generated and reported during classification modelling was the area under the curve (AUC) of a receiver operating characteristic (ROC) plot, a plot of sensitivity vs. 1 minus selectivity, which may also be described as the true positive rate vs. false positive rate. The AUC is a comprehensive measure of the accuracy and describes the classification ability of the model as the discriminant parameters or thresholds are changed (James *et al.*, 2017). An AUC close to 1.00 describes perfect predictive ability, while a value of 0.5 indicates random or chance classification.

Table 3.8 Classification performance indicators (Oliveri and Downey, 2012)

Statistical Indicator	Formula	Description	Eqn.
Accuracy	$\frac{TP + TN}{TP + TN + FP + FN}$	The percentage of samples correctly classified or predicted. Also referred to as the classification or prediction rate.	(3.3)
Misclassification	$\frac{FP + FN}{TP + TN + FP + FN}$	The percentage of samples incorrectly classified or predicted.	(3.4)
Efficiency	$\sqrt{\frac{TP \cdot TN}{(TP + FN) \cdot (TN + FP)}}$	Geometric mean of sensitivity and specificity	(3.5)
Precision	$\frac{TP}{TP + FP}$	Fraction of samples correctly accepted of all the accepted samples, also referred to as the predictive power	(3.6)
Sensitivity or Recall	$\frac{TP}{TP + FN}$	Proportion of samples correctly accepted by the model	(3.7)
Specificity or Selectivity	$\frac{TN}{TN + FP}$	Proportion of samples correctly rejected by the model	(3.8)

True Positives (TP) - Positive outcome correctly predicted as positive outcome; True Negatives (TN) - Negative outcome correctly predicted as negative outcome; False Positives (FP) - Negative outcome incorrectly predicted as positive outcome; False Negative (FN) - Positive outcome incorrectly predicted as negative outcome.

Model selection criteria

For an authenticity screening model, it is recommended to take a conservative approach: to fine-tune the model to only accept authentic samples and earmark all non-conforming or questionable samples for further testing with officially-recognised methods provided by the Department of Agriculture (2000). It is therefore advantageous to optimize the model based on the sensitivity, the proportion of samples correctly accepted by the model. A model with sensitivity close to 1.00 would be sought, as this would indicate minimal false negatives, or authentic samples rejected as non-conforming. As a stand-alone authenticity method, the specificity would be considered to be of higher importance, as the highest priority would be to have all non-conforming products be identified in one test. A model with specificity close to 1.00 would be appropriate, as this would indicate minimal false positives, or non-conforming samples accepted as authentic.

For selection of the best performing model, high sensitivity and specificity were sought, but higher sensitivity was prioritized over specificity as the focus of the preliminary classification model was on screening. Consequently, the best-performing models, with regard to classification technique, pre-processing

combination and number of PCs, LVs or *K* neighbours, were selected based on the highest sensitivity (of the authentic class), efficiency and validation classification rate, combined.

3.8.6. NIR INSTRUMENT COMPARISON

General dilution detection with the data acquired by the VIAVI MicroNIR instrument was also attempted, following the same PLS-DA modelling approach and selection criteria as the general dilution detection models built using the BÜCHI data, in order to conduct an NIR instrument comparison. The models were compared on the basis of their accuracy, sensitivity and specificity.

3.9. REFERENCES

AACC. (1999a). Solids in Syrups—Refractometer Method (method 80-51.01). *Approved Methods of the AACC*.

AACC. (1999b). Near-Infrared Methods—Guidelines for Model Development and Maintenance Procedure (method 39-15.01). *Approved Methods of the AACC*.

Bakier, S. (2009). Capabilities of near-infrared spectroscopy to analyse changes in water bonding during honey crystallisation process. *International Journal of Food Science & Technology*, **44**, 519–524.

BÜCHI. (2017). *Operation Manual NIRFlex N-500*. Flawil, Switzerland: BÜCHI Labortechnik AG.

Department of Agriculture. (2000). *Regulations Relating to the Grading, Packing and Marking of Honey and Mixtures of Bee Products Intended for Sale in The Republic of South Africa*. Pretoria: Department of Agriculture.

Department of Health. (1986). *Foodstuffs , Cosmetics and Disinfectants Act 54 of 1972*. *Government Gazette*.

Downey, G., Fouratier, V. & Kelly, J.D. (2003). Detection of honey adulteration by addition of fructose and glucose using near infrared transflectance spectroscopy. *Journal of Near Infrared Spectroscopy*, **11**, 447–456.

Friedrich, D.M., Hulse, C.A., Gunten, M. von, Eric P. Williamson & Christopher G. Pederson, N.A.O. (2014). Miniature near-infrared spectrometer for point-of-use chemical analysis. In: *Proceedings of Society of Photo-Optical Instrumentation Engineers*. Pp. 1–11.

James, G., Witten, D., Hastie, T. & Tibshirani, R. (2017). *Introduction to Statistical Learning*. 8th edn. New York: Springer.

Jansen, J.J., Hoefsloot, H.C.J., Greef, J. Van Der, Timmerman, M.E., Westerhuis, J.A. & Smilde, A.K. (2005). ASCA: analysis of multivariate data obtained from an experimental design. *Journal of Chemometrics*, **19**, 469–481.

Kelly, J.D., Petisco, C. & Downey, G. (2006). Potential of near Infrared Transflectance Spectroscopy to Detect Adulteration of Irish Honey by Beet Invert Syrup and High Fructose Corn Syrup. *Journal of Near Infrared Spectroscopy*, **14**, 139–146.

Masehela, T.S. (2017). *An assessment of different beekeeping practices in South Africa based on their needs (bee forage use), services (pollination services) and threats (hive theft and vandalism)*.

Oliveri, P. & Downey, G. (2012). Multivariate class modeling for the verification of food-authenticity claims. *Trends in analytical chemistry*, **35**, 74–86.

Oliveri, P. & Simonetti, R. (2016). Chemometrics for Food Authenticity Applications. In: *Advances in Food Authenticity Testing* (edited by G. Downey). Pp. 701–728. London: Elsevier.

Rinnan, Å. (2014). Pre-processing in vibrational spectroscopy - when, why and how. *Analytical Methods*, **6**, 7124–7129.

Roggo, Y., Chalus, P., Maurer, L., Lema-martinez, C., Edmond, A. & Jent, N. (2007). A review of near infrared spectroscopy and chemometrics in pharmaceutical technologies. *Journal of Pharmaceutical and Biomedical Analysis*, **44**, 683–700.

Shenck, J.S., Workman Jr., J.J. & Westerhaus, M.O. (2001). Application of NIR Spectroscopy to Agricultural Products. In: *Handbook of Near-Infrared Analysis* (edited by D.A. Burns & E.W. Ciurczak). Pp. 419–474. Basel: Marcel Dekker, Inc.

Smilde, A.K., Jansen, J.J., Hoefsloot, H.C.J., Lamers, R.A.N., Greef, J. Van Der & Timmerman, M.E. (2005). ANOVA-simultaneous component analysis (ASCA): a new tool for analyzing designed metabolomics data. *Systems biology*, **21**, 3043–3048.

Snee, R.D. (1977). Validation of regression models: methods and examples. *Technometrics*, **19**, 415–428.

The United States Pharmacopeial Convention. (2014). Food Chemicals Codex (9th Edition) [Internet document] . *The United States Pharmacopeial Convention*URL https://app.knovel.com/hotlink/toc/id:kpFCCE0021/food-chemicals-codex/food-chemicals-codex. Accessed 24/10/2018.

Toher, D. (2007). *A comparison of model-based and regression classification techniques applied to near infrared spectroscopic data in food authentication studies*.

Ulberth, F. (2016). Advances in Testing for Adulteration in Honey. In: *Advances in Food Authenticity Testing* (edited by G. Downey). Pp. 729–753. London: Elsevier.

Wan, K.X., Vidavsky, I. & Gross, M.L. (2002). Comparing Similar Spectra : From Similarity Index to Spectral Contrast Angle. *American Society for Mass Spectroscopy*, **13**, 85–88.

Woodcock, T., Downey, G., Kelly, J.D. & O'Donnell, C. (2007). Geographical classification of honey samples by near-infrared spectroscopy: A feasibility study. *Journal of Agricultural and Food Chemistry*, **55**, 9128–9134.

Chapter 4 Results and Discussion

4.1. SPECTROSCOPIC CHARACTERIZATION

4.1.1. Inspection of raw spectra

Inspection of raw NIR data is an important, but often neglected step that must be taken prior to MDA. At this stage, differences in absorption intensity of raw spectra cannot be correlated to chemical composition yet, as there are still physical sources of variation present in the data, such as light scattering. Raw spectra of Dilution Trial months 0, 3, 6 and 9 (D_0, D_3, D_6, and D_9) were plotted (**Figure 4.1**) and inspected to identify differences and trends in their spectral acquisition month classes. Baseline shifts and linear trends are evident in the D_0 spectra (**Figure 4.1a**), with two groups of samples exhibiting a vastly different baseline offset. Additionally, two sample spectra demonstrated flattened peaks, indicating possible specular reflectance, in the 1900 – 2500 nm region. In D_6, three sample spectra demonstrated slightly flattened peaks, indicating possible specular reflectance, in the 1900 – 2500 nm region (**Figure 4.1c**). Linear trends in the 1900 – 2500 nm region are evident in all months.

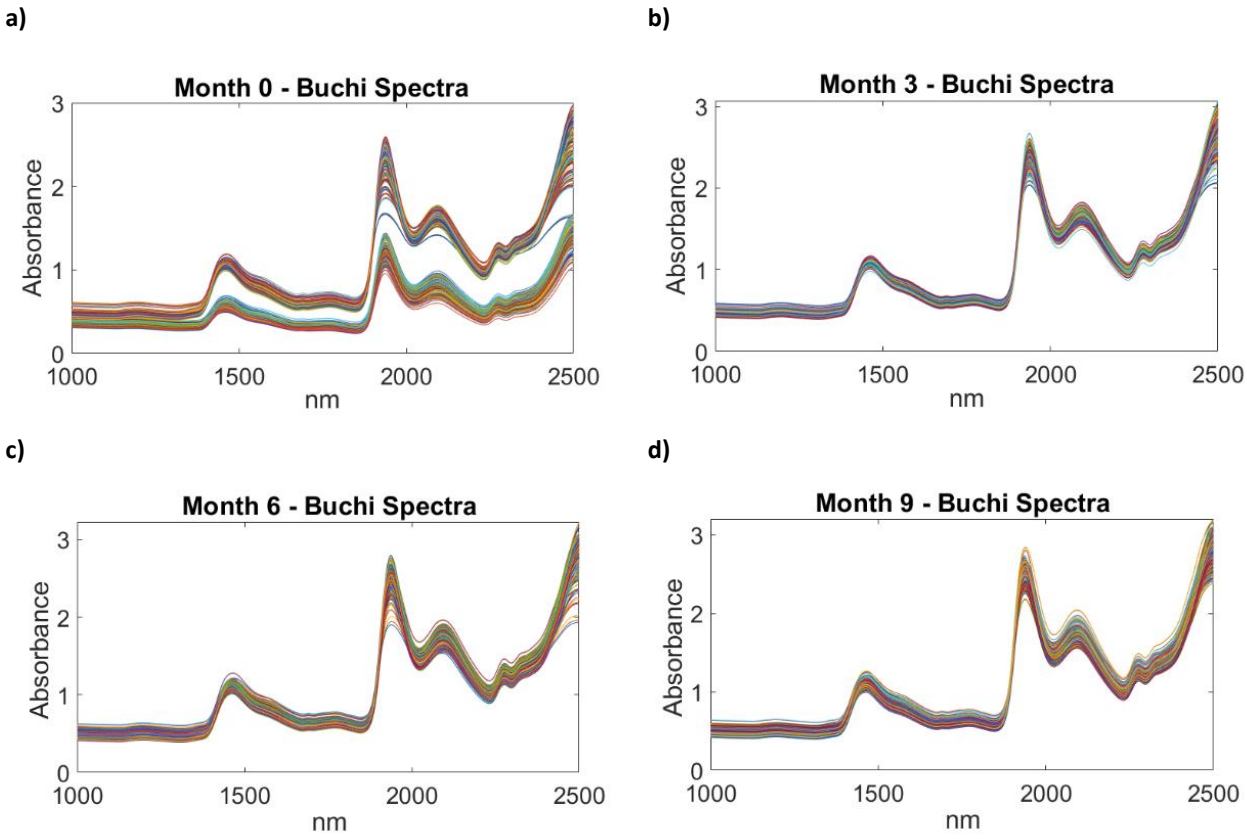

Figure 4.1 a) Raw spectra of Month 0 Dilution Trial (D_0), b) Raw spectra of Month 3 Dilution Trial (D_3), c) Raw spectra of Month 6 Dilution Trial (D_6), d) Raw spectra of Month 9 Dilution Trial (D_9).

From visual inspection it became evident that both additive and multiplicative effects were present in the spectral data. Differences in absorbance intensity of spectra were also visible. In spectra of the same

product this is most often correlated to the particle size differences within the samples (Shenk, 2001). Specular, or direct reflectance (**Figure 4.1a**), is characterized by a loss of fine structure within a spectrum and cannot be improved with pre-processing techniques (Rinnan *et al.*, 2009). This could be due to the size of crystals within these samples being of a particular size that results in more specular (surface) than diffuse (internal) reflectance over this specific wavelength range. Literature is unanimous in its recommendation of removing these samples, as they are likely to remain outliers, regardless of spectral processing. Hotelling's T^2 and Q-residuals plots generated during further exploratory data analysis will be used to assess whether these samples are candidates for exclusion.

4.1.2. Mean class and class difference spectra

Difference spectra allow wavebands, where the largest differences in absorption lie, to be identified for each class relative to the average authentic sample. Spectra within each dilution class [Authentic (0%), HF-diluted (10-20%), IS-diluted (10-20%), HFCS (100%), ICSS (100%)] were averaged and plotted (**Figure 4.2a**). Additionally, the averaged dilution classes and pure diluents were subtracted from the average authentic honey sample to create average difference spectra (**Figure 4.2b**). The differences in absorption intensity of raw spectra cannot yet be correlated to chemical composition or level of dilution, as there are still physical sources of variation present in the data such as light scattering.

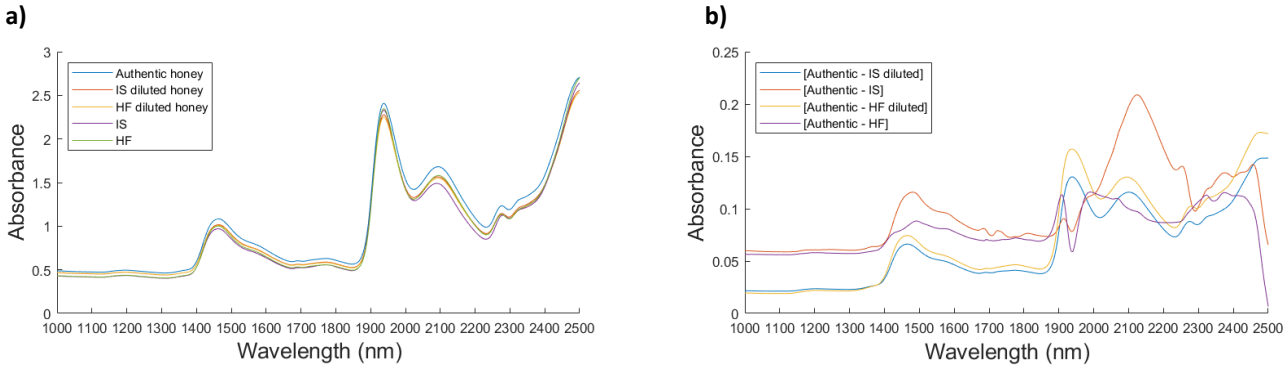

Figure 4.2 a) Average spectrum of each dilution class over D_0 – D_9, irrespective of irradiation, and b) Average difference spectrum of each dilution class over D_0 – D_9 [authentic class with HF-diluted (10-20%), IS-diluted (10-20%), HFCS (100%) and ICSS (100%) classes subtracted], irrespective of irradiation.

On inspection, the D_0 – D_9 dilution classes shared absorption bands in similar regions with slight variation in the intensity of the absorption, which can be attributed to light scattering effects. In all averaged class spectra, substantial absorption occurred in five regions, 1440-50, 1940, 2080, 2280 and 2500 nm, while smaller noticeable features could be found at 1190, 1580, 1690, 1780 and 2320 nm. Similar bands have been reported by other NIR studies on honey (Downey *et al.*, 2003; Kelly *et al.*, 2006; Woodcock *et al.*, 2007; Chen *et al.*, 2011; Herrero Latorre *et al.*, 2013; Bázár *et al.*, 2016; Guelpa *et al.*, 2017; Li *et al.*, 2017; Thamasopinkul *et al.*, 2017). Substantial differences in the dilution class spectra could be seen across the 1400 – 2500 nm region, which for sugar solutions corresponds to the 1st overtones of OH, CH and CH_2 stretching and deformation, and combination bands of OH, CH and CH_2 (Golic *et al.*, 2003). Differences between the pure

ICSS and HFCS samples in **Figure 4.2b** could be seen at 1420-1500, 1680-1730, 1800, 1880-1900, 1940, 2110, 2250, 2360 and 2460 nm.

Average and average difference spectra of the irradiated and non-irradiated classes revealed little difference in the absorption bands and band intensity of the two classes, with one noticeable double band feature around the 1940 nm region (**Figure 4.3**). The double peak band is moisture-related, attributed to O-H stretching and deformation combination bands of H_2O (Osborne *et al.*, 1993) and has frequently been reported in honey spectra (Downey *et al.*, 2003; Woodcock *et al.*, 2007; Herrero Latorre *et al.*, 2013; Bázár *et al.*, 2016; Thamasopinkul *et al.*, 2017).

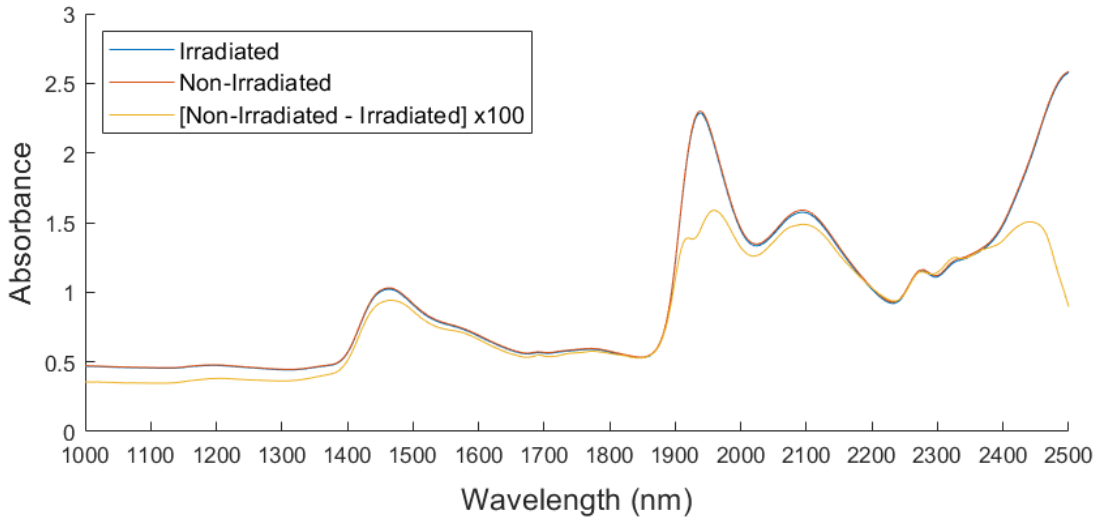

Figure 4.3 Average spectrum of the irradiation treatment classes over D_0 – D_9, irrespective of dilution and average difference spectrum of the irradiation treatment classes over D_0 – D_9, amplified by 100 (non-irradiated class with irradiated class subtracted), irrespective of irradiation.

4.1.3. Absorption band assignment

The major absorption bands were identified using the tables of Osborne *et al*. (1993) (**Figure 4.4**). The spectral band assignments concurred with those described in other research on *Apis mellifera* honey (Downey *et al.*, 2003; Woodcock *et al.*, 2007; Herrero Latorre *et al.*, 2013; Bázár *et al.*, 2016; Guelpa *et al.*, 2017; Thamasopinkul *et al.*, 2017), sugar solutions (Rambla *et al.*, 1997; Golic *et al.*, 2003) and water (Segtnan *et al.*, 2001).

On an averaged spectrum of pure honey, absorption bands were found at 1440 nm (O-H 1st overtone stretch and C-H stretch and deformation of sugars), 1450 nm (O-H 1nd overtone stretching bands of H_2O), 1940 nm (O-H stretching and deformation combination bands of H_2O), 2080nm (O-H stretch and deformation and C-O stretching bands of sugars) and 2280nm (C-H stretch and deformation combination bands of sugars) (Osborne *et al.*, 1993).

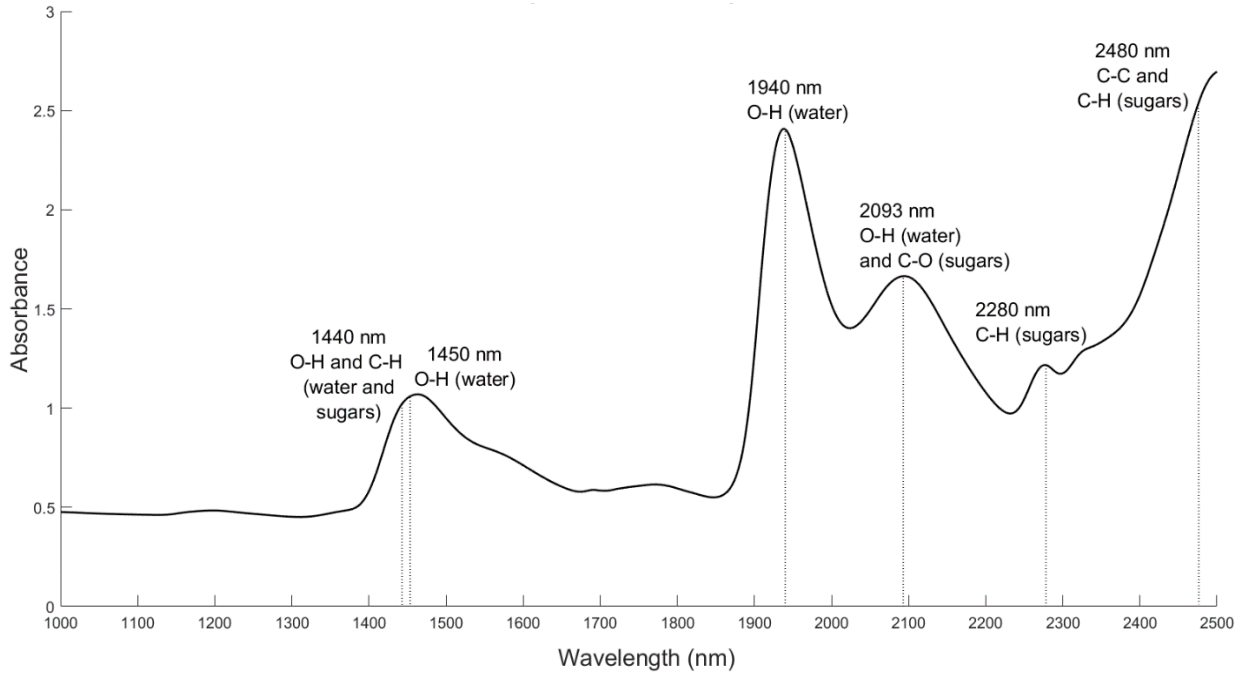

Figure 4.4 Average authentic honey spectrum over D_0 – D_9, with identified major absorption bands.

Another large peak could be found at around 2480 nm (C-H and C-C stretching of carbohydrates or sugars) but will likely be disregarded, as its proximity to the detector's end of range means it may be compromised due to scattering effects. 'Sugars' here refers to predominant honey constituents of fructose (37-39% w/w), glucose (30-32% w/w) and sucrose (0,5-2% w/w) (Ulberth, 2016), which contain varying numbers of C-C, C-H, O-H, C-O, C=O bonds. The characteristic NIR absorbances of these sugars, and in particular fructose and glucose have been well-described (Rambla *et al.*, 1997; Golic *et al.*, 2003) and have been extensively documented in other honey investigations (Downey *et al.*, 2003; Kelly *et al.*, 2006; Woodcock *et al.*, 2007; Bázár *et al.*, 2016).

The selected diluents also contain glucose and fructose, but in similar and not identical quantities. The HFCS used in this trial had a fructose content of 55% (db), while the ICSS contained 50% (db) fructose. In comparison, honey contains between 45 and 50% (db) fructose (Ulberth, 2016). The resulting difference in fructose content after dilution is likely to be evident in the spectra of the 10% and 20% diluted classes, with the HF-diluted samples, and to a lesser extent the IS-diluted samples, expected to have increased absorbance at 1583, 2123 and 2271 nm (Rambla *et al.*, 1997). The authentic honey samples, which will retain a higher proportion of glucose than the diluted samples, are likely to have greater characteristic glucose absorption peaks at 1587, 2121 and 2271 nm (Rambla *et al.*, 1997). Glucose and fructose absorption were also identified in the 2nd derivative spectra of sugar solutions at 2266, 2276, 2322, 2354, 2376, 2420, 2448 and 2484 nm for fructose and 2276, 2324, 2452 and 2460 nm for glucose (Downey *et al.*, 2003). Due to the overlapping nature of NIR peaks, it is likely that the 1583-1587 nm and 2121-2123 nm absorbances will be evident as shifted peaks instead of defined peaks, while the effects of absorbance by glucose and fructose at 2271 nm are likely

to be indistinguishable from one another. However, this was not evident in the averaged class spectra (**Figure 4.2a**) or the 2nd derivative dilution class difference spectra (**Figure 4.5b**).

Additionally, the °Brix of the diluents differed; HFCS was 75.5 °Brix and the ICSS 76.0 °Brix, meaning that the HF-diluted samples had a marginally lower sugar concentration than the IS-diluted samples for the duration of the nine-month storage period. This may have created opportunities for fermentation and the chemical change induced by it to occur over time. A thin layer of foam or bubbles, a reliable indicator of fermentative microbiological activity in honey, was found on the surface of a small number of diluted honey samples during every month's spectral acquisition, particularly honey varieties that had a starting °Brix below 80.0. Variation around the O-H related peaks at 1440-50 and 1940 nm was evident in both the averaged class spectra (**Figure 4.2a**) or the 2nd derivative dilution class difference spectra (**Figure 4.5b**).

4.2. EXPLORATORY DATA ANALYSIS

4.2.1. Derivation

Difference spectra of the dilution classes and pure diluents (**Figure 4.5**), irradiation classes (**Figure 4.8**) were processed with 2nd derivative with Savitzky-Golay smoothing (3rd order, 11 smoothing points). All minima, or peaks that correlate to prominent absorptions in the original spectrum, can be found pointing downward in the negative region of the plot. Prominent bands were identified on plots of each dilution class subtracted from the authentic class and the irradiation treatment class subtracted from the non-irradiated class (**Figure 4.6**).

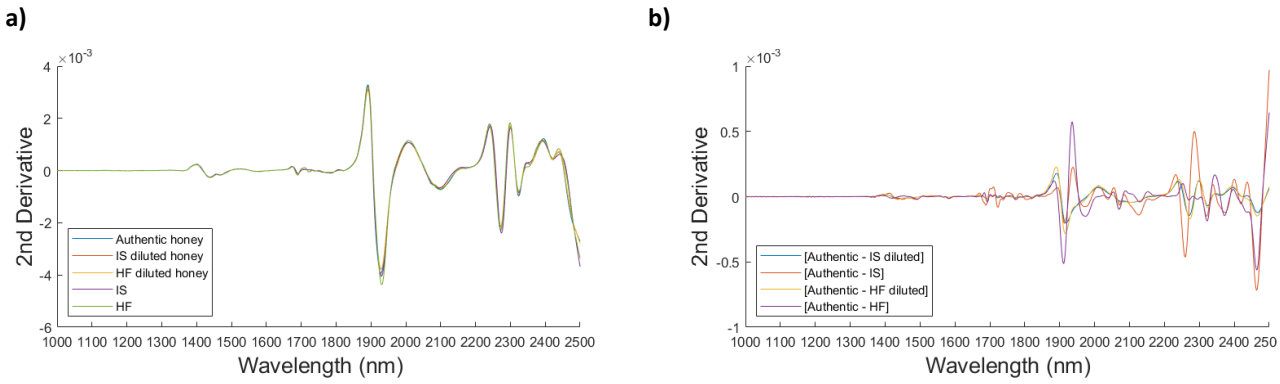

Figure 4.5 Average 2nd derivative (3, 11) a) spectra and b) difference spectra of $D_0 - D_9$ within each dilution class (authentic class with IS-diluted and HF-diluted classes subtracted), irrespective of irradiation.

Variation between the different dilution classes was evident (**Figure 4.5b**) These plots confirm that the dilution of honey with the chosen diluents does change the composition or physical properties of honey in a way that can be detected by NIR spectroscopy. Beyond the shared absorbance peaks indicated, noticeable differences in the absorption bands of the two diluted classes were observed at 1919, 2075 and 2110 nm. When individual diluent level classes were plotted, unique spectral differences could be seen at 1953, 2075 and 2110 nm (**Figure 4.7**).

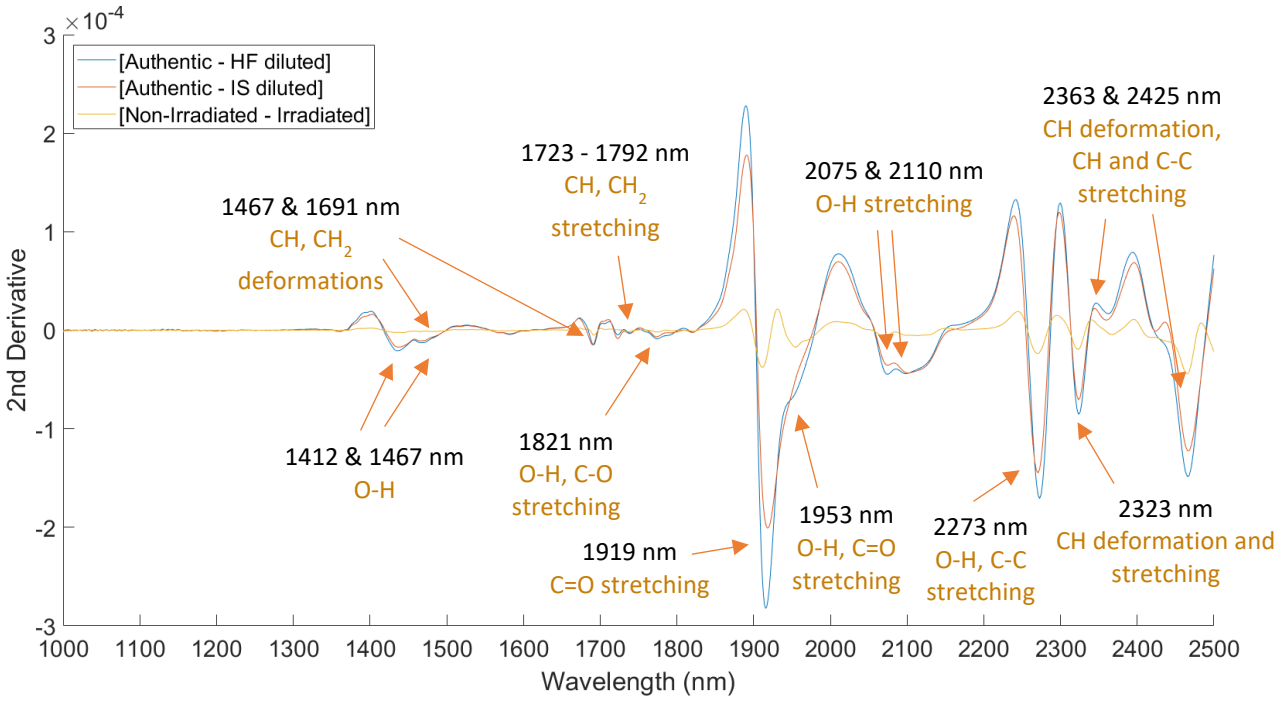

Figure 4.6 Second derivative difference spectra of D_0 – D_9 within each dilution class (authentic class with IS-diluted and HF-diluted classes subtracted) and irradiation treatment class (non-irradiated – irradiated), with prominent negative peaks indicated.

Downey *et al.* (2003) identified general absorption bands at 1460–1466, 1936–1938, 2094–2100 and 2276–2278 nm in NIR spectra of authentic honey as well as fructose and glucose solutions. In the same study, minima identified in 2nd derivative processed spectra were found to be specific to the authentic honey (1436, 1722, 1928, 2100, 2276 and 2322 nm), fructose solutions (2266, 2276, 2322, 2354, 2376, 2420, 2448 and 2484 nm), and glucose solutions (2276, 2324 and 2454 nm).

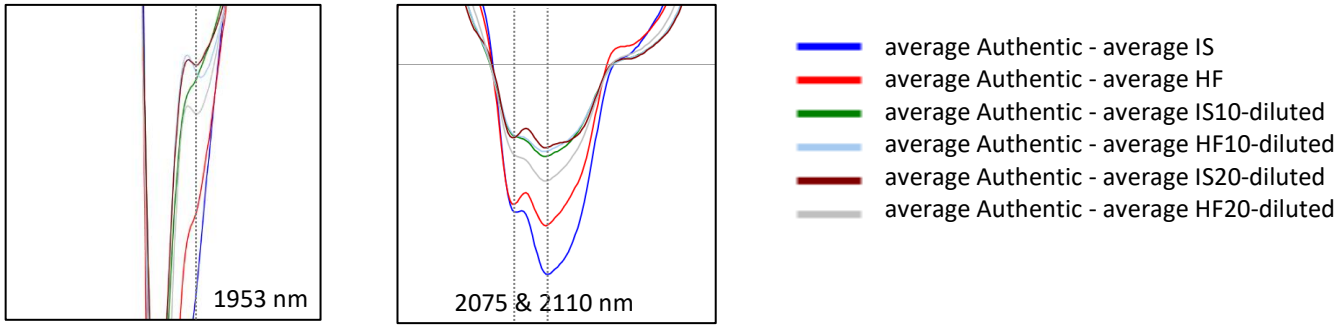

Figure 4.7 Enlarged sections of second derivative difference spectra of D_0 – D_9 within each dilution class (authentic class with HF-diluted (10-20%), IS-diluted (10-20%), HFCS (100%) and ICSS (100%) classes subtracted) with prominent negative peaks indicated.

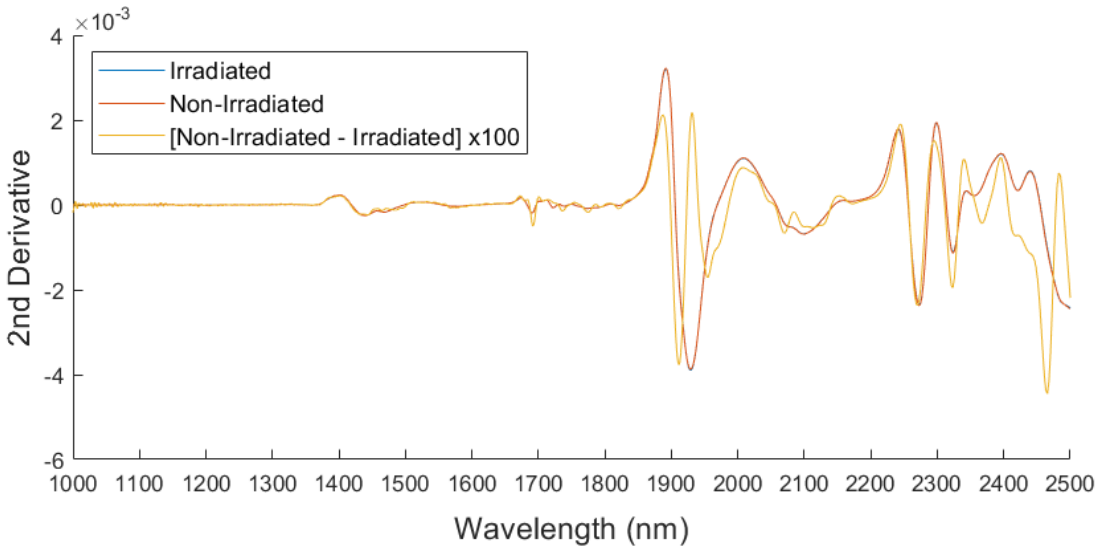

Figure 4.8 Second derivative difference spectra of D_0 – D_9 irradiation class (irradiated class subtracted from non-irradiated class), irrespective of dilution, with substantial peaks indicated.

Differences in very similar wavelength regions were observed in the 2nd derivative non-irradiated and irradiated spectra, as in the dilution class spectra. However, the magnitude of the variation displayed was far less than that of the diluted classes. This suggests that the effect of irradiation is far less prominent than the effect of dilution, as was anticipated.

4.2.2. Principal Component Analysis

Dilution trial

PCA was calculated on the combined D_{All} dataset, after the spectral range was reduced to 1300 – 2450 nm as it contained most spectral variation and the least observable noise. SNV and detrend (2nd order polynomial) pre-processing was applied. An influence plot, of Hotelling's T^2 against Q-residuals (95%), was constructed to assess whether outlying samples should be removed (**Figure 4.9**). Influential spectra were removed if sufficient evidence of spectral errors or non-conformities could be found. A number of samples found in the upper right quadrant or 'outlier' region, which had high leverage and were not well-modelled were identified as potential outliers, but only seven were removed, as evidence of spectral non-conformities in these samples could be found.

PCA was re-calculated on the combined D_{All} dataset after outlier removal, for evaluation of scores and loading line plots. The variance was considered to be predominantly explained by PC1 (77%), PC2 (15%), PC3 (4%), PC4 (2%) and PC5 (1%) at which point the explained variance curve had reached a plateau. Score plots of PCs 1-5 are shown, to illustrate distinct clustering and meaningful separation of the different experimental design factors (**Figures A1** to **A4, Appendix I**). PCs 6 – 7, each accounting for less than 1% of the variation, did not reveal any meaningful clustering or separation.

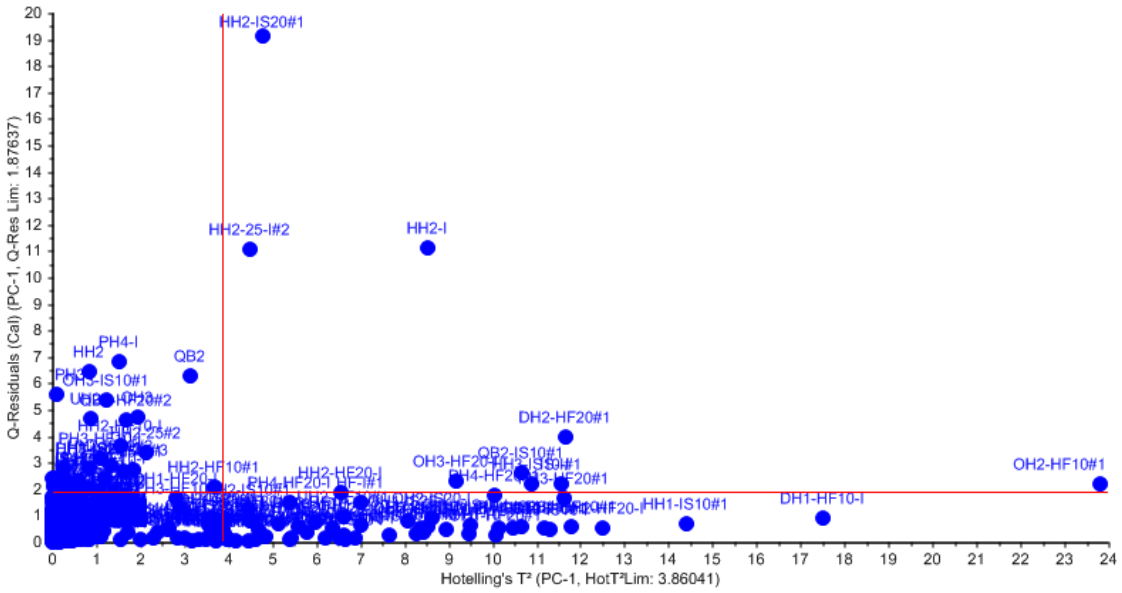

Figure 4.9 Hotelling's T^2 (95%) and Q-residuals (95%) plot of PC1 of the A_{All} dataset, prior to outlier removal.

The scores plot of **PC1 (77%)** vs. **PC2 (15%)** revealed two distinct clusters, a smaller dispersed cluster in the PC1(+) region and a larger, densely packed cluster in the PC1(-) region. The smaller cluster consisted of some samples from the D_0 acquisition class, confirmed by highlighting the diluent type (**Figure 4.10a**) and acquisition month classes (**Figure 4.10a**). This group of spectra were the 81 spectra from D_0 that exhibited a vastly different baseline offset, but was clearly sufficiently populous and carried enough leverage to prevent being pushed into the outlier region of the influence plot (**Figure 4.9**). The separation of diluent type is only partial, as the larger cluster contained samples of all three diluent type classes (**Figure 4.10a**). There were no trends among the diluted or individual diluent type classes evident in any of the other principal components.

The PC1 loadings line plot showed a positive peak at 1940 nm, as well as features at 1430 and 1580 nm (all three regions associated with OH stretching or deformation of H_2O; 1580 nm also associated with fructose), 1880 (unassigned, but located in region associated with OH, CH and CH_2 deformations, 1st overtone) and 2150-2400 nm (CH and CH_2 combinations, fundamental absorptions; or OH, CH and CH_2 deformations of H_2O and sugars, 1st overtone). The correlation loadings showed that all the identified features were significant and interpretable (**Figures 4.10b**) **i-ii**). The positive peak at 1940 nm, related to moisture content or the interaction of moisture with other constituents, appears to be driving the separation of the smaller diluted-only cluster from the larger cluster in PC1. It is worth noting that during spectral acquisition, traces of crystallization were observed in some honey samples after the standardized liquefication protocol was followed. Bakier (2009) found that the peak area of NIR absorption between 1876 -2014 nm showed a strong correlation to changes in water activity induced by crystallization of honey. It is strongly suspected that interference due to crystallization is present in the spectral data and is being explained by PC1.

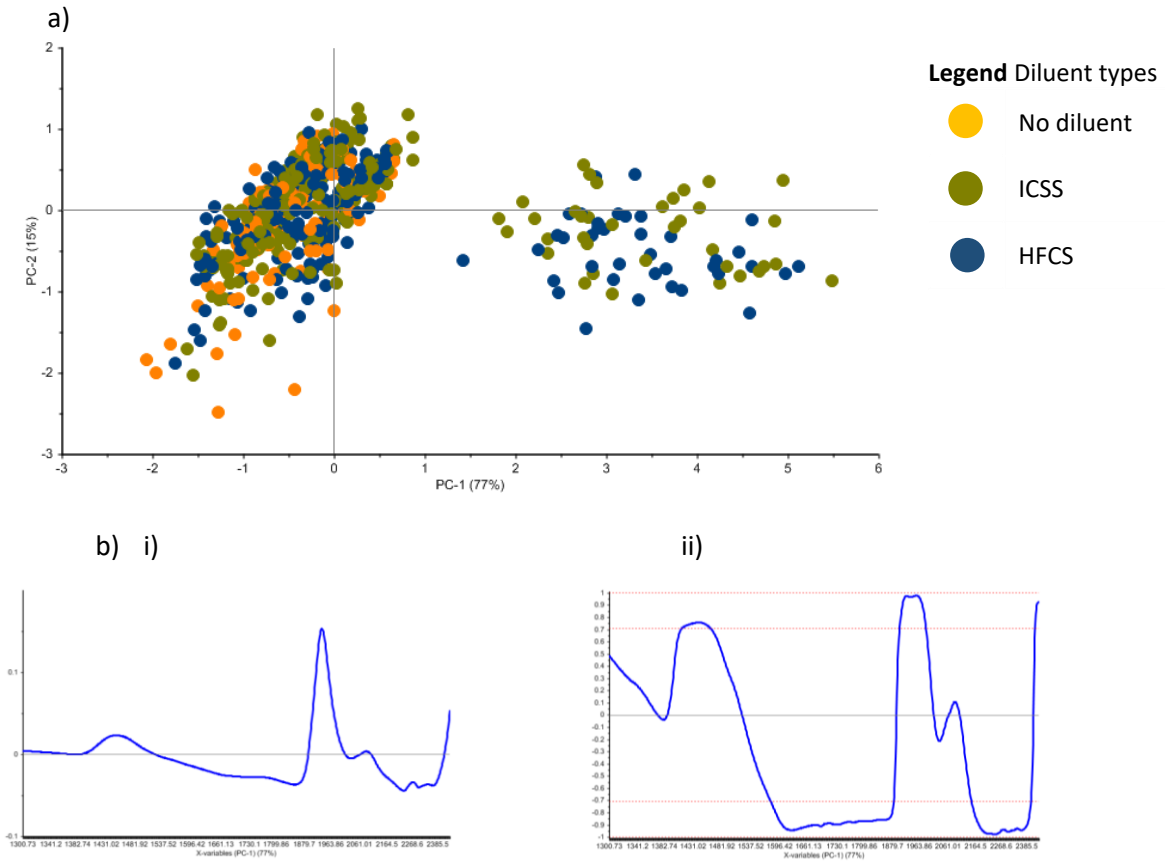

Figure 4.10 a) PCA score plot of PC1 (77%) vs. PC2 (15%), with diluent type classes highlighted - no diluent (**orange**), ICSS (**green**), HFCS (**dark blue**), b) **PC1** i) loadings line and ii) correlation loadings line plot of D_{All} data (SNV, DT (2) and MC).

No area of the plot could be designated to a specific diluent class, although some overlapping clustering of the non-adulterated class and the two diluent classes could be seen in the first principal component. This can be attributed to the strong similarities in chemical composition of the selected diluent syrups and the honey samples used to simulate dilution. It was not possible to attribute the separation to a single component in honey, but it appears that moisture, followed by the sugar components of honey are responsible. This is expected, as dilution with corn syrup is known to cause a change in the predominant water species present in honey (Bázár *et al.*, 2016). The high fructose content of the diluents is also expected to slightly increase the fructose: glucose ratios of the diluted honey.

PC3 (4%) vs. **PC4 (2%)** revealed a trend in the acquisition month classes, with months 0 and 3 lying predominantly in the PC4(+) region and months 6 and 9 predominantly in the PC4(-) region (**Figure 4.11a**). The **PC4** loadings line plot showed positive peaks at 1434 (OH stretching of H_2O and R-OH, 1st overtone), 1917 (OH stretching and deformation of H_2O and R-OH, combination bands) and 2147 nm (CH combination bands of sugars) and a negative peak at 1984 nm (OH stretching and deformation of H_2O and R-OH, combination bands) (**Figure 4.11b**) **i**). The correlation loadings showed no interpretable bands or peaks (**Figure 4.11b**) **ii**), so interpretations should be made with caution. Moisture appeared to be driving the graduated trend among

the acquisition month classes, which could also be considered ageing classes. While the moisture content of samples during spectral acquisition is kept constant by the adjustment of °Brix, the ageing of honey may have an effect on the interaction of moisture with other honey constituents. Again, absorption between 1876 - 2014 nm may be affected by changes in water activity induced by the crystallization of honey over prolonged storage (Bakier, 2009).

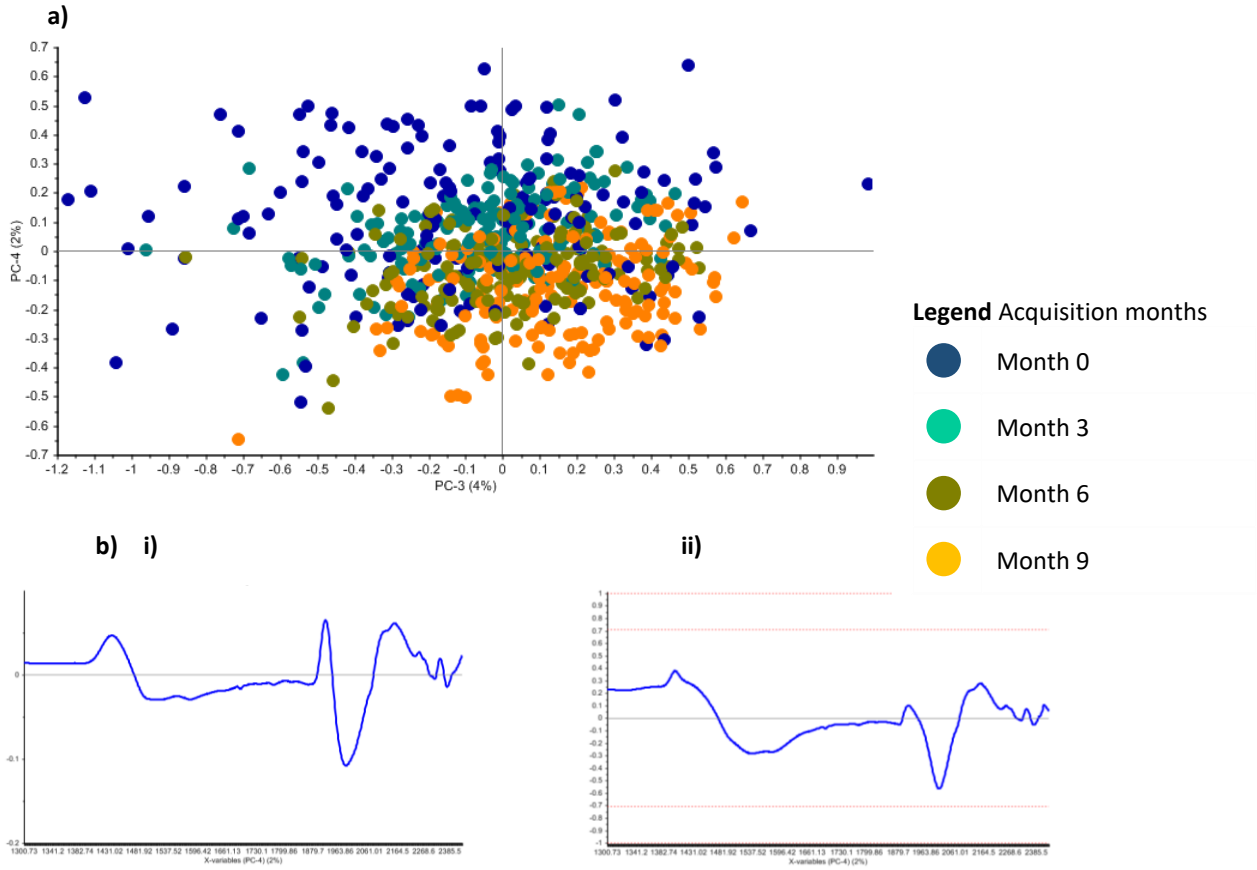

Figure 4.11 a) PCA score plot of PC3 (4%) vs. PC4 (2%), with acquisition month classes highlighted – month 0 (**dark blue**), month 3 (**light blue**), month 6 (**green**), month 9 (**orange**), b) **PC4** i) loadings line and ii) correlation loadings line plot of D_{All} data (SNV, DT (2) and MC).

PC4 (2%) vs. PC5 (1%) did not appear to contain meaningful clustering or separation in any of the four highlighted class groupings (**Figures A1** to **A4, Appendix I**). Additionally, no clustering or separation based on diluent level (**Figure A2, Appendix I**), nor irradiation treatment (**Figure A4, Appendix I**) could we seen in any of the PC1-5 scores plots.

Storage Trial

PCA was calculated on the combined A_{All} dataset, after the spectral range was again reduced to 1300 – 2450 nm, and SNV and detrend (2nd order polynomial) as well as 2nd Savitzky-Golay derivative (3nd order polynomial, 15 smoothing points) pre-processing were applied separately. The PCA of the 2nd Savitzky-Golay derivative (3nd order polynomial, 15 smoothing points) pre-processed data was added, as it revealed information on an experimental design factor that was not evident in the SNV and detrend (2nd order

polynomial) PCA. An influence plot, of Hotelling's T^2 against Q-residuals (95%), was constructed to assess whether outlying samples should be removed (**Figure 4.12**). Nine samples found in the upper right quadrant or 'outlier' region, which had high leverage and were not well-modelled were evaluated as potential outliers, but only three were removed, as evidence of spectral non-conformities could be found in these spectra.

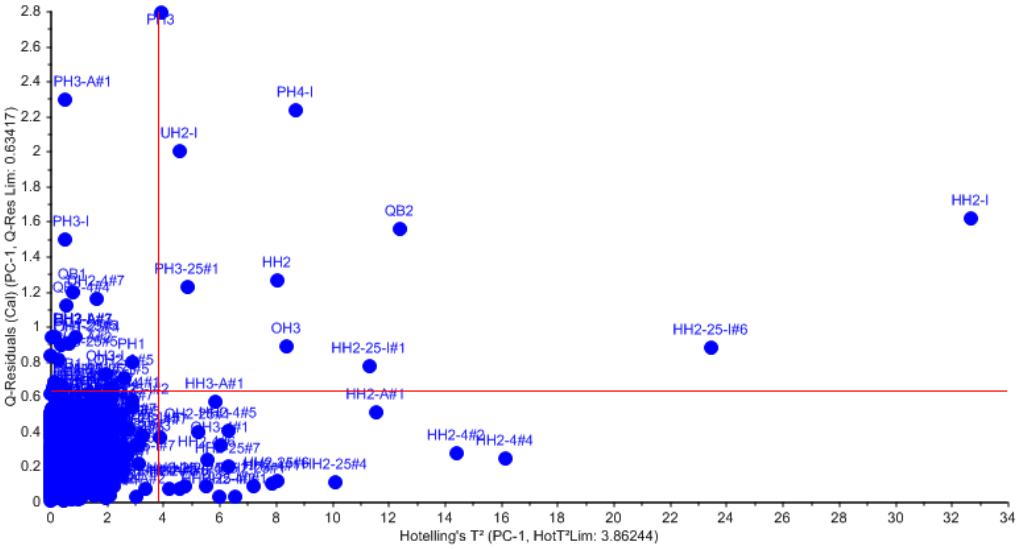

Figure 4.12 Hotelling's T^2 (95%) and Q-residuals (95%) plot of PC1 of the A_{All} dataset, prior to outlier removal.

PCA was re-calculated on the combined A_{All} dataset after outlier removal, for evaluation of scores and loadings plots. For the SNV and detrend (2nd order polynomial) data, the variance was predominantly explained by PC1 (72%), PC2 (14%), PC3 (7%), PC4 (3%) and PC5 (2%) after which the explained variance curve began to plateau. Score plots of PCs 1-5 are shown, to illustrate distinct clustering and meaningful separation of the different experimental design factors (**Figures A6** to **A9, Appendix I**). PCs 6 – 7, which accounted for less than 1% of the variation each, did not reveal any meaningful clustering or separation.

From the scores plots of **PC1 (72%)** vs. **PC2 (14%)** of the SNV and detrend (2nd order polynomial) pre-processed data, partial clustering of honey type classes could be seen, although no distinct separation was observed (**Figure 4.13a**). Most notably, honey types 2, 4, 5, 8, 9 and 12 were predominantly found in the PC1(-) region, while honey types 1, 6, 7, 10, 11, 16 and 17 were associated with the PC1(+) region. Types 3, 13, 14 and 15 were evenly positioned close to 0. A positive peak at 1940 (OH stretching and deformation of H_2O and R-OH, combination bands), and negative features at 1490 (OH stretching of H_2O and R-OH, 1st overtone), 2064-2367 nm (OH, CH and C=O combination bands of H_2O and sugars) in the PC1 loadings line contributed to the separation and were interpretable (**Figure 4.13c**) **i-ii**). Variation between the honey type classes appeared to be driven by moisture content or interactions, as well as naturally occurring sugar content variations or crystallization. Woodcock *et al.* (2007) found that honey samples of different provenance exhibited much variation around 1935 and 2097 nm, due to O-H and C-H combination bands, respectively. Accordingly, it is expected for there to be considerable variation in these regions between honey samples of different provenance, which was intentionally maximized for the present study.

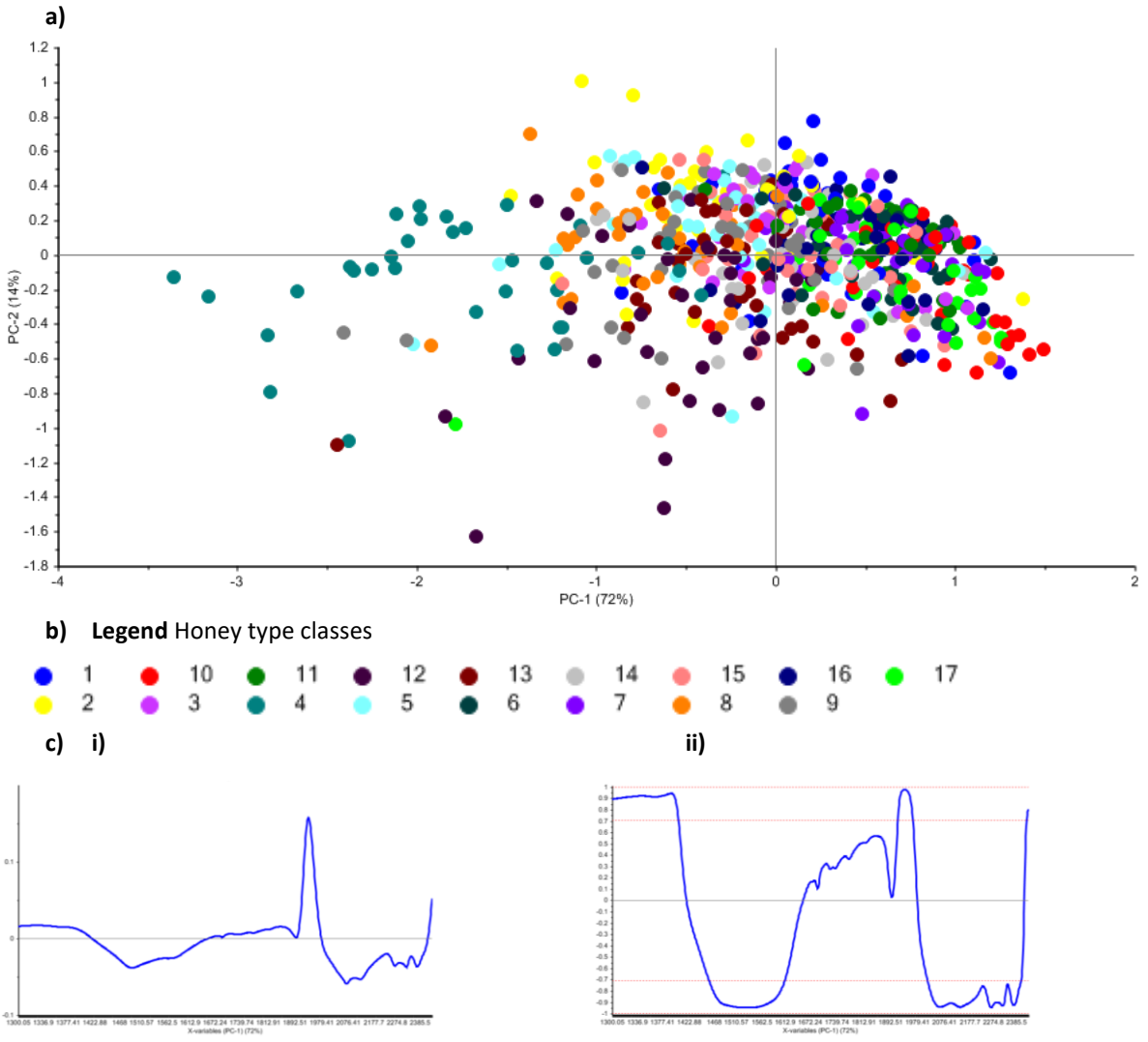

Figure 4.13 a) PCA score plot of PC1 (72%) vs. PC2 (14%), with honey type classes highlighted according to b) bulk honey sample number key, c) PC1 i) loadings line and ii) correlation loadings line plot of A_{All} data (SNV, DT (2) and MC).

The scores of **PC2 (14%)** vs. **PC3 (7%)** of the SNV and detrend (2nd order polynomial) pre-processed data revealed two clusters, a sparse cluster in the in the PC3 (+) region and a large, densely packed cluster in the PC3 (-) region (**Figures A6** to **A9, Appendix I**). The two clusters contained similar proportions of all the treatment classes investigated and could not be attributed to any specific experimental design effect.

In contrast, the scores of **PC2 (12%)** vs. **PC3 (6%)** of the 2nd Savitzky-Golay derivative (3nd order polynomial, 15 smoothing points) pre-processing data contains variation that separates the 40°C storage temperature class from the other classes in the PC3 direction (**Figure 4.14a**). The 40°C storage temperature class is distinctly positioned in the PC3 (-) region, while the remaining classes are distributed across the positive and negative regions. The loadings line and correlation loadings for PC3 revealed interpretable peaks at 2246, 2343, 2401 and 2443 nm in the positive region, and at 1490, 1691, 2073, 2131, 2265, 2323 and 2367 nm in the negative region (**Figure 4.14b**) **i-ii**). The loading line plots were quite varied and complex,

corresponding to regions related to the 1st overtones of OH, CH and CH_2 stretching and deformation, and combination bands of OH, CH and CH_2 (Golic *et al.*, 2003). Most notably, two of the largest peaks in the negative region, 2265 and 2323, were related to fructose and glucose (Downey *et al.*, 2003). This could be due to sucrose breaking down into its fructose and glucose components over time and at elevated temperatures, but potentially also influenced by decomposition reactions of fructose and glucose into furans, such as the well-known storage and heating marker, 5-HMF (Da Silva *et al*., 2016).

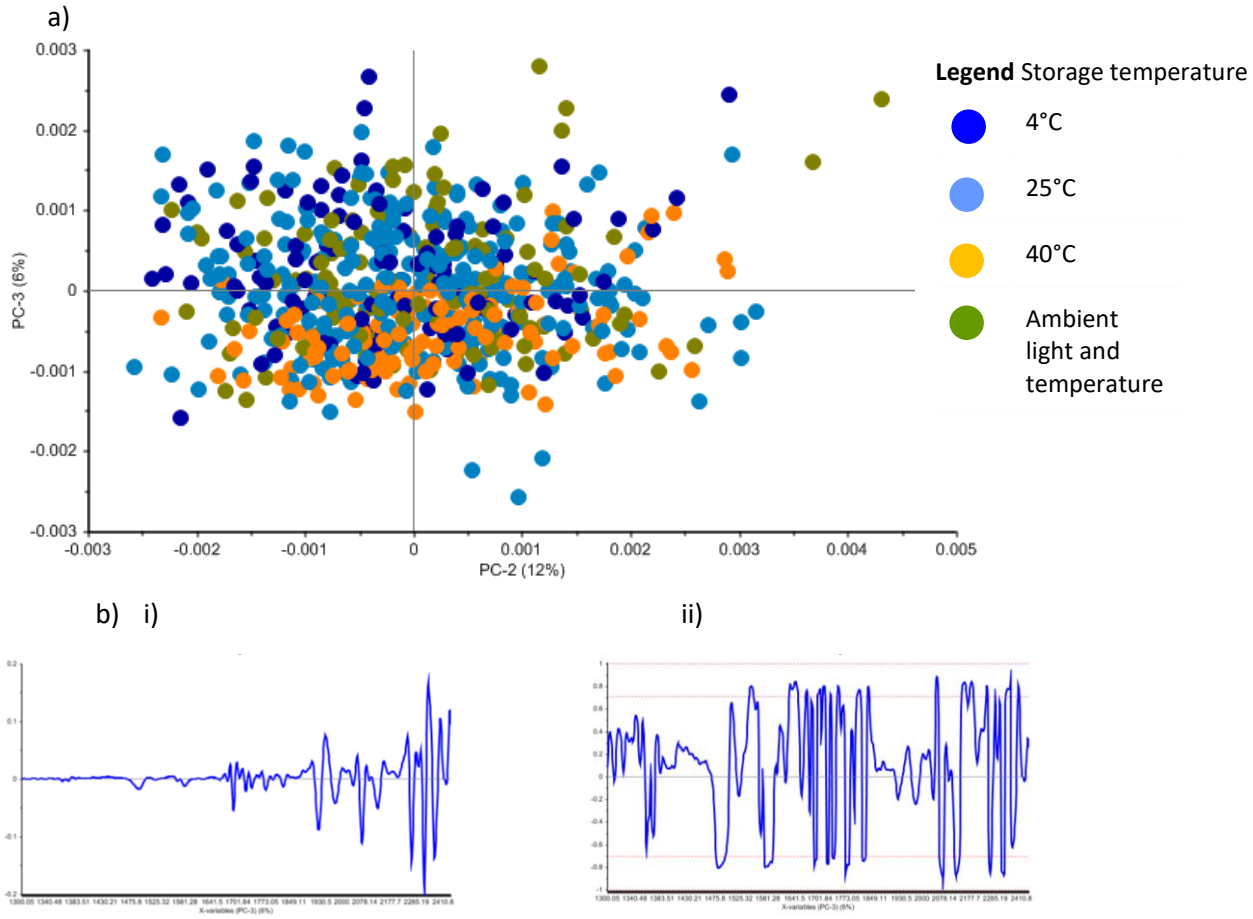

Figure 4.14 a) PCA score plot of PC2 (12%) vs. PC3 (6%), with storage temperature classes highlighted – 4°C (**dark blue**), 25°C (**bright blue**), 40°C (**orange**), ambient light and temperature (**green**), b) **PC3** i) loadings line and ii) correlation loadings line plot of A_{All} data (2nd derivative SG (3, 15)).

PC3 (7%) vs. **PC4 (3%)** of the SNV and detrend (2nd order polynomial) pre-processed data revealed a distinction in the spectral acquisition month classes (**Figures 4.15a**), with M_0 and M_3 positioned in the negative region of PC4 and M_6 and M_9 positioned in the positive region, forming an acquisition date gradient. In the PC4 loadings line, prominent peaks were found at 1440, 1921, 2110, 2153 nm in the positive direction, and 1974 nm in the negative direction, contributing to separation (**Figure 4.15b**) **i**). The correlation loadings did not reveal any interpretable bands or peaks (**Figure 4.15b**) **ii**), thus interpretations should be made with caution.

Moisture appeared to be driving the graduated trend among the acquisition month classes, which could also be considered ageing classes. Features attributed largely to moisture were associated with the positive region, and therefore the younger samples. While the moisture content of samples during spectral acquisition is kept constant by the adjustment of °Brix, the ageing of honey may have an effect on the interaction of moisture with other honey constituents. Again, absorption between 1876 -2014 nm may be affected by changes in water activity induced by the crystallization of honey over prolonged storage (Bakier, 2009).

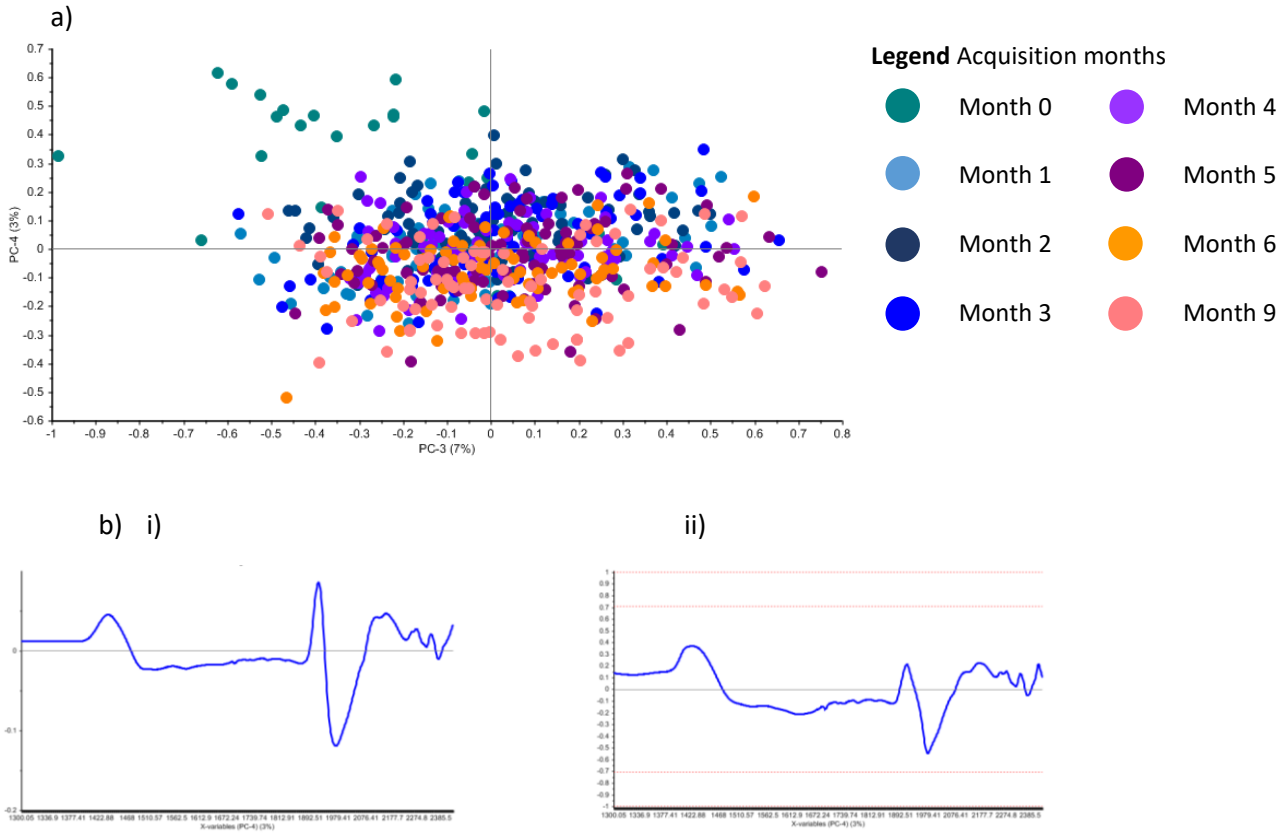

Figure 4.15 a) PCA score plot of PC3 (7%) vs. PC4 (3%), with acquisition month classes highlighted – month 0 (**teal**), month 1 (**light blue**), month 2 (**dark blue**), month 3 (**bright blue**), month 4 (**indigo**), month 5 (**purple**), month 6 (**orange**) and month 9 (**pink**), b) **PC4** i) loadings line and ii) correlation loadings line plot of A_{All} data (SNV, DT (2) and MC).

Scores plots of PC4 (3%) vs. PC5 (2%) did not reveal any distinct clustering or separations in any of the four highlighted class groupings (**Figures A6** to **A9, Appendix I**). No separation based on irradiation treatment (**Figure A9, Appendix I**) could be seen in any of the PC1-5 scores plots. The irradiation treatment classes showed the least distinction between classes, likely due to the largely insignificant changes between the irradiated and non-irradiated classes. On the whole, clear separation of the dilution experimental design factors was lacking in PCA, indicating a need for alternative exploratory data analysis tools, as well as suggesting that a PCA-based classification method, such as SIMCA, would likely not be a suitable solution for this authentication problem.

4.2.3. ANOVA Simultaneous Component Analysis (ASCA)

ASCA was conducted separately on the Storage and Dilution Trial datasets. In the latter, the syrup control samples were omitted, to prevent skewing of the results. For both trials, a wavelength range of 1300 – 2450 nm was chosen, as it contained most spectral variation and the least observable noise. SNV, detrend (2nd order polynomial) and mean-centering pre-processing was applied to remove unwanted multiplicative and additive effects from the spectra of both datasets. A t-test at the 0.05 significance level with 100 permutations was performed in order to determine the statistical significance of each factor. A small p-value (≤ 0.05) indicates strong evidence contradicting the null hypothesis, prompting its rejection, while a large p-value (> 0.05) indicates weak evidence contradicting the null hypothesis, which is consequently not rejected.

Storage Trial

The honey type, age and storage temperature factors were found to have a significant (p = 0.05) effect on the spectral data, while irradiation treatment did not (**Table 4.1**). Honey type variation was intentionally maximized for this study, so this was expected. Honey type, age and temperature factors all showed significant two-way interaction effects among themselves.

Table 4.1 ASCA results of the Storage Trial dataset, SNV, detrend (2nd order polynomial) and MC pre-processing

Term	PCs	Cumulative Eigenvalue	Effect	P-value	Significant (p = 0.05)
Experimental design factors					
(F1) – Honey type	16	0.37	49.78	0.0016	**Yes**
(F2) - Age	6	0.03	3.48	0.0016	**Yes**
(F3) - Temperature	2	0.04	6.02	0.0016	**Yes**
(F4) - Irradiation	1	0	0.05	0.0274	No
Interaction of factors					
(F1) x (F2)	20	0.07	9.62	0.0016	**Yes**
(F1) x (F3)	20	0.05	6.56	0.0016	**Yes**
(F1) x (F4)	18	0.01	1.21	0.1032	No
(F2) x (F3)	20	0.02	2.29	0.0016	**Yes**
(F2) x (F4)	10	0	0.54	0.3484	No
(F3) x (F4)	3	0	0.38	1	No
Mean	-	-	0	-	-
Residuals	-	-	24.07	-	-

Dilution Trial

The honey type, diluent type and age factors had a significant effect on the spectral data, while diluent level and irradiation treatment did not (**Table 4.2**). These results explained to some extent why strong trends were not evident in the PCA, as the effect of the variation caused by diluent type was significant but still small compared to the variation contributed by the honey type and age factors. Honey type and age, as well as honey type and irradiation showed significant interaction effects. The latter finding was unexpected, but could be substantiated with experimental observations, discussed further in **5.1.4 Classification of Irradiation Treatment**.

Table 4.2 ASCA results of the Dilution Trial dataset, SNV, detrend (2nd order polynomial) and MC pre-processing

Term	PCs	Cumulative Eigenvalue	Effect	P-value	Significant (p = 0.05)
Experimental design factors					
(F1) – Honey type	16	0.32	45.56	0.01	**Yes**
(F2) – Diluent type	2	0.01	1.85	0.04	**Yes**
(F3) - Diluent level	2	0.01	1.62	0.44	No
(F4) - Age	6	0.05	6.64	0.01	**Yes**
(F5) - Irradiation	1	0	0.18	0.06	No
Interaction of factors					
(F1) x (F2)	20	0.03	4.25	0.98	No
(F1) x (F3)	20	0.03	4.39	0.95	No
(F1) x (F4)	20	0.07	10.08	0.02	**Yes**
(F1) x (F5)	18	0.01	1.48	0.03	**Yes**
(F2) x (F3)	4	0.01	1.52	0.78	No
(F2) x (F4)	11	0.01	1.51	0.98	No
(F2) x (F5)	4	0	0.1	0.8	No
(F3) x (F4)	11	0.01	1.51	0.67	No
(F3) x (F5)	4	0	0.06	0.96	No
(F4) x (F5)	10	0	0.39	0.58	No
Mean	-	-	0	-	
Residuals	-	-	37.78	-	

The lack of agreement between the ASCA results of the two trials, with respect to the irradiation treatment, could also be as a result of the size of the represented populations: the number of irradiated samples included in the Storage Trial dataset was 17, while in the Dilution Trial dataset it was 85, i.e. 5 times larger, and included samples that were not pure honey.

The results of ASCA must be interpreted with caution, as the significance of a design factor may not be a direct indicator of the success of a classification model, as it is a measure of the global variation of that factor, while detection of adulteration by dilution may be dependent on subtle or waveband-dependent differences in spectral data.

4.2.4. Spectral Contrast Angle (SCA)

The spectral contrast angle (SCA) method was employed to compare the similarity between dilution and irradiation treatment classes. The spectral contrast angles of the dilution and irradiation treatment classes were compared, using an average spectrum of each class. MSC pre-processed spectral data was used to remove effects of scattering. A vector was generated to represent the prominent absorbance peaks within each averaged class spectrum under consideration, with the angle between vectors of two spectra being calculated as a measure of the similarity of that spectral pair.

A total of 13 substantial absorbance peaks present in the dilution classes of spectra under investigation were identified, based on the largest 2nd derivative difference peaks previously identified in **2.1. Derivation**. The absorbance values of the substantial peaks were averaged across replicates within each class. Class-representing vectors were calculated for the authentic, HF-diluted (10-20%) and IS-diluted (10-20%) classes, respective and irrespective of irradiation (**Table 4.3**). Spectral contrast angles were then computed for the Authentic vs. IS-diluted, Authentic vs. HF-diluted, Authentic vs. diluted (combined), and IS-diluted vs. HF-diluted class combinations (**Table 4.4**). A spectral contrast angle close to zero implies a strong degree of similarity between two spectra, while an angle close to 0.5π suggests a large degree of dissimilarity.

Similarly, a total of 7 substantial absorbance peaks present in the irradiation treatment classes of spectra under investigation were identified, based on the largest 2nd derivative difference peaks (**Figure 4.6**). The absorbance values of the substantial peaks were averaged, and class-representing vectors were calculated for the irradiated and non-irradiated classes, respective and irrespective of dilution (**Table 4.5**). Spectral contrast angles were then computed for the All Non-Irradiated vs. All Irradiated, Authentic Non-Irradiated vs. Authentic Irradiated, and Diluted Non-Irradiated vs. Diluted Irradiated class combinations (**Table 4.6**).

Table 4.3 Identified substantial absorbance peaks and calculated class-representative vectors of dilution classes

Wavelength (nm)		Authentic (a)	IS-diluted (b)	HF-diluted (c)	Diluted combined (d)
1	**1436**	0.9873	0.9309	0.9241	0.9275
2	**1467**	1.082754	1.0191	1.0119	1.0155
3	**1691**	0.6023	0.5563	0.5508	0.5535
4	**1723**	0.6079	0.5608	0.5547	0.5577
5	**1739**	0.6167	0.5689	0.5623	0.5656
6	**1774**	0.6286	0.5796	0.5721	0.5759
7	**1792**	0.6175	0.5686	0.5612	0.5649
8	**1821**	0.5852	0.5371	0.5300	0.5335
9	**1919**	2.0854	1.9775	1.9513	1.9644
10	**1953**	2.2725	2.1589	2.1346	2.1468
11	**2075**	1.6447	1.5297	1.5136	1.5217
12	**2273**	1.2291	1.1310	1.1147	1.1229
13	**2323**	1.2974	1.1943	1.1744	1.1843
	Vector (r)	4.4487	4.1734	4.1237	4.1486

a) average of 399 spectra, b) average of 813 spectra, c) average of 813 spectra, d) average of 1626 spectra

Table 4.4 Spectral Contrast Angles of dilution classes

	Authentic vs. IS-diluted	Auth. vs. HF-diluted	Auth. vs. Diluted	HF-diluted vs. IS-diluted
SCA (θ)	0.0131	0.0142	0.0136	0.0024

Table 4.5 Identified substantial absorbance peaks and calculated class-representative vectors of irradiation classes

Wavelength (nm)		All Irr. (a)	All non-Irr. (b)	Auth. Irr. (c)	Auth. Non-Irr (d)	Diluted Irr. (e)	Diluted Non-Irr. (f)
1	**1691**	0.5608	0.5651	0.6049	0.5998	0.5608	0.5651
2	**1736**	0.5721	0.5764	0.6182	0.6126	0.5721	0.5764
3	**1774**	0.5838	0.5882	0.6316	0.6257	0.5838	0.5882
4	**1911**	1.7085	1.7166	1.8152	1.7905	1.7085	1.7166
5	**1955**	2.1443	2.1535	2.2660	2.2331	2.1443	2.1535
6	**1975**	1.8017	1.8119	1.9182	1.8892	1.8017	1.8119
7	**2046**	1.3962	1.4059	1.5020	1.4810	1.3962	1.4059
8	**2070**	1.5198	1.5301	1.6341	1.6113	1.5198	1.5301
9	**2099**	1.5728	1.5831	1.6914	1.6678	1.5728	1.5831
10	**2271**	1.1333	1.1414	1.2313	1.2141	1.1333	1.1414
11	**2323**	1.2017	1.2108	1.3066	1.2883	1.2017	1.2108
Vector (r)		4.6051	4.6322	4.9261	4.8573	4.6051	4.6322

a) average of 1014 spectra, b) average of 1011 spectra, c) average of 198 spectra, d) average of 201 spectra, e) average of 816 spectra, f) average of 810 spectra

Table 4.6 Spectral Contrast Angles of irradiation treatment classes

	All Irr. vs. All Non-Irr.	Authentic Irr. vs. Authentic Non-Irr.	Diluted Irr. vs. Diluted Non-Irr.
SCA (θ)	0.00117	0.00124	0.00128

Using the spectral contrast angle as an approximation of spectral similarity, the observation could be made that the SCA of the irradiated and non-irradiated authentic classes was highly similar to that of the irradiated and non-irradiated diluted classes. The irradiation of samples could be said to be affecting the authentic and diluted samples equally. The SCA of all irradiated vs. all non-irradiated classes was less than ten times smaller than the SCA of the authentic vs. diluted classes. From this, the conclusion could be drawn that the irradiation of samples affected the spectral data very minimally. In numerical terms, if the maximum SCA of 0.5π is considered to be 100% dissimilarity, irradiation treatment induced a 0,737 – 0,807% change in SCA, while dilution exacted a change of 8,25 – 8.89%. However, it must be noted that SCA relies on the condensation of a 1501 variable spectrum to a 11 to 13 variable array to a single vector and should be regarded as a generalization.

4.3. MULTIVARIATE DATA ANALYSIS

4.3.1. PLS-DA

Preliminary classification models were built using both SIMCA and PLS-DA, of which PLS-DA proved to be the most effective. All PLS-DA models were built using all months' spectra within the Dilution Trial subset, and in selected models both the Storage and Dilution Trial, with all identified and verified outliers excluded. The spectra acquired in each month were treated as independent samples, given that the age or spectral acquisition date introduced the 2nd largest source of variation into the Dilution Trial dataset, more than diluent, dilution level and irradiation combined.

After PLS compression, the invert syrup and irradiated invert syrup samples from D_0, D_3, D_6, and D_9 were frequently found in the 'outlier' region but were not removed (Hotelling's T^2 and Q-residuals influence plot not shown). These samples, whose raw spectrum did not show signs of specular reflectance, are likely correctly captured but badly represented in relation to the entire sample set as they are the only pure invert syrup samples present. As these samples are expected to stand out from the honey samples, their inclusion in the dataset for further analysis is justified.

The Duplex algorithm was used to select calibration (70%) and validation (30%) sets that maintained representative diversity of the full dataset, for all classification approaches (Snee, 1977). Once split, the sets were checked to ensure the approximate proportions of authentic: diluted or irradiated: non-irradiated samples were retained. Venetian blinds, 10-fold cross-validation was used, and the number of latent variables used for each model was determined by selecting the number of components that yielded the

lowest error of cross-validation and the best validation performance in terms of accuracy, sensitivity and specificity.

4.3.1.1. Comparison of Wavelength Ranges

Dilution detection, regardless of diluent or irradiation, also referred to as authentic vs. diluted classification models, were built using the original 1000-2500 nm range, as well as ranges of 1300-2450 and 1300-1800 nm. The 1300-2450 nm range was found to cover all substantial absorption and excluded regions that contained some noise or scattering of light in the raw spectra, while 1300-1800 nm was proposed as it has been found to contain sufficient spectral information to differentiate between authentic and HF-diluted honey samples in a similar study (Bázár *et al.*, 2016).

The results of the dilution detection models generated from different wavelength ranges (**Table 4.7**) were used to select an effective wavelength range. The models built on all three ranges showed similar, acceptable classification performances. All three ranges were more or less equally efficient (68.6-69.1%), but the ranges of 1000-2500 and 1300-2450 nm provided better accuracies (>70.0%), and of the two, 1300-2450 nm had better sensitivity. This range was used for all models built hereafter.

Table 4.7 Calibration and validation results of the best-performing PLS-DA models for general dilution classification: distinguishing between authentic vs. diluted classes, all BÜCHI D_{All} spectra, three spectral ranges. Sensitivity and specificity reported for the authentic class.

Range (nm)	Pre-processing	LVs	Calibration accuracy (%)	Validation accuracy (%)	Validation misclassification (%)	Sensitivity (%)	Specificity (%)	Efficiency (%)
1000-2500	SNV, 2nd derivative SG (3, 11) + MC	9	71.87	71.08	28.92	64.44	72.96	68.57
1300-2450	2nd derivative SG (3, 11) + MC	11	73.72	70.59	29.41	66.67	71.70	69.14
1300-1800	MC	9	63.86	66.67	33.33	73.33	64.78	68.92

4.3.1.2 Effect of Irradiation

To assess the implications of irradiation on the spectral data in a relatively simple, indirect manner, two dilution detection models were built with only irradiated spectra (346) and only non-irradiated spectra (345) with the 1300-2450 nm range, and compared to the previously constructed dilution detection model based on all spectra (691).

Dilution detection models generated from different irradiation treatment data subsets (**Table 4.8**) both had acceptable, but lower than desirable classification performances. The non-irradiated dataset model had marginally better validation accuracy, sensitivity and specificity, and therefore also an increased overall efficiency, than the irradiated dataset model. Score plots of both models (**Fig 4.16**) showed a large overlap of the authentic and diluted classes, giving further evidence of their unexceptional performance.

Table 4.8 Calibration and validation results of the best-performing PLS-DA models for dilution classification: distinguishing between authentic vs. diluted classes, irradiated dataset and non-irradiated dataset spectral subsets from BÜCHI D_{All} dataset, 1300 – 2450 nm spectral range. Sensitivity and specificity reported for the authentic class.

Data set	Pre-processing	LVs	Calibration accuracy (%)	Validation accuracy (%)	Validation misclassification (%)	Sensitivity (%)	Specificity (%)	Efficiency (%)
Irradiated	SNV, DT (2) + MC	6	62.55	62.14	37.86	66.67	60.76	63.64
Non-irradiated	SNV, 2nd derivative SG (3, 11) + MC	7	66.53	67.96	32.04	76.19	65.85	70.83

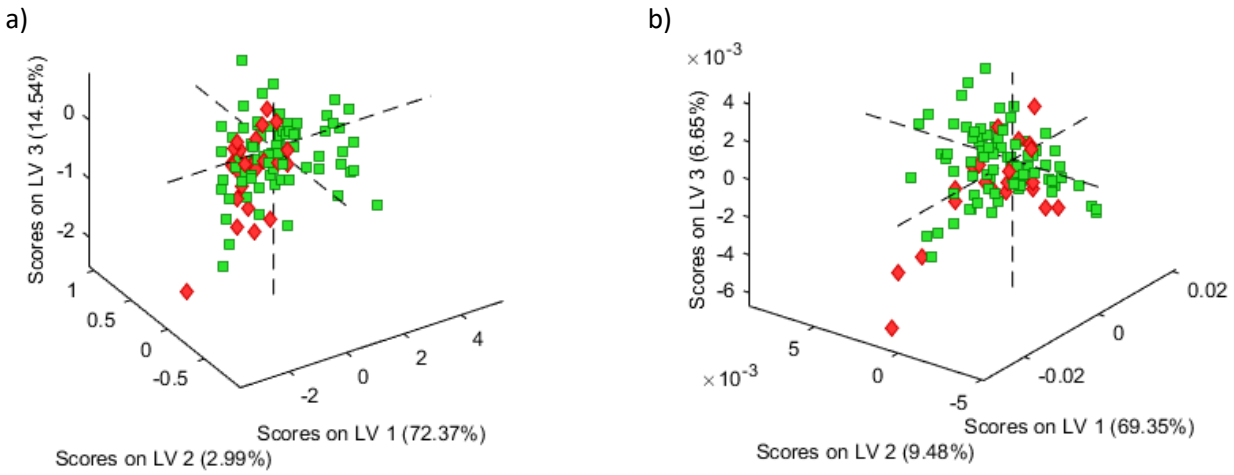

Figure 4.16 Authentic vs. diluted PLS-DA scores plots of **LV1** vs. **LV2** vs. **LV3,** for the a) irradiated dataset (MSC and MC, 9 LVs), and b) non-irradiated dataset (SNV, DT(2) and MC, 11 LVs), with authentic (**red**) and diluted (**green**) classes marked.

Despite irradiation not contributing to the overall variation significantly, the non-irradiated model proved to be a consistently better performing model. The irradiation and honey type interaction effect was previously found to be significant with ASCA, which would suggest that not all honey varieties respond in the same way to irradiation treatment, discussed in greater detail in **5.1.4 Classification of Irradiation Treatment.**

The VIP scores of the 'irradiated only' and 'non-irradiated only' models (**Figure 4.17** and **4.18**) were investigated in order to locate differences and compare the contributing variables. Large contributions from 2272 and 2437 nm, associated with C-H bonds and specifically fructose, and a split peak at 1925-1959 attributed to moisture, distinguished the non-irradiated VIP score contributions from the irradiated VIP scores, suggesting that irradiation treatment had interfered with these specific regions (Downey *et al.*, 2003; Thamasopinkul *et al.*, 2017).

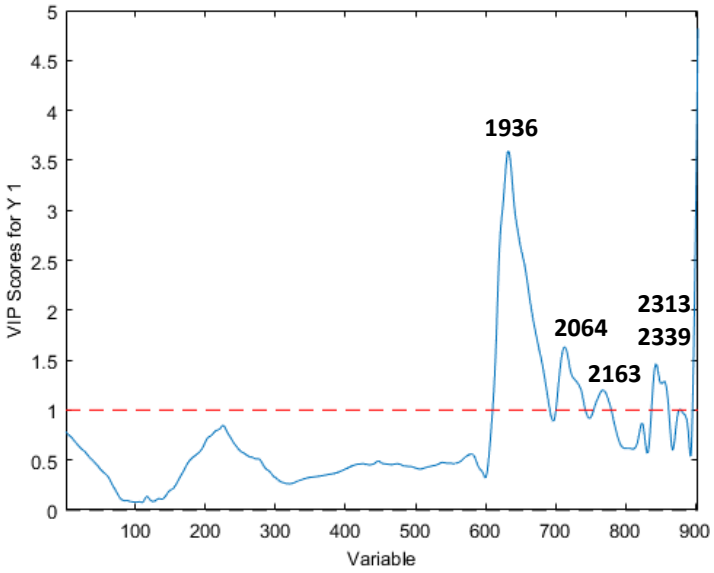

Wavelength assignments

1936 and **2064 nm** - O-H stretching and deformation (Osborne *et al.*, 1993)

2313 nm – C-H bonds (Herrero Latorre *et al.*, 2013)

2339 nm – C-H deformation and stretching; fructose (Downey *et al.*, 2003)

Figure 4.17 VIP scores showing the contribution of each wavelength to the Authentic vs. Diluted Irradiated model. The assignment of each wavelengths are given.

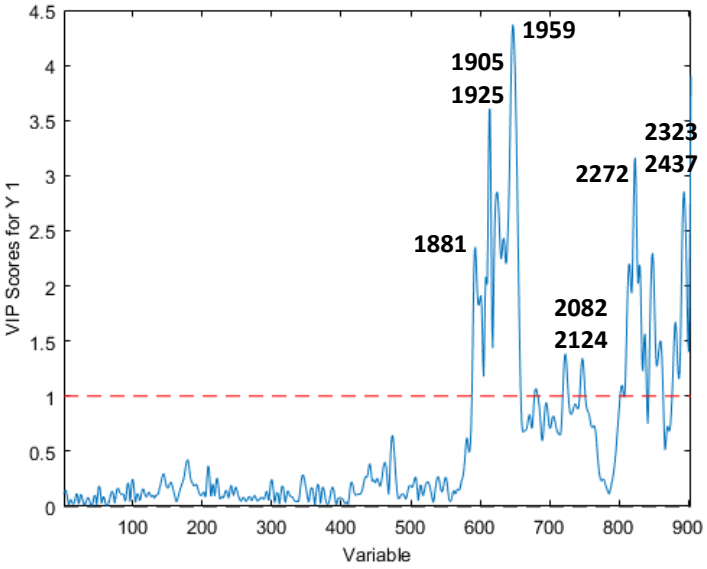

Wavelength assignments

1925, 1959 and **2082 nm** O-H stretching and deformation (Osborne *et al.*, 1993)

2124 nm C-H stretching and deformation; fructose (Rambla *et al.*, 1997)

2272 nm C-H stretching and deformation; fructose and glucose (Rambla *et al.*, 1997, Woodcock *et al.*, 2007)

2323 and **2437 nm** C-H deformation and stretching; fructose (Downey *et al.*, 2003)

Figure 4.18 VIP scores showing the contribution of each wavelength to the Authentic vs. Diluted Non-irradiated model. The assignment of each wavelengths are given.

4.3.1.3 Diluent and Dilution Detection

To build an 'optimised' diluent detection model, the Storage and Dilution datasets, excluding all identified and verified outliers, were combined to form a larger reference library with more realistic variation. This was done to simulate the comprehensive database that would need to be constructed prior to implementation of an authentication system. For 'optimization' the sensitivity of the models was prioritised over selectivity, as a conservative approach was desired for screening purposes: only accepting authentic samples and earmarking all other questionable samples for further authenticity testing with officially recognised methods. The performance of the ICSS and HFCS samples in preliminary multi-class models was uneven (**Figure 4.19** and **Table 4.9**), thus separate models, to be implemented sequentially, were proposed.

Classification					**Validation**				
n = 829	Actual Authentic	Actual IS-diluted	Actual HF-diluted	**Total**	n = 355	Actual Authentic	Actual IS-diluted	Actual HF-diluted	**Total**
Predicted Authentic	352	76	69	**497**	Predicted Authentic	126	44	34	**204**
Predicted IS-diluted	29	79	15	**123**	Predicted IS-diluted	11	36	9	**56**
Predicted HF-diluted	77	30	102	**209**	Predicted HF-diluted	31	14	50	**95**
Total	**458**	**185**	**186**		**Total**	**168**	**94**	**93**	

Figure 4.19 Confusion matrices describing the calibration and validation performance of the multi-class authentic vs. IS-diluted and HF-diluted honey model (SNV, 1st derivative SG (3, 11) and MC, 7 LVs).

Table 4.9 Performance measures of the validation of the multi-class authentic vs. IS-diluted vs. HF-diluted honey model (SNV, 1st derivative SG (3, 11) and MC, 7 LVs)

Performance measure	**Diluted**	**IS-diluted**	**HF-diluted**
Accuracy (%)	63.86	73.10	70.67
Precision (%)	61.76	64.29	52.63
Sensitivity (%)	75.00	38.30	53.76
Specificity (%)	52.44	89.80	78.26
Efficiency (%)	62.71	58.64	64.87

TN – true negative; FN – false negative; FP – false positive; TP - true positive.

A preliminary multi-class model (**Figure 4.19**) revealed the IS-diluted and HF-diluted classes consistently had a high number of true negatives relative to false positives, resulting in high specificity and contributing to these classes being more accurately predicted than the authentic class. However, the IS-diluted class also showed the lowest sensitivity: other samples are seldom wrongly predicted as IS-diluted, but the IS-diluted samples themselves were also least likely to be correctly predicted. The accuracy measure gives the misleading impression that the ICSS and HFCS dilution detection is performing well, when authentic class has a higher sensitivity and is therefore better distinguished than the IS-diluted class. Both dilution types were most commonly misclassified as authentic and not as the other diluent, which was unexpected based on the information known about the diluents. The ICSS used in this trial is most similar to a typical honey in terms of TSS and fructose: glucose ratio, while the HFCS is most similar to the invert syrup. Honey typically has a °Brix of 78-82 and an expected fructose content of 45 to 50% (db) (Ulberth, 2016), while the ICSS used had a higher °Brix (76%) and lower fructose content (50% db), and HFCS had both a lower °Brix (75.5%) and higher fructose content (55% db). The diluent misclassifications may be as a result of the size of the authentic class, and the consequence that has on the 'predict most probable' threshold. The samples were found to cluster within their classes on scores plots of LV 1-3 (**Figure 4.20**) but overlapped and could not be separately distinguished.

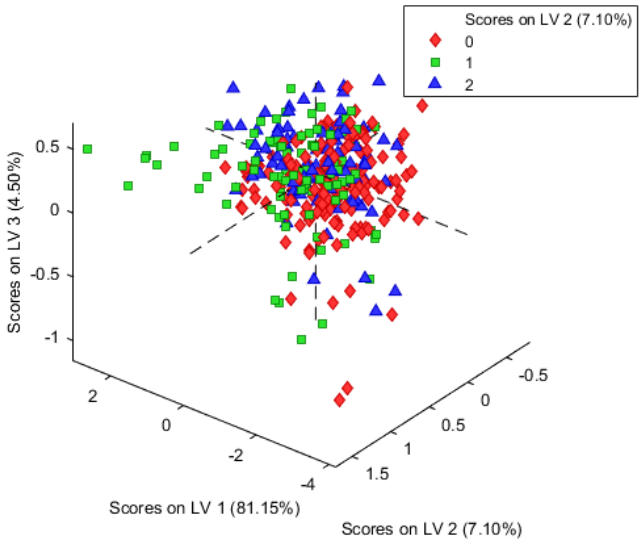

Figure 4.20 Authentic vs. IS- and HF-diluted PLS-DA scores plots of **LV1** vs. **LV2** vs. **LV3** (SNV, 1st derivative SG (3, 11) and MC, 7 LVs), with authentic (**green**), IS-diluted (**red**) and HF-diluted (**blue**) classes shown.

Ultimately, three different PLS-DA modelling approaches were taken to develop an acceptable dilution detection tool: a two-class model for general dilution detection, regardless of irradiation, based on all Diluted and Storage Trial spectra (1102); a multi-class model for diluent detection, regardless of irradiation, based on all Diluted and Storage Trial spectra (1102); and two two-class models for diluent detection of HFCS and ICSS individually, regardless of irradiation, based on relevant spectra in the Diluted and Storage Trial datasets.

Multi-class classification with PLS-DA was performed with authentic, IS-diluted and HF-diluted as the three classes under investigation (**Table 4.10**).

The multi-class model was the worst-performing model, which with the findings in **Figure 4.19** and **Table 4.9**, suggests that the difficulty lies in distinguishing between the adulterants themselves. The multi-class model scores plots showed largely overlapping diluent classes (**Figure 4.21**). The dilution class average difference spectra (**Figure 4.2**) had also revealed that the two diluents exhibited differences in similar regions, but with slightly different intensities, possibly too subtle for the model to distinguish between. The two-class authentic vs. diluted model had passable performance, with accuracy, sensitivity and specificity just below that of the individual diluent two class models.

Table 4.10 Calibration and validation results of the best performing PLS-DA models for specific dilution classification: distinguishing between authentic, IS-diluted and HF-diluted classes, all BÜCHI D_{All} spectra with spectral range of 1300-2450 nm. Sensitivity of the authentic class indicated in bold.

Model	Pre-processing	LVs	Calibration accuracy (%)	Validation accuracy (%)	Validation misclassification (%)	Sensitivity (%)	Specificity (%)	Efficiency (%)
Two-class *Authentic vs. Diluted*	MC	8	72.01	68.73	31.27	**79.76**	58.82	68.50
Multi-class *Authentic vs. HF-diluted vs. IS-diluted*	SNV, DT (2) + MC	7	61.28	62.82	37.18	**Authentic 71.43** IS-diluted 54.26 HF-diluted 55.91	Authentic 63.19 IS-diluted 86.87 HF-diluted 78.80	Authentic 67.18 IS-diluted 68.65 HF-diluted 66.38
Two-class *Authentic vs. IS-diluted*	SNV, DT (2) + MC	7	78.54	75.95	24.05	**86.31**	57.45	70.41
Two-class *Authentic vs. HF-diluted*	1st derivative SG (3, 11) + MC	7	75.93	73.95	26.05	**82.14**	59.14	69.70

The scores and prediction plots of the IS-dilution model (**Figure 4.22** and **4.23**) showed overlapping of the authentic and diluted class. The scores plot revealed a distinct region close to 0 on LV 1-3 in which all authentic samples were clustered, while IS-diluted samples were distributed along the direction of LV 3. The scores and prediction plots of the HF-dilution model similarly showed poorly separated classes (**Figure 4.26**

and **4.27**). Both authentic and HF-diluted classes were clustered close to 0 of LV 1-3 in the scores plot, but the authentic class was distributed more in the direction of LV 2 and HF-diluted in the direction of LV1.

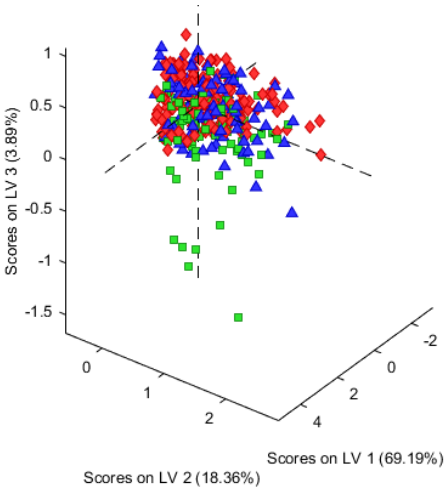

Figure 4.21 Authentic vs. IS- and HF-diluted PLS-DA scores plots of **LV1** vs. **LV2** vs. **LV3** (SNV, DT (2) and MC, 7 LVs), with authentic (**green**), IS-diluted (**red**) and HF-diluted (**blue**) classes shown.

The separate two-class models for detection of HF and IS dilution were the best performing in terms of sensitivity and accuracy and will be the most effective solution for screening. However effective, this solution will be clumsy to implement in practice as each new sample will have to be passed through two models, and the dilemma exists in which samples may be accepted as authentic by one model and rejected by the other. The VIP scores of the individual diluent models were compared to see which wavelengths were contributing to the separation in each case (**Figure 4.24** and **Figure 4.28**).

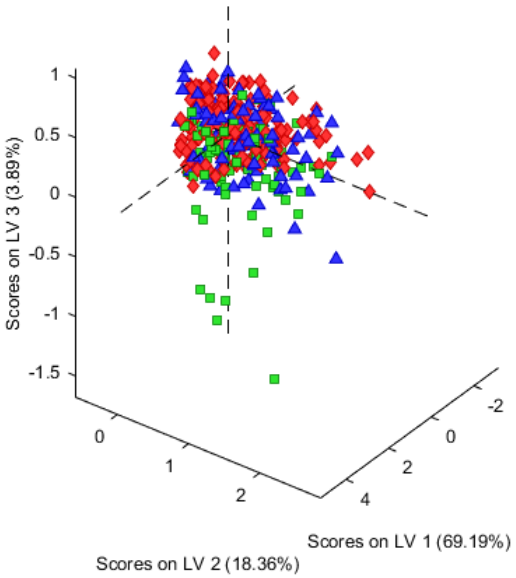

Figure 4.22 Authentic vs. IS-diluted PLS-DA (SNV, DT(2) and MC, 7 LVs), scores plot of **LV1 (69.19%)** vs. **LV2 (18.36%)** vs. **LV3 (3.89%)**, authentic (**red**) and IS-diluted (**green**) classes, HF-diluted (**blue**) class shown but not predicted.

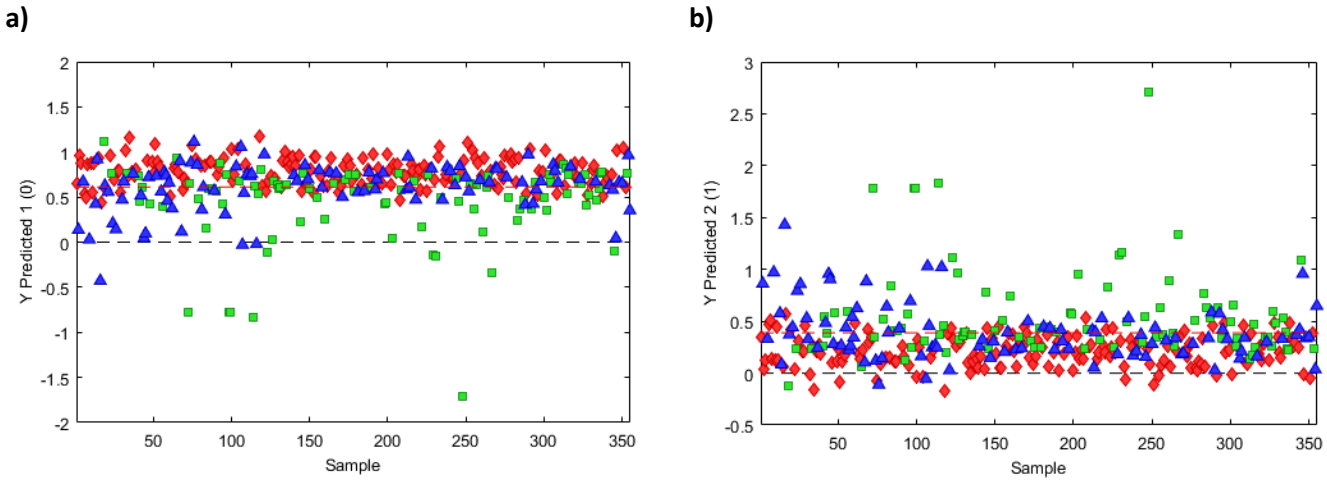

Figure 4.24 Authentic vs. IS-diluted PLS-DA (SNV, DT(2) and MC, 7 LVs), Y prediction plots, with authentic (**green**), IS-diluted (**red**) and HF-diluted (**blue**) classes shown, a) Predicted as 0 (authentic (**red**)), b) Predicted as 1 (IS-diluted (**green**)).

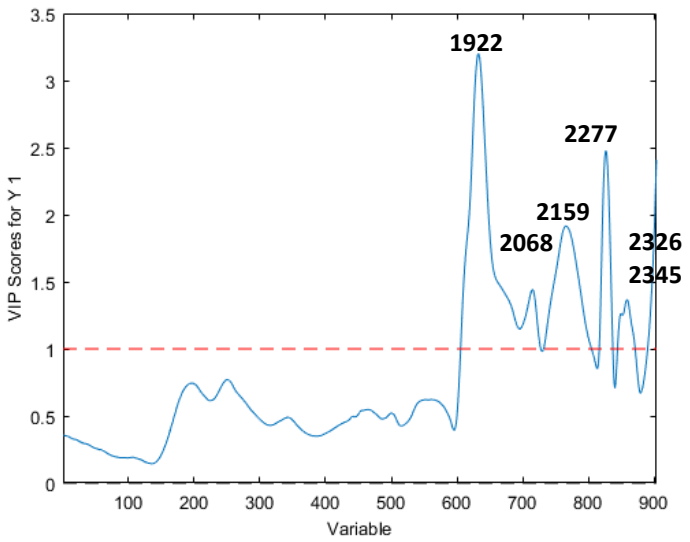

Assigned wavelengths

1922 nm - O-H stretching and deformation (Woodcock *et al.*, 2007)

2068 nm - O-H stretching and deformation (Osborne *et al.*, 1993)

2277 nm - C-H stretching and deformation; fructose and glucose (Rambla *et al.*, 1997, Woodcock *et al.*, 2007)

2326 nm – C-H deformation and stretching; fructose and glucose (Downey *et al.*, 2003)

2350 nm – C-H deformation and stretching; fructose (Downey *et al.*, 2003)

Figure 4.23 Authentic vs. IS-diluted PLS-DA (SNV, DT (2) and MC, 7 LVs) VIP scores showing the contribution of each variable, with the assignment for each wavelength.

The VIP scores of the IS-dilution model revealed a large contribution from an O-H related feature, as well as three smaller sugar-related C-H features (**Figure 4.24**). It is proposed that this is due to ICSS having a sugar profile closer to that of a typical honey than the HFCS sample used in this trial. Not much literature is available on IS specific dilution of honey, but it is expected that it will disrupt the water structures of honey in a similar way that HFCS has been reported to (Bázár *et al.*, 2016). The receiver operating characteristic (ROC) curve (**Figure 4.25**), which gives an indication of the predictive ability of the model, had an area under the curve (AUC) of above 0.8, showing that while the model was far from achieving perfect classification accuracy, it did have some predictive power.

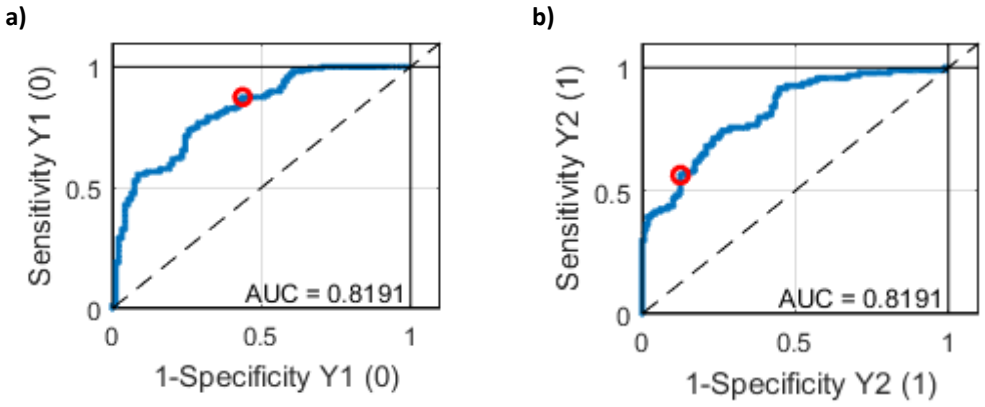

Figure 4.25 Authentic vs. IS-diluted PLS-DA (SNV, DT (2) and MC, 7 LVs), ROC curve, sensitivity and 1-specificity of the a) authentic class and b) IS-diluted class.

The HF-dilution model differed from the IS-dilution model, with greater contributions coming from C-H bonds and specific wavelengths correlated to fructose content (**Figure 4.28**). This is anticipated, as HFCS has the highest fructose content, higher than ICSS and the naturally occurring range for honeys. There was still some contribution from moisture, which is also consistent with HFCS dilution, which is known to cause a change in the predominant water bonding and water species present in samples (Bázár *et al.*, 2016). The ROC curve had a lower AUC, revealing that the model had slightly less predictive power than the IS-dilution model (**Figure 4.29**).

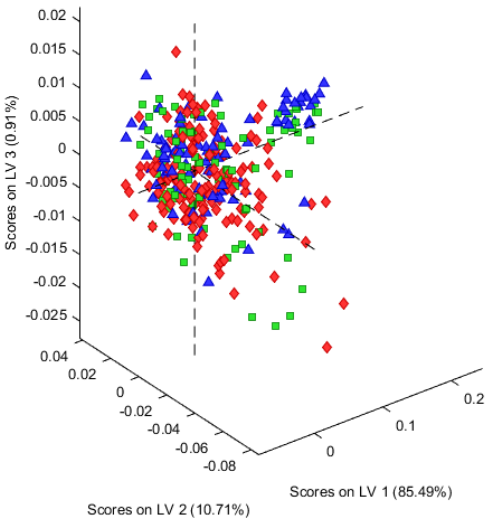

Figure 4.26 Authentic vs. HF-diluted PLS-DA (1st derivative SG (3, 11) and MC, 7 LVs), scores plot of **LV1 (85.49%)** vs. **LV2 (10.71%)** vs. **LV3 (0.91%)**, authentic (**red**) and HF-diluted (**blue**) classes, IS-diluted (**green**) class shown, but not predicted.

a) b)

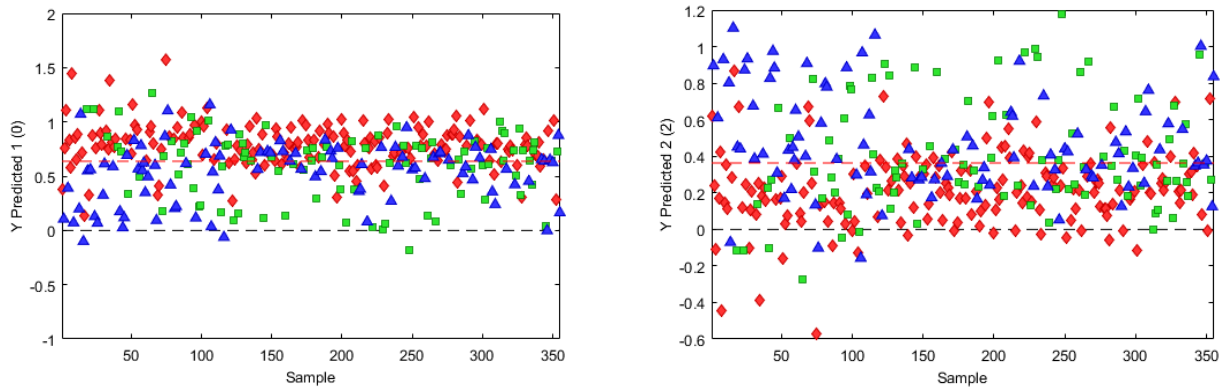

Figure 4.28 Authentic vs. HF-diluted PLS-DA (1st derivative SG (3, 11) and MC, 7 LVs), Y prediction plots, with authentic (**red**), IS-diluted (**green**) and HF-diluted (**blue**) classes shown (IS-diluted (**green**) class shown, but not predicted), a) Predicted as 0 (authentic (**red**))**,** b) Predicted as 1 (HF-diluted (**blue**)).

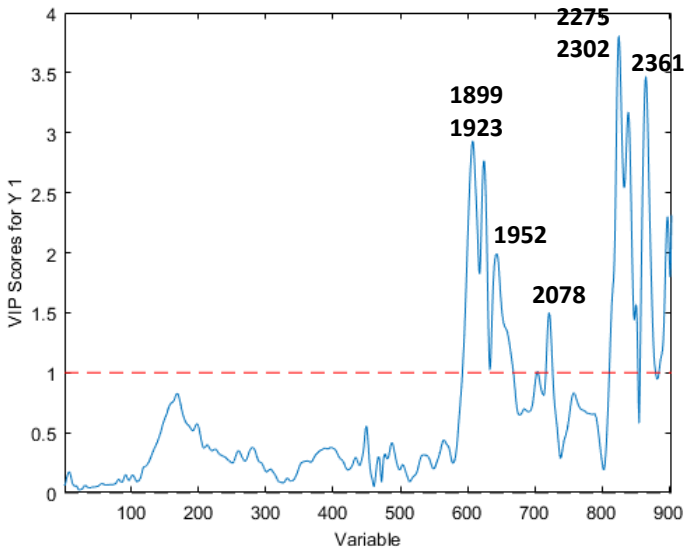

Assigned wavelengths

1923 & 1952 nm - O-H stretching and deformation (Woodcock *et al*., 2007, Herrero Latorre *et al*., 2013)

2078 nm - O-H stretching and deformation (Osborne *et al*., 1993)

2275 nm - C-H stretching and deformation; fructose and glucose (Rambla *et al*., 1997, Woodcock *et al*., 2007)

2302 nm – C-H deformation and stretching (Thamasopinkul *et al.*, 2017)

2361 nm – C-H deformation and stretching; fructose (Downey *et al.*, 2003)

Figure 4.27 Authentic vs. HF-diluted PLS-DA (1st derivative SG (3, 11) and MC, 7 LVs), VIP scores showing the contribution of each variable, with the assignment for each wavelength.

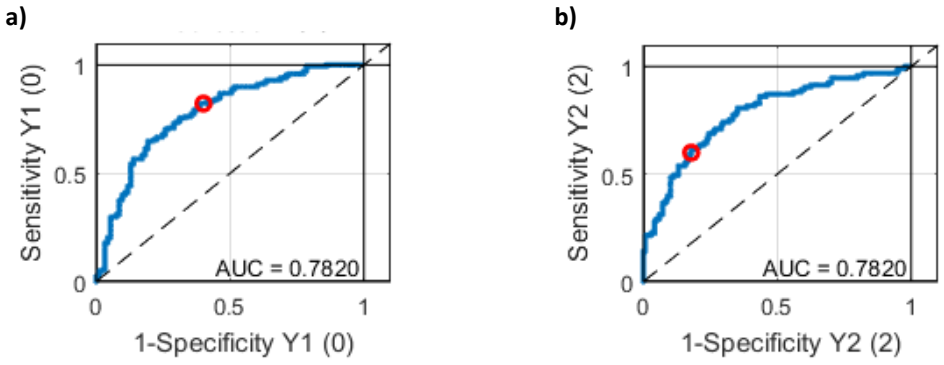

Figure 4.29 Authentic vs. HF-diluted PLS-DA (1st derivative SG (3, 11) and MC, 7 LVs), ROC curve, sensitivity and 1-specificity of the a) authentic class and b) HF-diluted class.

4.3.1.4 Classification of Irradiation Treatment

An attempt at detection of irradiation treatment, regardless of dilution, using all Dilution Trial spectra (691) was made. It was reasoned that the ASCA findings that irradiation treatment not having overall significance within the dataset did not discount the possibility of irradiation affecting either a selection of samples or a specific wavelength or wavelength regions. The same modelling approach was applied to attempt classification of irradiation treatment, using all spectra within the dilution trial subset, excluding all identified and verified outliers. Two-way classification with PLS-DA was performed with non-irradiated and irradiated classes, and with different wavelength ranges. The featured models (**Table 4.11**) gave the best performance, but overall the results were unsatisfactory, with low model accuracies and model efficiency. The scores and prediction plots of the model (**Figure 4.30** and **4.31**) showed an absence of any distinct grouping of the irradiated and non-irradiated classes. The ROC curve (**Figure 4.32**) lay close to the diagonal threshold and had a low AUC close to 0.5, indicative of poor predictive power.

Table 4.11 Calibration and validation results of PLS-DA models for irradiation treatment classification: distinguishing between non-irradiated and irradiated classes, all BÜCHI D_{All} spectra, with different spectral ranges.

Range (nm)	Pre-processing	LVs	Calibration accuracy (%)	Validation accuracy (%)	Validation misclassification (%)	Sensitivity (%)	Specificity (%)	Efficiency (%)
1000-2500	2nd derivative SG (3, 11) + MC	11	67.22	59.71	40.29	50.49	68.93	58.99
1300-2450	SNV, 2nd derivative SG (3, 11) + MC	10	65.50	58.33	41.67	42.57	73.79	56.05
1300-1800	2nd derivative SG (3, 11) + MC	5	63.66	58.33	41.67	65.35	51.46	57.99

Observations on Irradiation

While ASCA indicated that irradiation treatment was not significant on the whole variation of the dataset, it did have a significant interaction effect with the honey type experimental factor, implying significant interaction of irradiation treatment on specific honey types. This was also evident in the experimental observations, as a small number of honey samples returned from undergoing irradiation treatment topped with a distinct, thick aerated layer (**Figure 4.33**). While similar in colour to the layer often found on top of fermenting samples, examination of several affected samples established that it was both thicker and made up of smaller, more densely packed bubbles when compared to non-irradiated fermenting honey.

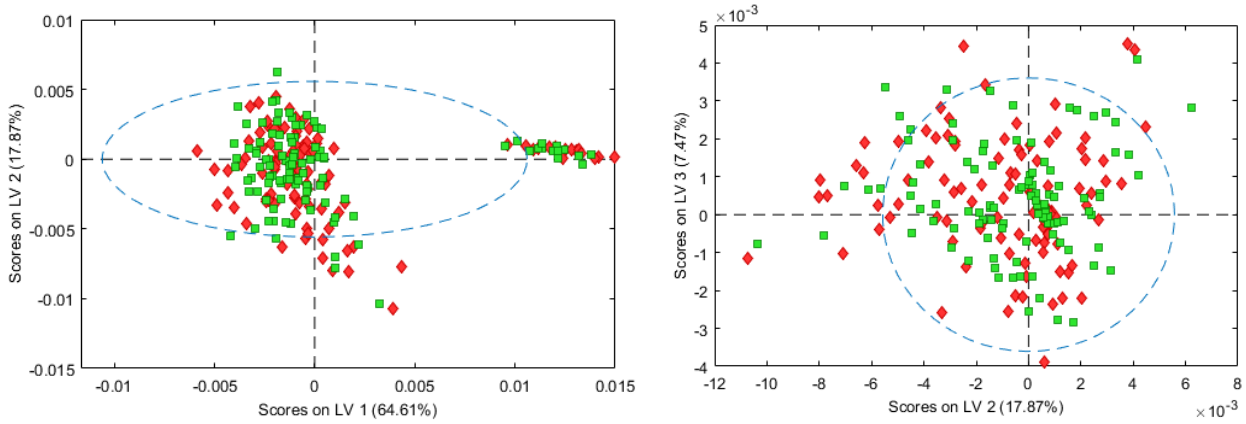

Figure 4.30 Irradiation treatment classification PLS-DA (2nd derivative SG (3, 11) and MC, 11 LVs) scores plot, with irradiated (**green**) and non-irradiated (**red**) classes shown, a) **LV1 (64.61%)** vs. **LV2 (17.87%),** b) **LV2 (17.87%)** vs. **LV3 (7.47%).**

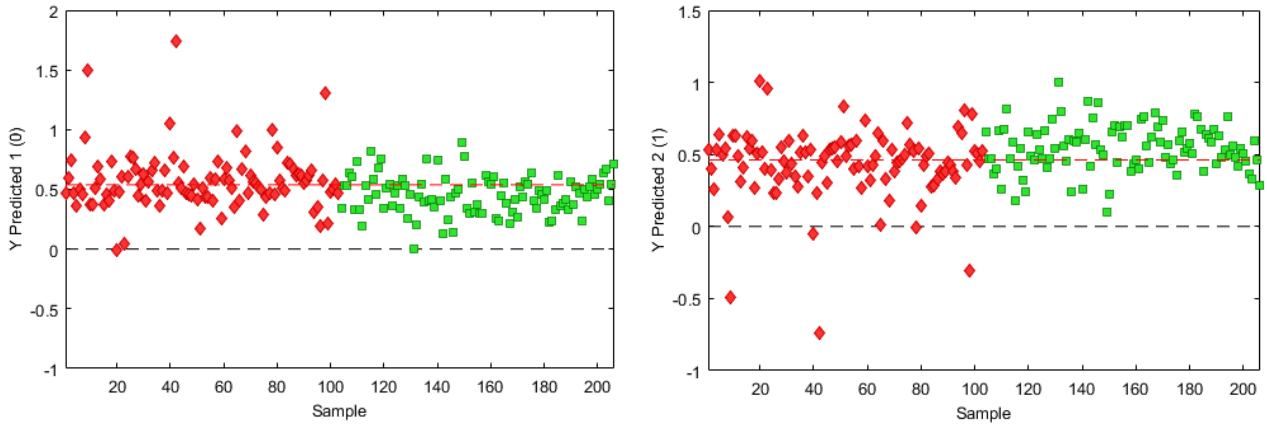

Figure 4.31 Irradiation treatment classification PLS-DA (2nd derivative SG (3, 11) and MC, 11 LVs) Y prediction plots, with irradiated (**green**) and non-irradiated (**red**) classes shown, a) Predicted as 0 (non-irradiated (**red**))**,** b) Predicted as 1 (irradiated (**green**)).

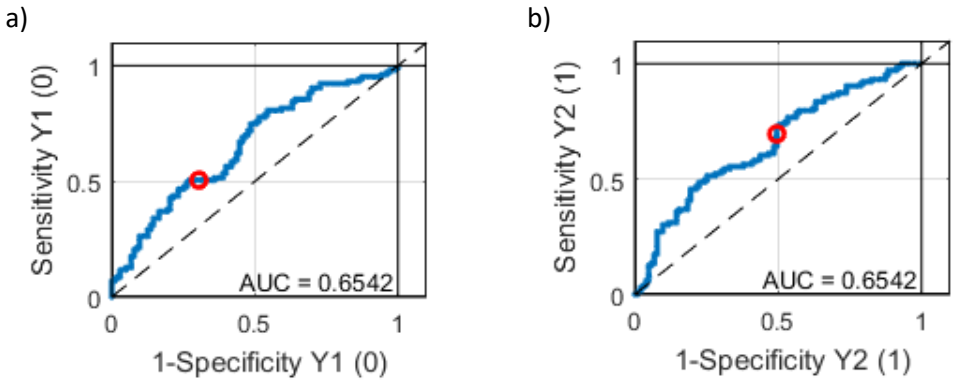

Figure 4.32 Irradiation treatment classification PLS-DA (2nd derivative SG (3, 11) and MC, 11 LVs), ROC curve, sensitivity and 1-specificity of the a) non-irradiated class and b) irradiated class.

Additionally, the samples with this aerated layer did not have the characteristic flavours and odours associated with fermentation. While there was no mention of this phenomenon to be found in literature, its occurrence in honey has been documented by the irradiation facility (C. Balt, 2019, Managing Director, High Energy Processing Cape, Cape Town, South Africa, personal communication, 13 November). Irradiation of water produces H_2 as a by-product, and has been reported to induce H_2 and CO_2 gas formation in carbohydrate solutions (Fan, 2013), but it is unknown why it would affect different honey varieties with vast inconsistency. Viscosity of honey, a well-studied parameter that varies with botanical origin and moisture content (Bhandari *et al.*, 1999), may also play a role in honey retaining gas or allowing it to disperse into the headspace of the container.

a) **b)**

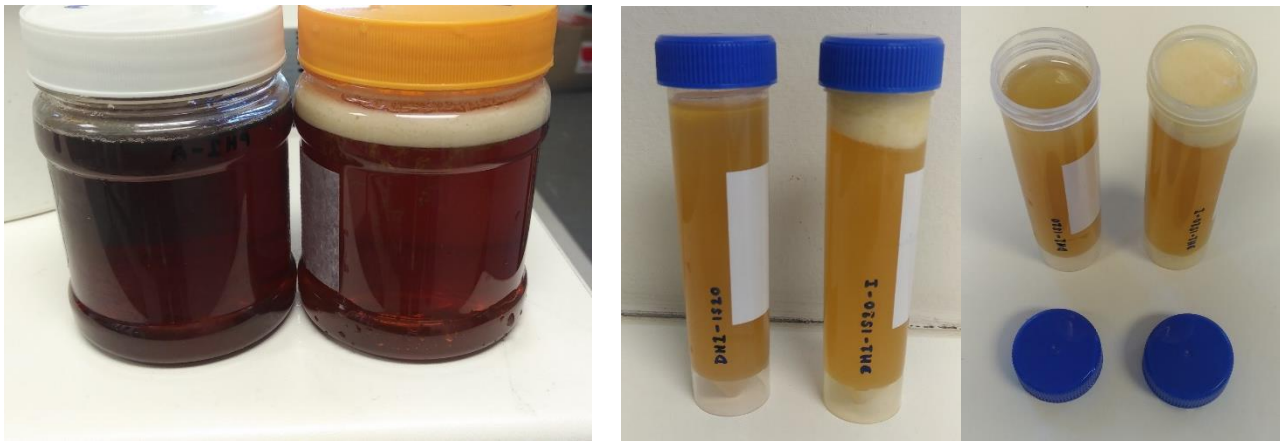

Figure 4.33 Non-irradiated (L) and irradiated (R) samples of the same honey type and dilution level, exhibiting the aerated layer phenomenon, a) Peel's Honey Macadamia Honey, no dilution; b) Dad's Honey Protea Fynbos Honey diluted with 20% invert syrup, side and top view.

The irradiation-related layer was removed prior to sample preparation for spectral acquisition, as were all traces of fermentation. The discrete phenomena were only fully characterized retrospectively, as the fermentation layers reformed after removal and further storage and the irradiation layers did not.

Unfortunately, incomplete record of samples that exhibited this was kept, as the earliest instances were regarded as fermentation, and no samples were retained for further analysis to identify the gas.

4.3.2 COMPARISON OF INSTRUMENTS

The classification ability of PLS-DA models based on the BÜCHI NIRFlex-500 data was compared to models based on data acquired with the VIAVI MicroNIR 1700 instrument, with the MicroNIR's two sample presentation formats. The MicroNIR instrument covers the 2nd and 3rd overtones, in comparison to the BÜCHI instrument, which covers the 1st, 2nd, 3rd overtones and combinations.

Separate two-class models for detection of HFCS and ICSS dilution were built from the MicroNIR (Teflon cup) (1188 spectra) and MicroNIR (Vial) (1187 spectra) datasets, with confirmed outliers removed, using a spectral range of 908-1651 nm as light scattering was present above 1651 nm (**Table 4.12**). This region contains the OH stretching 1st and 2nd overtones, OH combinations 1st overtone, CH stretching 1st, 2nd and 3rd overtones, and CH_2 stretching 2nd and 3rd overtones (Golic *et al.*, 2003). Glucose and fructose absorptions have been reported in this spectral range at 960-984 nm and 1040 nm, attributed to O-H stretching (2nd overtone) and C-H and CH_2 stretching (1st overtone combination bands) (Golic *et al.*, 2003). Rambla *et al.* (1997) found features at 1587 nm in glucose solutions [1 – 19% (w/w)], and 1583 nm in fructose solutions [1 – 16% (w/w)]. Water, making up approximately 30 % of the honey samples at the time of spectral acquisition, makes a substantial contribution to the overall spectrum obtained. Segtnan *et al.* (2001) studied the structure of water with NIR spectroscopy, and found peaks at 1441, 1462, 1490, and 1650 nm in 2nd derivative spectra, which were assigned to H-bonding of various H_2O species.

BÜCHI data models had highest accuracies (73.95-75.95%) and sensitivities (82.14-86.31%), but MicroNIR (Teflon cup) data models had higher specificity (63.74-72.37%), resulting in high efficiency. In general, The MicroNIR (vial) models underperformed in comparison to the other two datasets. Based on the priority of maximising either sensitivity or specificity, the BÜCHI or MicroNIR (Teflon cup) models, respectively, would be most suitable for authentication applications. Additionally, IS-diluted models consistently performed better in terms of accuracy and sensitivity than HF-diluted models.

VIP scores of the MicroNIR (Teflon cup) authentic vs. IS-diluted indicated wavelengths at 964 (O-H stretching, 2nd overtone), 995, 1057 (C-H stretching and CH_2 stretching, 1st overtone combination bands), 1150, 1187 and 1236 nm were responsible for the separation of classes (Golic *et al.*, 2003). For the MicroNIR (Teflon cup) authentic vs. HF-diluted model, 951 (O-H stretching, 2nd overtone), 1143, 1193, 1236-1249, 1348, and 1391 nm were most prominent (Golic *et al.*, 2003). The MicroNIR (vial) authentic vs. IS-diluted indicated wavelengths at 1150, 1187, 1236, 1410-1441 (O-H bonds, 1st overtone) and 1552 nm made the greatest contributions (Segtnan *et al.*, 2001).

Table 4.12 Calibration and validation results of the best performing PLS-DA models for specific diluent classification: distinguishing between authentic, IS-diluted and HF-diluted classes, all BÜCHI, MicroNIR (Teflon cup) and MicroNIR (vial) D_{All} spectra. The results of best performing instrument are highlighted.

Model	Pre-processing	LVs	Calibration accuracy (%)	Validation accuracy (%)	Validation misclassification (%)	Sensitivity (%)	Specificity (%)	Efficiency (%)
BÜCHI NIRFlex-500 bench top instrument (1300-2450 nm)								
Two class *Authentic vs. IS-diluted*	SNV, DT (2) + MC	7	**78.54**	**75.95**	**24.05**	**86.31**	57.45	70.41
Two class *Authentic vs. HF-diluted*	1st derivative SG (3, 11) + MC	7	**75.93**	**73.95**	**26.05**	**82.14**	59.14	69.70
VIAVI MicroNIR 1700 handheld instrument with Teflon cup (908-1651 nm)								
Two class *Authentic vs. IS-diluted*	SNV, DT (4) + MC	8	75.82	75.47	24.53	76.72	**72.37**	**74.51**
Two class *Authentic vs. HF-diluted*	1st derivative SG (3, 11) + MC	9	72.35	70.00	30.00	73.02	**63.74**	**68.22**
VIAVI MicroNIR 1700 handheld instrument with vial attachment (908-1651 nm)								
Two class *Authentic vs. IS-diluted*	SNV, DT (3) + MC	9	75.04	70.85	29.15	78.31	53.66	64.82
Two class *Authentic vs. HF-diluted*	2nd derivative SG (3, 11) + MC	9	71.75	67.88	32.12	67.20	69.41	68.29

Meanwhile, in the authentic vs. HF-diluted model, wavelengths at 951 (O-H stretching, 2nd overtone), 1162, 1205 and 1490 nm (O-H stretching, 1st overtone) were responsible (Golic *et al.*, 2003; Herrero Latorre *et al.*, 2013). These wavelengths and regions share a large overlap with the VIP scores reported by Guelpa *et al.* (2017), that 1143.5-1162.1 nm and 1447.0-1453.2 nm (C-H stretching, 2nd overtone), 908.1–976.2 nm (C-H deformations, CH_2 and N-H bonds) and 1205.4–1267.4 nm (C-H bonds, 2nd overtone) were significant contributors to PLS-DA honey authentication models built with a similar instrument and wavelength range (908-1680 nm). This was the only authentication study to partially attribute discrimination, based on absorptions around 900-1000 nm, to protein structures, a finding which was not shared by the present study.

In contrast, the BÜCHI IS-dilution models largely relied on contributions from O-H related wavelengths (1922, 2068 and 2159 nm), and smaller sugar-related C-H features (2277, 2326 and 2345 nm) (Osborne *et al.*, 1993; Rambla *et al.*, 1997; Downey *et al.*, 2003; Woodcock *et al.*, 2007). The HFCS model had contributions from 2275, 2302 and 2361 nm, attributed to C-H stretching and deformation, and which have also been related to fructose and glucose (Rambla *et al.*, 1997, Woodcock *et al.*, 2007), with smaller peaks at 1923,

1952 and 2078 nm related to O-H stretching and deformation (Osborne *et al.*, 1993; Woodcock *et al.*, 2007; Herrero Latorre *et al.*, 2013). In essence, all significant wavebands in the BÜCHI models were above 1900, and therefore had no overlap with the wavebands contributing to the MicroNIR models, which were all below 1560 nm.

4.3.3 QUANTIFICATION

Quantification of the level of dilution using PLSR was unsatisfactory (**Figure 4.34** and **Table 4.13**). The IS-diluted quantification model (RMSEP = 7.083%, R^2_{Pred} = 0.751) predicted the level of dilution better than the HF-diluted model (RMSEP = 8.847%, R^2_{Pred} = 0.121) but both had mediocre performance that would be unsuitable for quantification applications. This inadequate performance is unsurprising, as the dataset was not designed with the intention of building a well-represented quantification reference library and higher dilution levels are poorly represented.

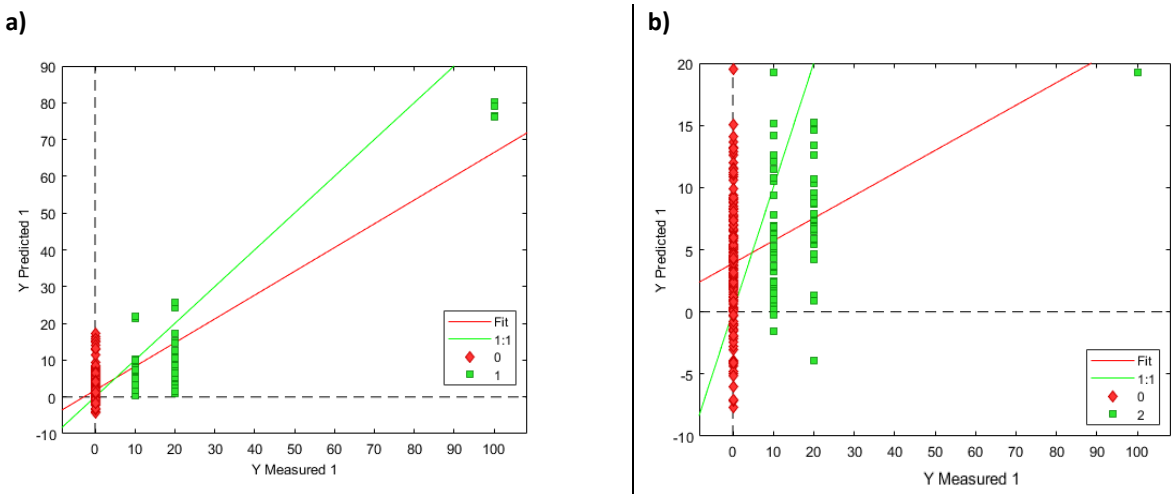

Figure 4.34 a) Authentic vs. IS-diluted PLSR (SNV, DT (2) and MC, 8 LVs) validation results of predicted dilution percentage, with pure adulterant syrups included, and b) Authentic vs. HF-diluted PLSR (1st derivative SG (3, 11) and MC, 5 LVs) validation results of predicted dilution percentage, with pure adulterant syrups included.

Table 4.13 Quantification results of Authentic vs. IS-diluted PLSR (SNV, DT (2) and MC, 8 LVs) and Authentic vs. HF-diluted PLSR (1st derivative SG (3, 11) and MC, 5 LVs), pure adulterant syrups included

Model	R^2_{Cal}	R^2_{CV}	R^2_{Pred}	RMSEC (%)	RMSECV (%)	RMSEP (%)
Authentic vs. IS-diluted	0.529	0.501	0.751	6.736	6.931	7.083
Authentic vs. HF-diluted	0.140	0.105	0.121	10.978	11.217	8.847

Models were recalculated with the pure adulterant syrups omitted (**Figure 4.35** and **Table 4.14**). This omission limits the applicability of the model, but may be a necessary concession, given the unsuitability of the dataset for prediction of diluent levels higher than 20%.

The recalculated models both performed slightly better in terms of root mean square error values, but still had unacceptably high root mean square error of prediction in relation to the reference values. The IS-dilution model had much poorer determination coefficients when the pure adulterant syrups were excluded, while those of the HF-dilution model improved negligibly. As a consequence of the poor performances of the PLSR models, further meaningful information relating the spectral features to the quantity of diluent present in samples could not be gleaned from examining the regression vectors, selectivity ratios or VIP scores.

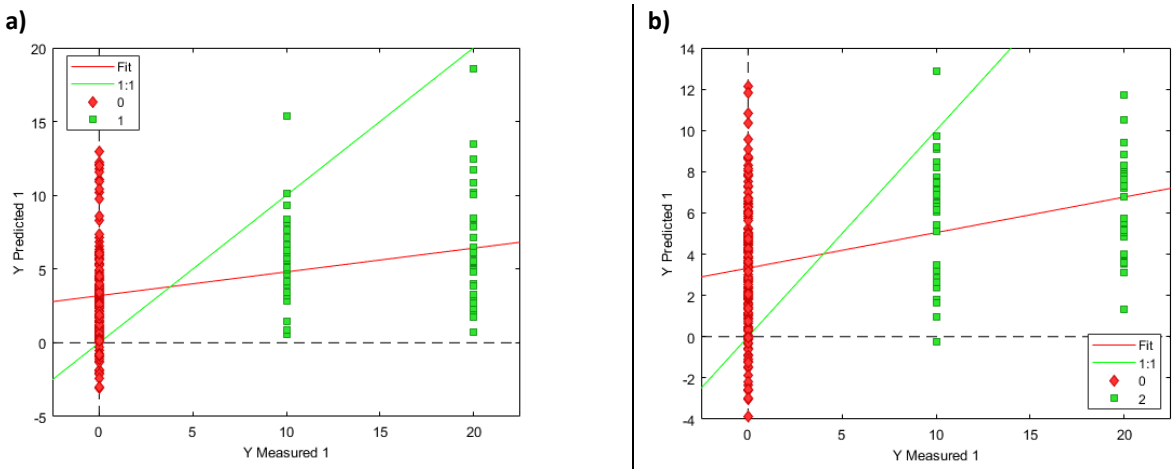

Figure 4.35 a) Authentic vs. IS-diluted PLSR (SNV, DT (2) and MC, 8 LVs) validation results of predicted dilution percentage, with pure adulterant syrups excluded, and b) Authentic vs. HF-diluted PLSR (1st derivative SG (3, 11) and MC, 7 LVs) validation results of predicted dilution percentage, with pure adulterant syrups excluded.

Table 4.14 Quantification results of Authentic vs. IS-diluted PLSR (SNV, DT (2) and MC, 8 LVs) and Authentic vs. HF-diluted PLSR (1st derivative SG (3, 11) and MC, 7 LVs), pure adulterant syrups excluded

Model	R^2_{Cal}	R^2_{CV}	R^2_{Pred}	RMSEC (%)	RMSECV (%)	RMSEP (%)
Authentic vs. IS-diluted	0.255	0.220	0.118	6.185	6.337	6.795
Authentic vs. HF-diluted	0.166	0.122	0.147	6.431	6.612	6.596

4.4 REFERENCES

Bakier, S. (2009). Capabilities of near-infrared spectroscopy to analyse changes in water bonding during honey crystallisation process. *International Journal of Food Science & Technology*, **44**, 519–524.

Bázár, G., Romvári, R., Szabó, A., Somogyi, T., Éles, V. & Tsenkova, R. (2016). NIR detection of honey adulteration reveals differences in water spectral pattern. *Food Chemistry*, **194**, 873–880.

Bhandari, B., D 'arcy, B. & Kelly, C. (1999). Rheology and Crystallization Kinetics of Honey: Present Status. *International Journal of Food Properties*, **2**, 217–226.

Chen, L., Xue, X., Ye, Z., Zhou, J., Chen, F. & Zhao, J. (2011). Determination of Chinese honey adulterated with high

fructose corn syrup by near infrared spectroscopy. *Food Chemistry*, **128**, 1110–1114.

Downey, G., Fouratier, V. & Kelly, J.D. (2003). Detection of honey adulteration by addition of fructose and glucose using near infrared transflectance spectroscopy. *Journal of Near Infrared Spectroscopy*, **11**, 447–456.

Fan, X. (2013). Radiation Chemistry of Food Components. In: *Food Irradiation Research and Technology* (edited by X. Fan & C.H. Sommers). Pp. 75–97. Blackwell Publishing.

Golic, M., Walsh, K. & Lawson, P. (2003). Short-wavelength near-infrared spectra of sucrose, glucose, and fructose with respect to sugar concentration and temperature. *Applied Spectroscopy*, **57**, 139–145.

Guelpa, A., Marini, F., Plessis, A. du, Slabbert, R. & Manley, M. (2017). Verification of authenticity and fraud detection in South African honey using NIR spectroscopy. *Food Control*, **73**, 1388–1396.

Herrero Latorre, C., Peña Crecente, R.M., García Martín, S. & Barciela García, J. (2013). A fast chemometric procedure based on NIR data for authentication of honey with protected geographical indication. *Food Chemistry*, **141**, 3559–3565.

Kelly, J.D., Petisco, C. & Downey, G. (2006). Potential of near Infrared Transflectance Spectroscopy to Detect Adulteration of Irish Honey by Beet Invert Syrup and High Fructose Corn Syrup. *Journal of Near Infrared Spectroscopy*, **14**, 139–146.

Li, S., Zhang, X., Shan, Y., Su, D., Ma, Q., Wen, R. & Li, J. (2017). Qualitative and quantitative detection of honey adulterated with high-fructose corn syrup and maltose syrup by using near-infrared spectroscopy. *Food Chemistry*, **218**, 231–236.

Osborne, B.G., Fearn, T. & Hindle, P.. (1993). *Practical NIR Spectroscopy with Applications in Food and Beverage Analysis*. Essex, England: Longman Scientific and Technical.

Rambla, F.J., Garrigues, S. & Guardia, M. De. (1997). PLS-NIR determination of total sugar, glucose, fructose and sucrose in aqueous solutions of fruit juices. *Analytica Chimica Acta*, **344**, 41–53.

Segtnan, V.H., Sasic, S., Isaksson, T. & Ozaki, Y. (2001). Studies on the Structure of Water Using Spectroscopy and Principal Component Analysis. *Analytical Chemistry*, **73**, 3153–3161.

Snee, R.D. (1977). Validation of regression models: methods and examples. *Technometrics*, **19**, 415–428.

Thamasopinkul, C., Ritthiruangdej, P., Kasemsumran, S., Suwonsichon, T., Haruthaithanasan, V. & Ozaki, Y. (2017). Temperature compensation for determination of moisture and reducing sugar of longan honey by near infrared spectroscopy. *Journal of Near Infrared Spectroscopy*, **25**, 36–44.

Ulberth, F. (2016). Advances in Testing for Adulteration in Honey. In: *Advances in Food Authenticity Testing* (edited by G. Downey). Pp. 729–753. London: Elsevier.

Woodcock, T., Downey, G., Kelly, J.D. & O'Donnell, C. (2007). Geographical classification of honey samples by near-infrared spectroscopy: A feasibility study. *Journal of Agricultural and Food Chemistry*, **55**, 9128–9134.

Chapter 5 General Discussion and Conclusion

5.1. GENERAL DISCUSSION

Exploratory data analysis

Exploration of the **Storage Trial** dataset with derivative spectra, PCA and ASCA indicated a few trends. Using ASCA, honey type was found to have the largest effect on the Storage Trial spectral data, followed by the age and the storage temperature. Irradiation treatment did not have a significant effect. PCA allowed the variation arising from the temperature and age factors to be identified: differences in C-H bond absorptions, thought to be related to fructose content, appeared to be driving the separation of 40°C storage treatment samples, while differences in the moisture content resulted in changes over time.

Exploratory data analysis of the **Dilution Trial** revealed information on the effects of syrup dilution on spectra data but was inconclusive on the matter of irradiation treatment. Some differences were evident in honey spectra after irradiation but were not evident in PCA. Using ASCA, it was determined that the honey type, diluent type and age factors had a significant effect on the Dilution Trial spectral data, while diluent level and irradiation treatment did not. In contrast, differences between authentic and diluted samples were evident in spectral data, and PCA revealed some incomplete separation of authentic and diluted classes. Comparison of SCA of the irradiated and non-irradiated classes revealed that irradiation was affecting the authentic and diluted samples to the same extent (0,737 – 0,807%), a difference which was tenfold smaller than the differences in the SCA of the authentic and diluted classes themselves (8,25 – 8,89%). This was taken as a generalised indication of minimal interference of irradiation treatment on the dilution-indicating information contained in the spectral data.

While the ASCA and SCA results are specific to the two datasets, which were created under controlled conditions, the results provide an estimation of where significant variation is likely to arise from when reference libraries are constructed.

Wavelength region performance

All three wavelength ranges were found to be more or less equally efficient (68.6-69.1%) as one another, but the ranges of 1000-2500 and 1300-2450 nm provided better prediction accuracies (>70.0%), and of the two, 1300-2450 nm had better sensitivity. Rambla *et al.* (1997) reported that fructose, glucose and sucrose exhibited the most similar absorptions in the region of 1300-1800 nm and more varied absorptions between 2050 to 2300 nm, concluding that the 1300-1800 nm region would be best suited for quantification of total sugars and the region above 2000 nm more suitable for quantification of individual sugars. While model-based authentication does not rely on quantification of individual sugars, it may rely on the subtleties of moisture and hydrocarbon absorptions, which contain more intricacies above 2000 nm. However, Chen *et al.* (2011) investigated the effectiveness of the spectral ranges 1000-2500 nm, 1000-1667 and 1667-2500 nm

for building PLS-DA honey authentication models, and found the range 1000-1667 nm to be most effective. In the present study, the 1300-1800 nm range was closest to the range of Chen *et al.* (2011), but did not show a remarkable improvement on the accuracy or efficiency of the model.

Multivariate data analysis

Multivariate data analysis was applied to investigate the effect of irradiation on the spectral data further, as well as attempt classification on the basis of syrup dilution and irradiation treatment. PLS-DA proved to be a better classification technique than SIMCA for the datasets in the present study. Poor performance of SIMCA is expected when clear separation of classes is not evident in PCA. In contrast, PLS is suitable for highly correlated data without encountering multicollinearity issues. It is an improvement upon PC compression, as it is a supervised method and it maximises the covariance of the response variables, where PCA simply maximises variance and is unsupervised (Oliveri and Simonetti, 2016).

Detection of irradiation was investigated as it would serve as a proxy test for imported honeys sold as local honeys. No local honey sold as a foodstuff would be voluntarily irradiated due to the cost involved, while all legally imported honeys would be irradiated. There were no previous findings in literature with which to compare the irradiation classification results, but accuracy of approximately 50% is considered random or chance classification. This strongly suggests that there is little or no utilizable effect of irradiation on the spectral data and that NIR is an unsuitable technique for irradiation detection.

Models built on irradiated spectral data did not match the performance of models built on non-irradiated or mixed irradiated and non-irradiated data, with respect to accuracy and efficiency, suggesting that classification may be impeded by irradiation treatment to a small degree. The VIP scores of the two models indicated large contributions from 2272 and 2437 nm, associated with C-H bonds and specifically fructose, and a split peak at 1925-1959 attributed to moisture (Downey *et al.*, 2003; Thamasopinkul *et al.*, 2017). These features distinguished the non-irradiated VIP score contributions from the irradiated VIP scores, suggesting that irradiation treatment had interfered with these specific regions. Irradiation is known to cause formation of H_2 and or CO_2 gas in honey, which was observed in a small number of samples and may have affected the spectral data obtained. But no conclusive explanation could be given for this impediment to classification. All evidence is suggestive of an effect of irradiation treatment on the performance of syrup dilution classification models. Despite these findings indicating that non-irradiated data yields better classification models, a robust authentication model will need to include both irradiated and non-irradiated data.

In general, PLS-DA classification provided acceptable model accuracy, sensitivity and selectivity for screening purposes, but inadequate for unequivocal predictions of authenticity. Building two-class classification models based on individual diluents improved the accuracy and sensitivity of the models. The ICSS detection model revealed large contributions from O-H related wavelengths (1922, 2068 and 2159 nm)

likely moisture-associated, as well as less prominent sugar-related C-H features (2277, 2326 and 2345 nm) (Osborne *et al.*, 1993; Rambla *et al.*, 1997; Downey *et al.*, 2003; Woodcock *et al.*, 2007). The fructose content of ICSS is similar to that of honey, therefore moisture or moisture-related bonding differences are a more likely source of variation.

In contrast, the HFCS detection model had its largest contributions from 2275, 2302 and 2361 nm, all of which are related to C-H stretching and deformation and associated with fructose and glucose (Rambla *et al*., 1997, Woodcock *et al*., 2007). Smaller peaks at 1923, 1952 and 2078 nm are attributed to O-H stretching and deformation and are likely moisture-related (Osborne *et al.*, 1993; Woodcock *et al.*, 2007; Herrero Latorre *et al.*, 2013). The large contribution is likely due to HFCS having the highest fructose content, in comparison to the natural range for honey, as well as ICSS. The ICSS model had more predictive power than the HFCS model, for the BÜCHI data as well as for both MicroNIR datasets.

Dilution detection models that included the Storage Trial data performed equally well in terms of accuracy and efficiency, when compared to models trained only on the Dilution Trial, i.e. authentic and diluted samples stored under identical conditions. In general, neither HFCS nor ICSS detection models could perform as well as those reported in literature.

Downey *et al.* (2003) investigated honey samples (n = 300) diluted with fructose and glucose solutions of different ratios and different levels (7, 14 and 21%). kNN (k = 4) and PLS-DA (10 LVs) of authentic vs. adulterated samples yielded accuracies of 89.3% and 98.0%. SIMCA was also performed on a subset of the data (only authentic vs. 7% adulteration samples) but could only accurately classify 35.3% of samples.

Kelly *et al.* (2006) achieved a high validation classification accuracy of 90.9% and sensitivity of 1 for both of the adulterated classes for discriminating between authentic and HFCS and beet invert syrup diluted honey samples (n = 179) with a SIMCA calibration. Kelly also remarked that the HFCS diluted samples did not cluster during PCA in the way that beet invert diluted samples did. They concluded that the limit of detection for quantification would closest to 20% for both adulterants investigated.

Chen *et al.* (2011) discriminated between authentic and commercially-obtained HFCS diluted (7-59%) honey samples (n = 144) with PLS-DA (1st derivative SG (13 pts) and MC pre-processing, 8 LVs), obtaining correct calibration classification of 95.8 for authentic and 97.9% for adulterated samples, as well as validation accuracy of 100% for both classes.

Zhu *et al.* (2010), when differentiating between authentic honey and honey diluted with glucose and fructose solutions, used least-squares support vector machines (LS-SVM) to obtain accuracy of 95.1% and an AUC of 0.952. Guelpa *et al.* (2017) discriminated between authentic local honey and imported or adulterated honey samples (n = 84) with the same benchtop instrument, with a high validation classification accuracy of 96.9%. Li *et al.* (2017) used NIRS and PLS-LDA to detect HFCS added to a set of honey samples (n = 205)

successfully, with a classification accuracy of 86.3%. In a previous publication, the same investigation was conducted with Raman spectroscopy, which outperformed NIR for authenticity classifications (Li *et al.*, 2012).

However, it is difficult to compare the results obtained in this study with those found in literature, due to differences in properties of adulterants used and experimental procedures followed. In one study, syrup with 8.5% fructose was used for dilution, a substantially different fructose content to that of honey (Ferreiro-González *et al.*, 2018). Another study using HFCS did not declare the composition of the diluent syrup (Li *et al.*, 2017). HFCS is favoured for honey dilution as the proportions of glucose: fructose in certain HFCS grades are similar to those of honey. Syrups that contain less than 50% (db) fructose, compared to honey's average of 50-55% (db), would substantially alter the glucose: fructose ratio of those diluted samples, and will be detected in the NIR spectral data. While dilution detection models should ideally be able to recognise similar and dissimilar diluent syrups, calibrating a model only on dissimilar, easy to detect diluents will provide an over-optimistic result of its overall performance. The syrups used in the present study had 50-55% (db) fructose to maintain that ratio, which could be a reason for the difficulty in classifying the diluted samples and the results comparing poorly to those found in literature.

It is also possible that some of the results in literature were optimistic due to inconsistent sample treatment, i.e. no liquefication (Chen *et al.*, 2011), no adjustment of °Brix (Chen *et al.*, 2011; Mouazen and Al-Walaan, 2014) and mixed filtration treatment of sample classes (Guelpa *et al.*, 2017). Studies that did not adhere to best practice liquefication, at no more than 40°C (Chen *et al.*, 2011; Guelpa *et al.*, 2017; Li *et al.*, 2017) may have inadvertently caused accelerated chemical change to occur in the honey samples studied (Bogdanov, 2009).

There were also physical effects in this study's spectra that were not successfully removed with the chosen spectral pre-processing techniques, such as light scattering due to presence of undissolved crystals which may have arisen due to the conservative heating practices. The two baseline clusters that arose in the D_0 data are likely due to sugar crystal sizes within the honey samples. Rinnan *et al.* (2009) demonstrated the additive and multiplicative differences in the spectra of sucrose samples over a range of crystal sizes (20-540 µm), which revealed that larger particle's spectra had greatly increased absorbance as a result of increased additive and multiplicative effects. Bakier (2009) found that crystallization affected the peak area of NIR absorption between 1876 -2014 nm and showed a strong correlation to changes in water activity induced by crystallization. Removal of a spectral offset present in spectra obtained at a different time phase was done by Toher (2007). This is recommended as an option for eliminating spectral offsets in future, such as those found in the present study, which was still evident in the spectra after pre-processing had been applied and was visible in PCA and PLS models.

Lastly, the number of unique honey samples used in this study was fairly limited. Including more biological variation could build a more robust model, better suited to its purpose, and would be necessary to

construct a reference library for a model able to fulfil the honey authentication screening needs of South Africa.

Comparison of NIR instruments

Classification models based on spectral information originating from the 2nd and 3rd overtones, captured by the MicroNIR instrument, was almost as effective as models based on spectral information from the 1st, 2nd, 3rd overtones and combinations, captured by the BÜCHI instrument. There were no similarities or overlap of the two instrument's VIP scores, as substantial wavebands contributing to the BÜCHI models were above 1900, and below 1560 nm for the MicroNIR models. Overall, the BÜCHI models had the highest proportion of samples both correctly accepted and rejected (199 out of a total of 262 validation samples), but the MicroNIR (Teflon cup) offers a reasonable trade-off of reduced sensitivity in return for higher specificity, with minimal effect on the accuracy and efficiency. The instrumental cost of the MicroNIR (Teflon cup), as well as its portability and ease of use makes it a viable, high-performing alternative to traditional benchtop instruments.

Quantification of diluent syrup

Quantification of the level of diluent syrup added to honey with PLSR was not satisfactory, providing further support for the ASCA findings on the insignificance of the diluent level experimental factor. The quantification results did not compare to the findings of other investigations into level of diluent with NIR spectroscopy. Bázár *et al.* (2016), reported R^2_{CV} = 0.987 and RMSECV = 1.48% when conducting PLSR on the spectra of honey samples diluted with HFCS (n = 40) at 0 to 40 %, in 10% increments. Ferreiro-González *et al.* (2018) also reported an acceptable performance (R^2_{Pred} = 0.986 and RMSEP = 4.71%) when using PLSR to predict the quantity of HFCS added to honey samples (n = 22), diluted at 0 to 100% also in 10% increments. Ferreiro-González *et al.* (2018) also showed that a high coefficient of variation for repeatability (CV = 3.90) could be obtained across measurements taken over three days. Kelly *et al.* (2006) achieved similar high RMSECV values of 11.9%, though had an acceptable R^2_{CV} of 0.72 for HFCS diluted honey samples (n = 179) at syrup dilution levels of 0, 10, 30, 50 and 70%, with a PLSR model with 8 LVs Li *et al.* (2017) used NIRS and PLS-LDA to quantify HFCS (1:1 fructose to glucose ratio) in sets of diluted honey samples (n = 180 and n = 60) with NIRS and PLSR was also not successful (R^2_{CV} = 0.018-0.078, RMSECV = 11.951-12.340) in a study by Li *et al.* (2012). The same study was able to achieve satisfactory quantification (R^2_{Pred} = 0.901-0.981, RMSEP = 1.789-4.041) of maltose syrup, however, indicating that a robust methodology had been employed, but was unsuitable for HFCS quantification.

PLSR models that made use of a wide and well-represented range of reference values generally obtained better determination coefficients than the present study, which was limited to 0, 10, 20 and 100% dilution levels. However, in all cases the number of samples between studies varied considerably, and caution should be taken when comparing the results directly.

The wavelength region utilized for quantification could also be reconsidered in further analyses. Golic *et al.* (2003) authored a study on the effects of concentration and temperature on the NIR spectra of fructose, glucose and sucrose solutions, and concluded that the absorption of C-H related bonds were a more robust measure for quantification, as O-H bond absorptions were greatly affected by fluctuations in temperature. On the basis of this, quantification based on the 2200 nm and upwards range, in contrast to the findings of (Bázár *et al.*, 2016), may be key to building a more robust quantification model.

Another proposed reason for the unsatisfactory performance is the inadequate removal of light scattering effects from the spectra by the selected pre-processing techniques. For quantification to be successful the Beer-Lambert law must hold, which will only be the case for pure transmission spectra in absence of scattering effects (Rinnan *et al.*, 2009). Scattering is likely to have been caused by the presence of sugar crystals (as a result of the conservative heating of samples) or trapped air bubbles (introduced during homogenization) present in the samples at the time of spectral acquisition.

5.2. CONCLUSION

NIR spectroscopy has been used, in combination with MDA, in a number of successful honey authentication and syrup dilution detection feasibility studies. While many of the proposed classification models have achieved excellent classification rates, they have not been extensively implemented in the honey industry and there are a few unaddressed sample standardization issues.

The effect of sample treatments thought to affect the spectral patterns of honey were investigated with ASCA, revealing that honey type, diluent type, storage temperature and age tended to have significant effects on the spectral dataset, while diluent level and irradiation treatment did not. This provided an indication of which experimental factors have detectable influence on the dataset, and where significant variation is likely to arise in future reference libraries.

Comparison of PLS-DA authentication models based on only irradiated and only non-irradiated spectral data suggest that irradiation of honey samples impeded the use of NIR spectroscopy for syrup dilution detection to a small degree. However, the effect of irradiation could not be utilized in a useful manner, as classification on the basis of irradiation treatment was not successful.

The PLS-DA models, proposed as a screening technique for syrup dilution, achieved mild success which was not optimal for confirming definite authenticity but adequate for screening purposes. Separate two-class PLS-DA models for each diluent yielded the best-performing authentication solution. A comparison of PLS-DA models based on spectra acquired using the benchtop BÜCHI instrument with the portable MicroNIR instrument and its two sample presentation formats indicated that the BÜCHI performed best, but that the MicroNIR (Teflon cup) is a reasonable, cost-effective alternative offering high accuracy and specificity, with slightly reduced sensitivity.

In contrast to previous studies, the models in the present study could not replicate the reported success of models in literature and were not suited to make unequivocal declarations of authenticity. The shortcomings of this methodology are highlighted by reduced model performance when irradiated samples were included, as well as when crystallization was present in samples. It is unclear whether the technique is unsuitable for honey authentication, or whether a revision of the method or experimental protocol may yield improved results. Nonetheless it is still recommended that other promising non-targeted techniques, such as NMR or MIR, should be further pursued to rule out possibilities for a more effective screening method with existing technology available.

Quantification of sugar syrup diluents, added to honey at low but realistic levels of 10 and 20%, was not successful with PLSR. Unsatisfactory prediction errors and coefficient of determination indices were obtained, for both diluent syrups. The determination coefficients were far below those obtained in similar studies of HFCS dilution. Consequently, the quantity of diluent present in samples could not be associated with the spectral information in a meaningful manner. It is expected that quantification was largely unsuccessful due to the limitations of the reference data which was not representative of the range of dilution levels, as well as remnants of light scattering present in the data. Based on the ASCA findings, it was not surprising that quantification, as well as detection of irradiation, were unsuccessful. Significance at $p = 0.05$ proved to be a useful indicator for whether or not an experimental design factor would be successfully quantified or classified.

Ultimately, the findings of the present feasibility study indicate that PLS-DA authentication models based on NIR spectral data offer a definite improvement upon having no screening tool in place and may assist in reducing the reliance of honey regulatory bodies on costly, outsourced analysis. However, such models may have their shortcomings and should not be considered a panacea for honey authentication.

5.3. REFERENCES

Bakier, S. (2009). Capabilities of near-infrared spectroscopy to analyse changes in water bonding during honey crystallisation process. *International Journal of Food Science & Technology*, **44**, 519–524.

Bázár, G., Romvári, R., Szabó, A., Somogyi, T., Éles, V. & Tsenkova, R. (2016). NIR detection of honey adulteration reveals differences in water spectral pattern. *Food Chemistry*, **194**, 873–880.

Bogdanov, S. (2009). *Harmonised Methods of the International Honey Commission*. *International Honey Commission*. Bern.

Chen, L., Xue, X., Ye, Z., Zhou, J., Chen, F. & Zhao, J. (2011). Determination of Chinese honey adulterated with high fructose corn syrup by near infrared spectroscopy. *Food Chemistry*, **128**, 1110–1114.

Downey, G., Fouratier, V. & Kelly, J.D. (2003). Detection of honey adulteration by addition of fructose and glucose using near infrared transflectance spectroscopy. *Journal of Near Infrared Spectroscopy*, **11**, 447–456.

Ferreiro-González, M., Espada-Bellido, E., Guillén-Cueto, L., Palma, M., Barroso, C.G. & Barbero, G.F. (2018). Rapid

quantification of honey adulteration by visible-near infrared spectroscopy combined with chemometrics. *Talanta*, **188**, 288–292.

Golic, M., Walsh, K. & Lawson, P. (2003). Short-wavelength near-infrared spectra of sucrose, glucose, and fructose with respect to sugar concentration and temperature. *Applied Spectroscopy*, **57**, 139–145.

Guelpa, A., Marini, F., Plessis, A. du, Slabbert, R. & Manley, M. (2017). Verification of authenticity and fraud detection in South African honey using NIR spectroscopy. *Food Control*, **73**, 1388–1396.

Herrero Latorre, C., Peña Crecente, R.M., García Martín, S. & Barciela García, J. (2013). A fast chemometric procedure based on NIR data for authentication of honey with protected geographical indication. *Food Chemistry*, **141**, 3559–3565.

Kelly, J.D., Petisco, C. & Downey, G. (2006). Potential of near Infrared Transflectance Spectroscopy to Detect Adulteration of Irish Honey by Beet Invert Syrup and High Fructose Corn Syrup. *Journal of Near Infrared Spectroscopy*, **14**, 139–146.

Li, S., Shan, Y., Zhu, X., Zhang, X. & Ling, G. (2012). Detection of honey adulteration by high fructose corn syrup and maltose syrup using Raman spectroscopy. *Journal of Food Composition and Analysis*, **28**, 69–74.

Li, S., Zhang, X., Shan, Y., Su, D., Ma, Q., Wen, R. & Li, J. (2017). Qualitative and quantitative detection of honey adulterated with high-fructose corn syrup and maltose syrup by using near-infrared spectroscopy. *Food Chemistry*, **218**, 231–236.

Mouazen, A.M. & Al-Walaan, N. (2014). Glucose adulteration in Saudi honey with visible and near infrared spectroscopy. *International Journal of Food Properties*, **17**, 2263–2274.

Oliveri, P. & Simonetti, R. (2016). Chemometrics for Food Authenticity Applications. In: *Advances in Food Authenticity Testing* (edited by G. Downey). Pp. 701–728. London: Elsevier.

Osborne, B.G., Fearn, T. & Hindle, P.. (1993). *Practical NIR Spectroscopy with Applications in Food and Beverage Analysis*. Essex, England: Longman Scientific and Technical.

Rambla, F.J., Garrigues, S. & Guardia, M. De. (1997). PLS-NIR determination of total sugar, glucose, fructose and sucrose in aqueous solutions of fruit juices. *Analytica Chimica Acta*, **344**, 41–53.

Rinnan, Å., Berg, F. van den & Engelsen, S.B. (2009). Review of the most common pre-processing techniques for near-infrared spectra. *Trends in Analytical Chemistry*, **28**, 1201–1222.

Toher, D. (2007). *A comparison of model-based and regression classification techniques applied to near infrared spectroscopic data in food authentication studies*.

Woodcock, T., Downey, G., Kelly, J.D. & O'Donnell, C. (2007). Geographical classification of honey samples by near-infrared spectroscopy: A feasibility study. *Journal of Agricultural and Food Chemistry*, **55**, 9128–9134.

Zhu, X., Li, S., Shan, Y., Zhang, Z., Li, G., Su, D. & Liu, F. (2010). Detection of adulterants such as sweeteners materials in honey using near-infrared spectroscopy and chemometrics. *Journal of Food Engineering*, **101**, 92–97.

Appendix I

Dilution Trial: *Diluent type class*

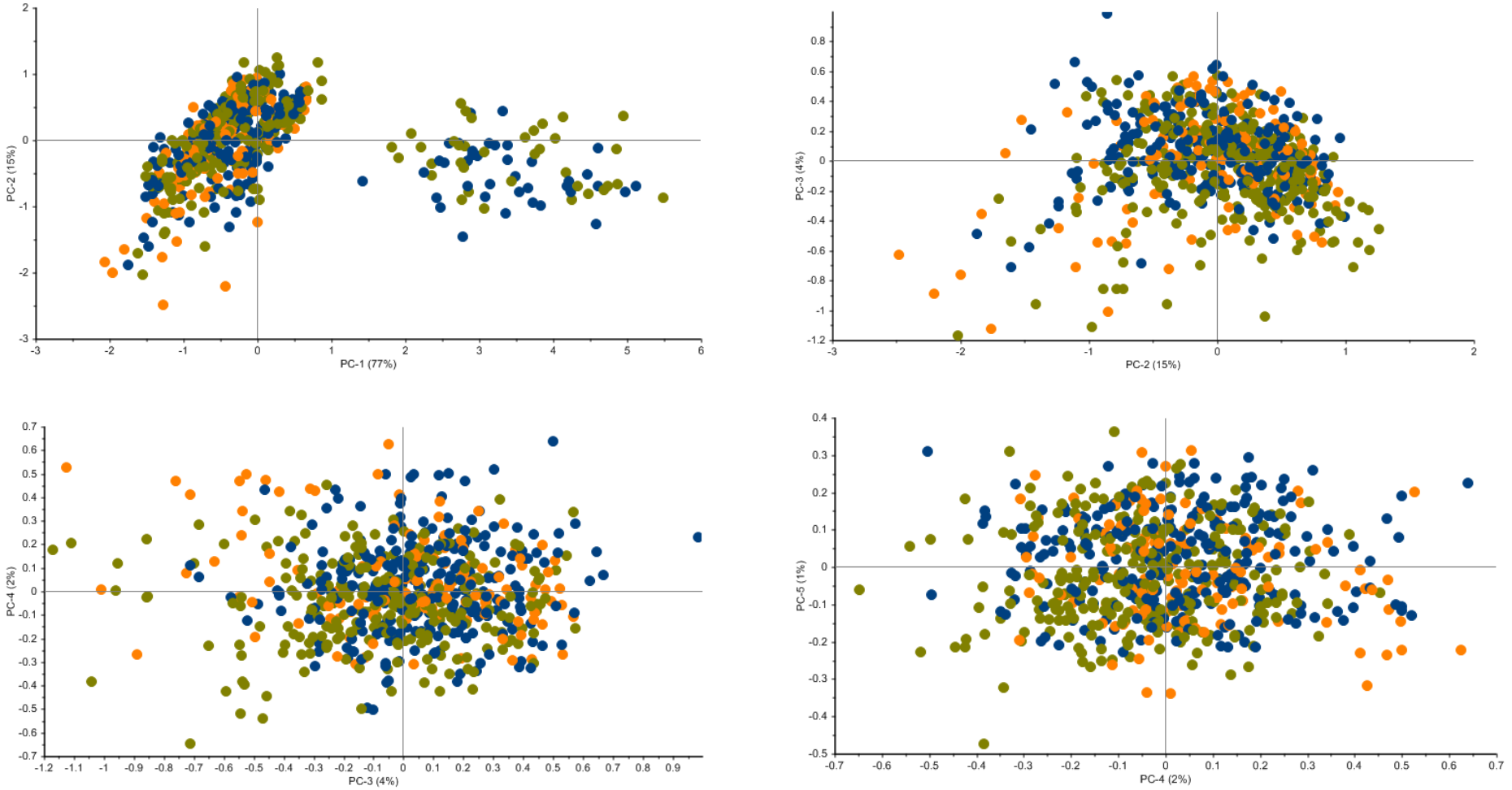

Figure A1 PCA Score plots of D_{All} data (SNV and detrend (2nd order polynomial)), a) PC1 (77%) vs. PC2 (15%), b) PC2 (15%) vs. PC3 (4%), c) PC3 (4%) vs. PC4 (2%), d) PC4 (2%) vs. PC5 (1%), with diluent type classes highlighted - no diluent (**orange**), invert cane sugar syrup (**green**), high-fructose corn syrup (**dark blue**).

Dilution Trial: *Diluent level class*

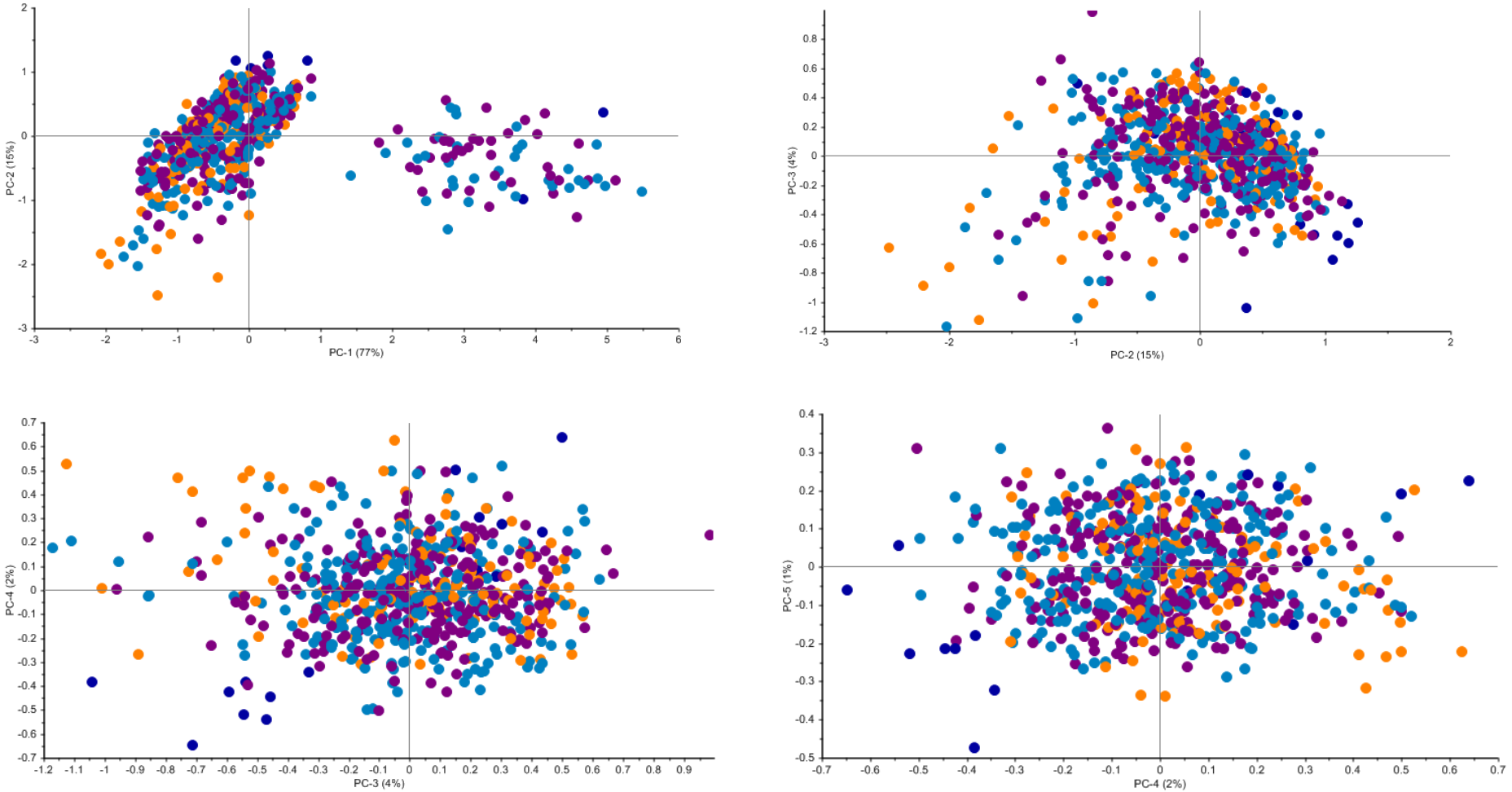

Figure A2 PCA Score plots of D_{All} data (SNV and detrend (2nd order polynomial)), a) PC1 (77%) vs. PC2 (15%), b) PC2 (15%) vs. PC3 (4%), c) PC3 (4%) vs. PC4 (2%), d) PC4 (2%) vs. PC5 (1%), with diluent level classes highlighted – 0% (w/w) / no diluent (**orange**), 10% (w/w) (**light blue**), 20% (w/w) (**purple**), 100% (w/w) (**dark blue**).

Dilution Trial: *Acquisition month class*

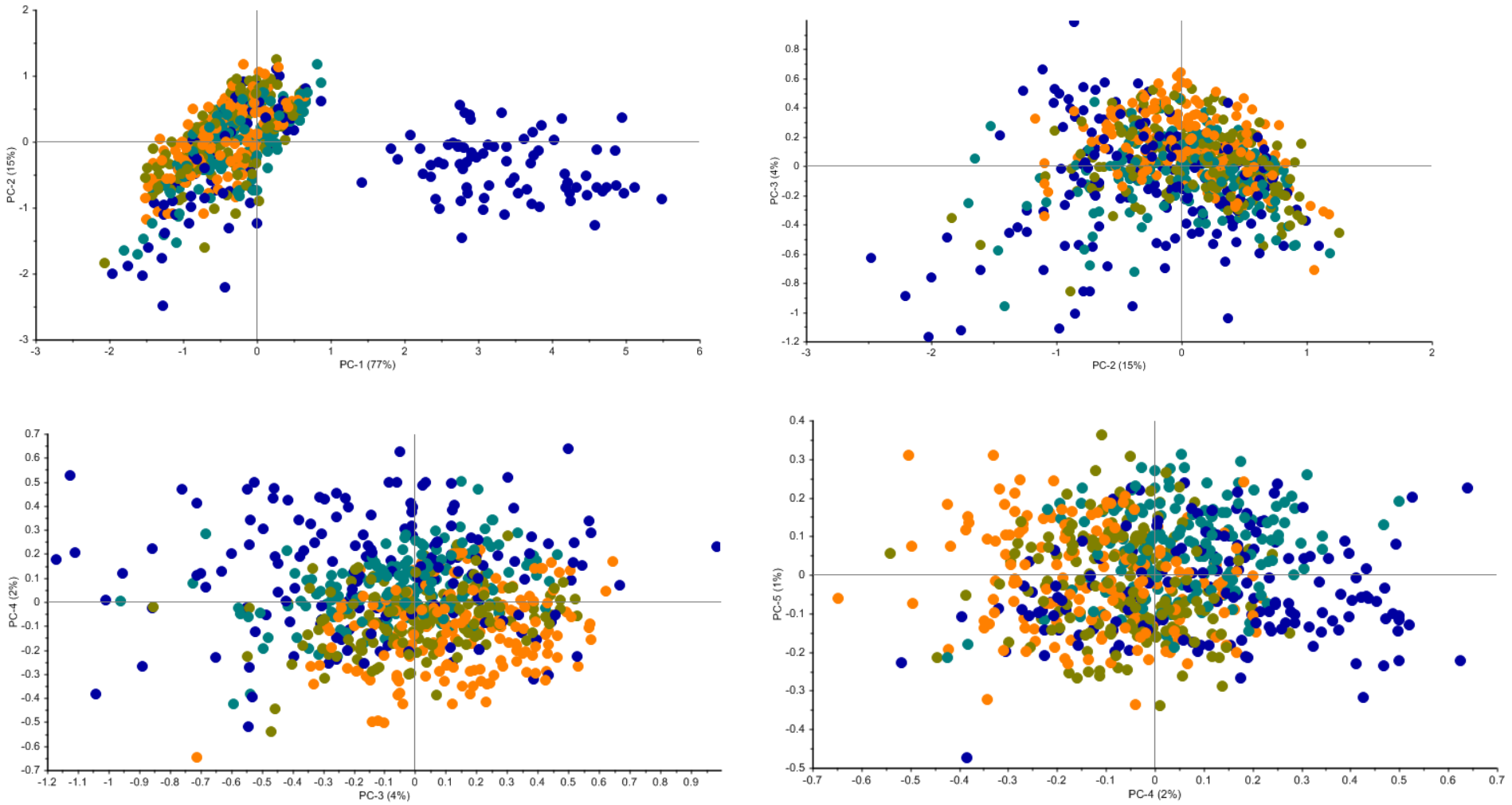

Figure A3 PCA Score plots of D_{All} data (SNV and detrend (2nd order polynomial)) a) PC1 (77%) vs. PC2 (15%), b) PC2 (15%) vs. PC3 (4%), c) PC3 (4%) vs. PC4 (2%), d) PC4 (2%) vs. PC5 (1%), with acquisition month classes highlighted – month 0 (**dark blue**), month 3 (**light blue**), month 6 (**green**), month 9 (**orange**).

Dilution Trial: *Irradiation treatment class*

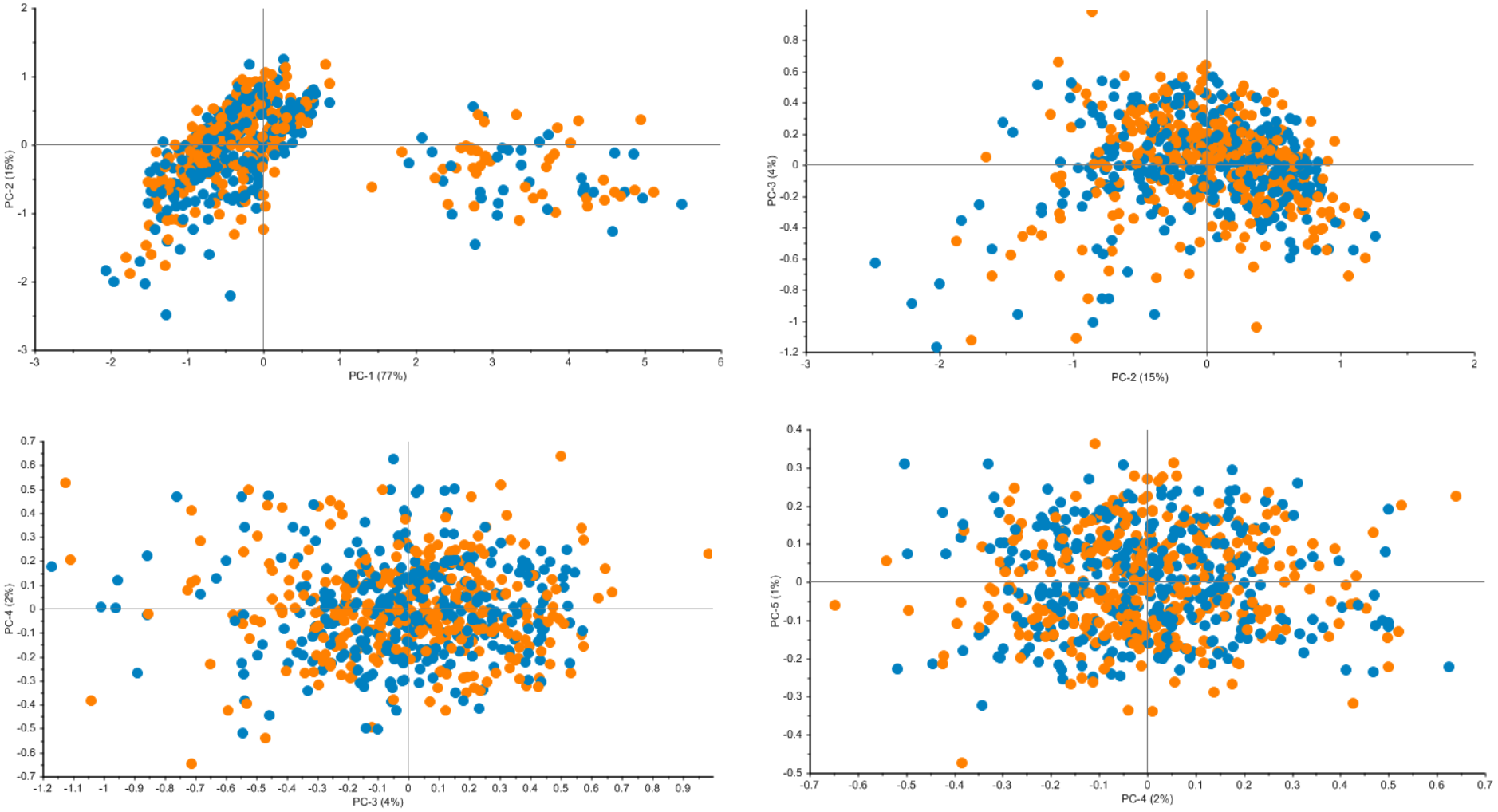

Figure A4 PCA Score plot of D_{All} data (SNV and detrend (2nd order polynomial)), a) PC1 (77%) vs. PC2 (15%), b) PC2 (15%) vs. PC3 (4%), c) PC3 (4%) vs. PC4 (2%), d) PC4 (2%) vs. PC5 (1%), with irradiation treatment classes highlighted – non-irradiated (**orange**), irradiated (**light blue**).

Dilution Trial: *Loadings line and correlation loadings line plots*

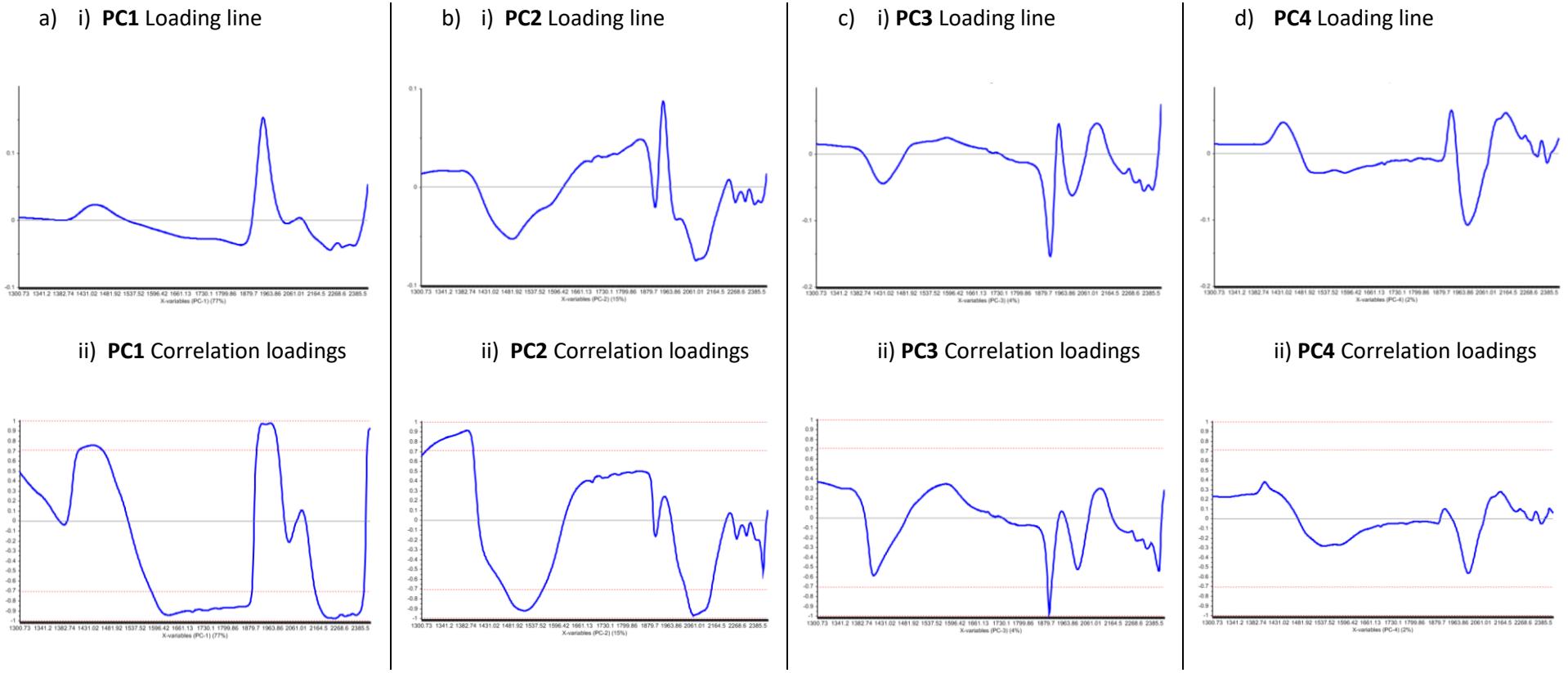

Figure A5 PCA a) i) loadings line and ii) correlation loadings line plot for **PC1 (77%),** b) i) loadings line and ii) correlation loadings line plot for **PC2 (15%),** c) i) loadings line and ii) correlation loadings line plot for **PC3 (4%),** d) i) loadings line and ii) correlation loadings line plot for **PC4 (2%)** of D_{All} data (SNV and detrend (2^{nd} order polynomial)).

Storage Trial: *Honey type class*

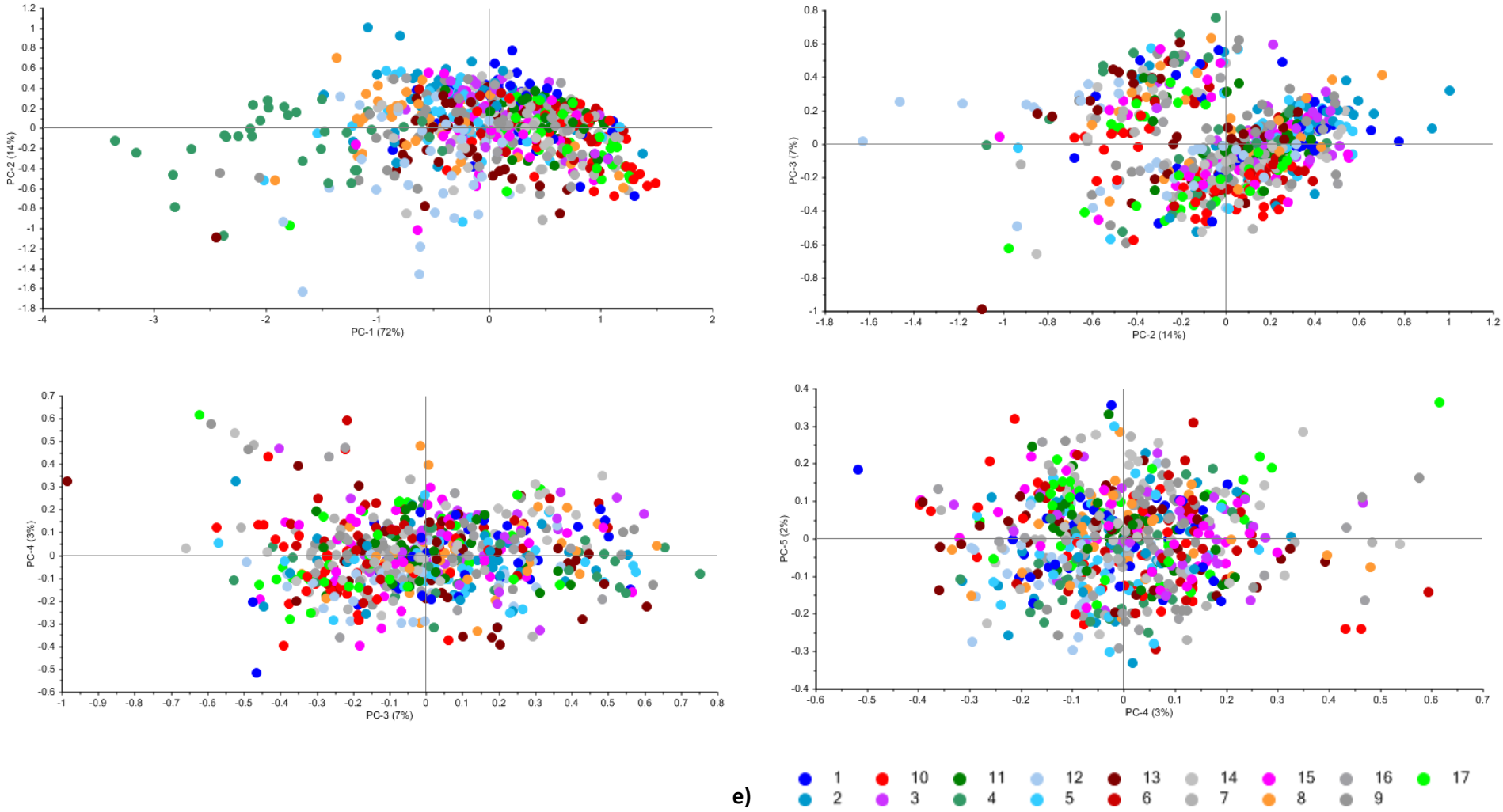

Figure A6 PCA Score plot of A_{All} data (SNV and detrend (2nd order polynomial)) a) PC1 (72%) vs. PC2 (14%), b) PC2 (14%) vs. PC3 (7%), c) PC3 (7%) vs. PC4 (3%), d) PC4 (2%) vs. PC5 (1%), with honey type classes highlighted according to e) bulk honey sample number key.

Storage Trial: *Storage temperature class*

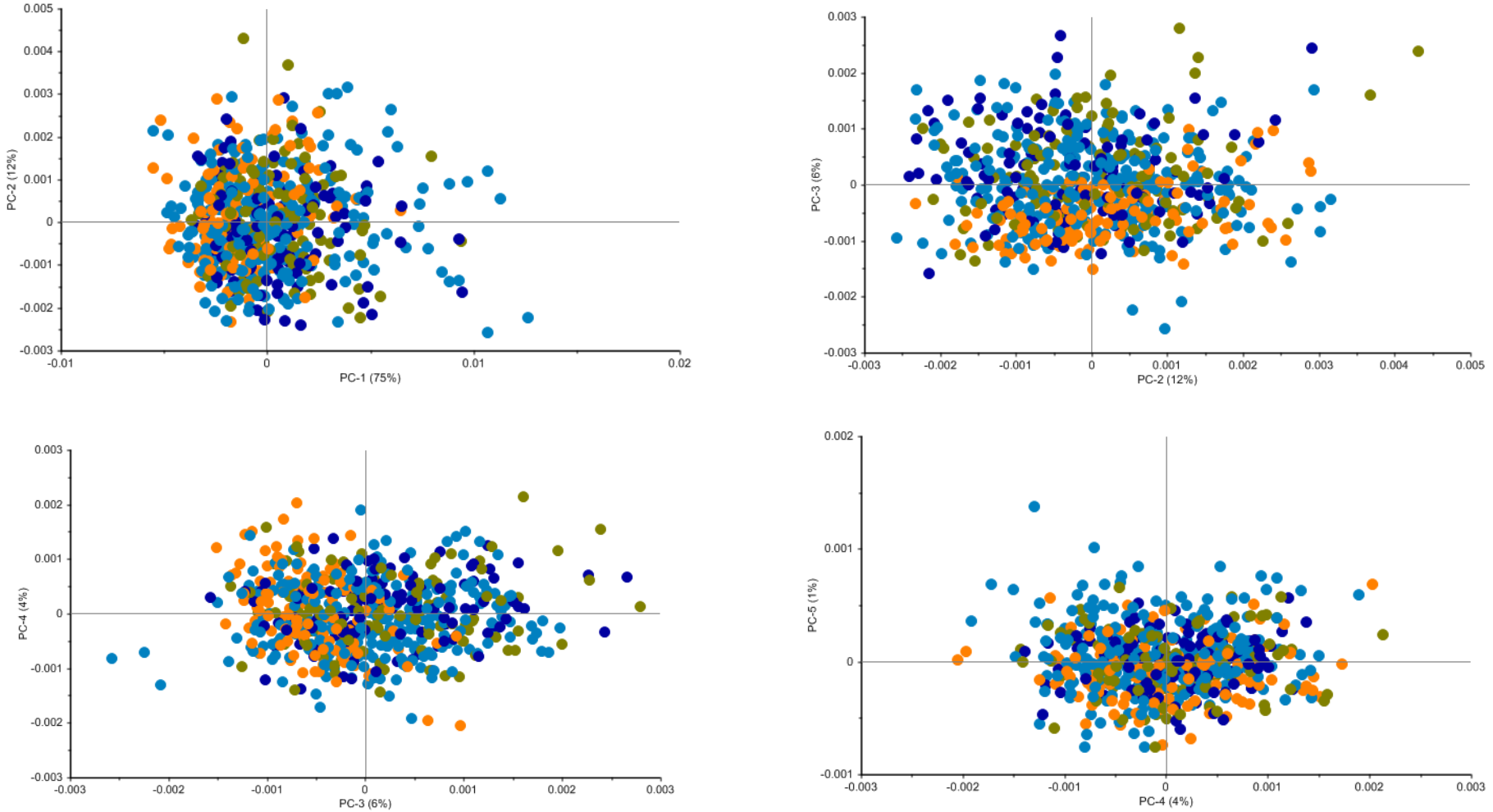

Figure A7 PCA Score plots of A_{All} data (2nd Savitzsky-Golay derivative (3nd order polynomial, 15 smoothing points)) a) PC1 (75%) vs. PC2 (12%), b) PC2 (12%) vs. PC3 (6%), c) PC3 (6%) vs. PC4 (4%), d) PC4 (4%) vs. PC5 (1%), with storage temperature classes highlighted – 4°C (**dark blue**), 25°C (**bright blue**), 40°C (**orange**), ambient light and temperature (**green**).

Storage Trial: *Acquisition month class*

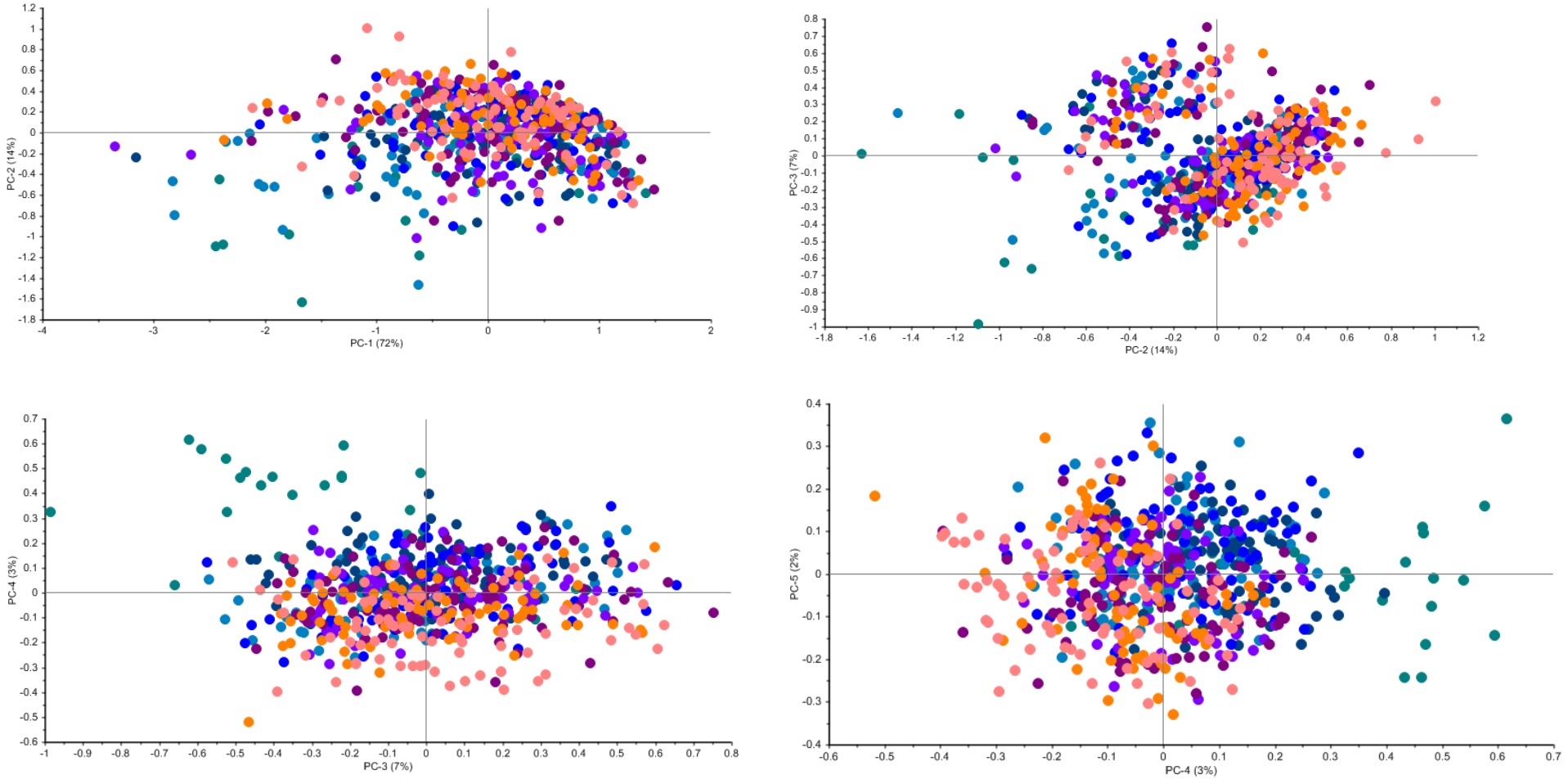

Figure A8 PCA Score plot of A_{All} data (SNV and detrend (2nd order polynomial)) a) PC1 (72%) vs. PC2 (14%), b) PC2 (14%) vs. PC3 (7%), c) PC3 (7%) vs. PC4 (3%), d) PC4 (2%) vs. PC5 (1%), with acquisition month classes highlighted – month 0 (**teal**), month 1 (**light blue**), month 2 (**dark blue**), month 3 (**bright blue**), month 4 (**indigo**), month 5 (**purple**), month 6 (**orange**) and month 9 (**pink**).

Storage Trial: *Irradiation treatment class*

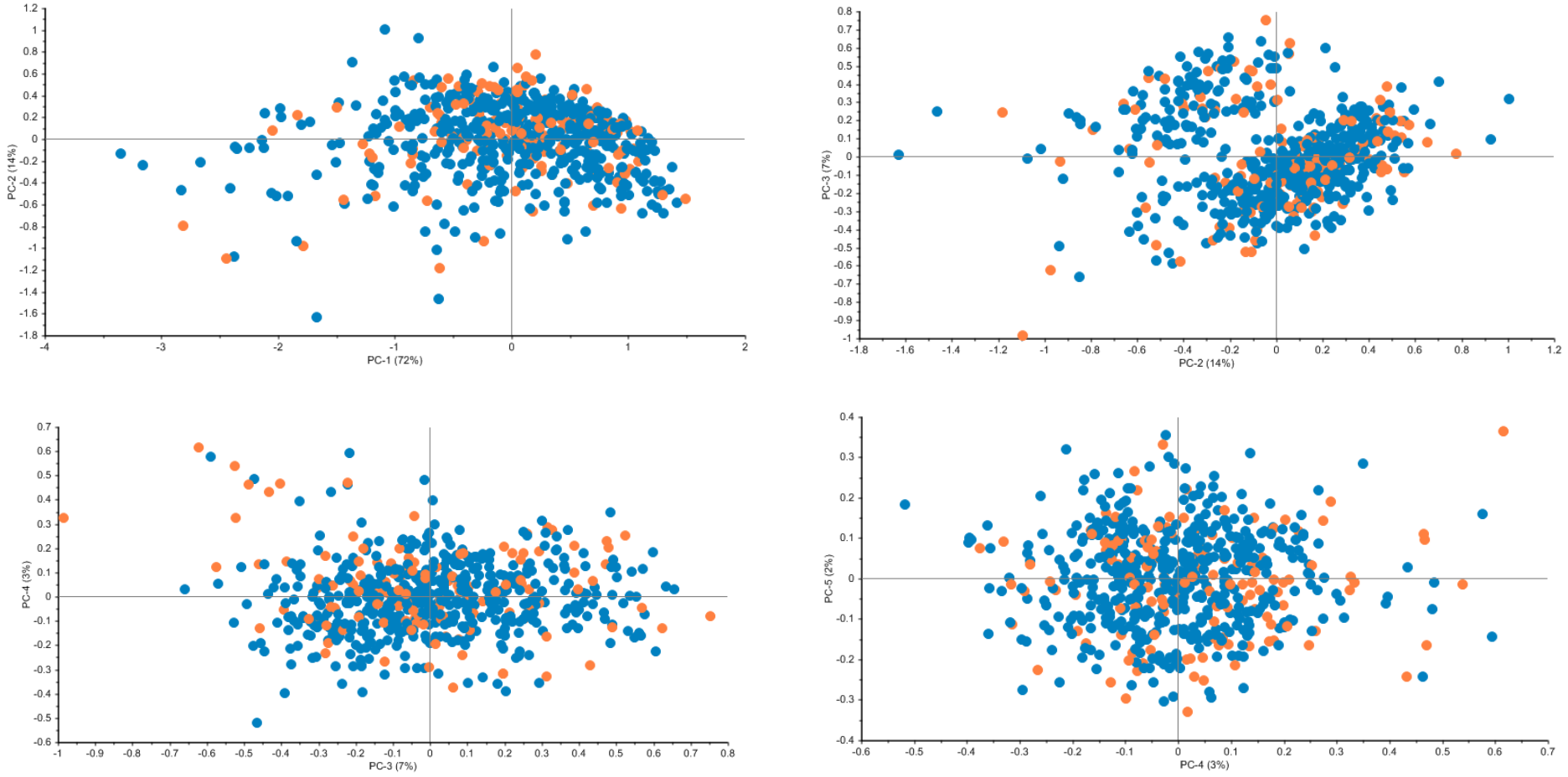

Figure A9 PCA Score plot of A_{All} data (SNV and detrend (2nd order polynomial)) a) PC1 (72%) vs. PC2 (14%), b) PC2 (14%) vs. PC3 (7%), c) PC3 (7%) vs. PC4 (3%), d) PC4 (2%) vs. PC5 (1%), with irradiation treatment classes highlighted – non-irradiated (**orange**), irradiated (**light blue**).

Storage Trial: *Loadings line and correlation loadings line plots of SNV and detrend pre-processed data*

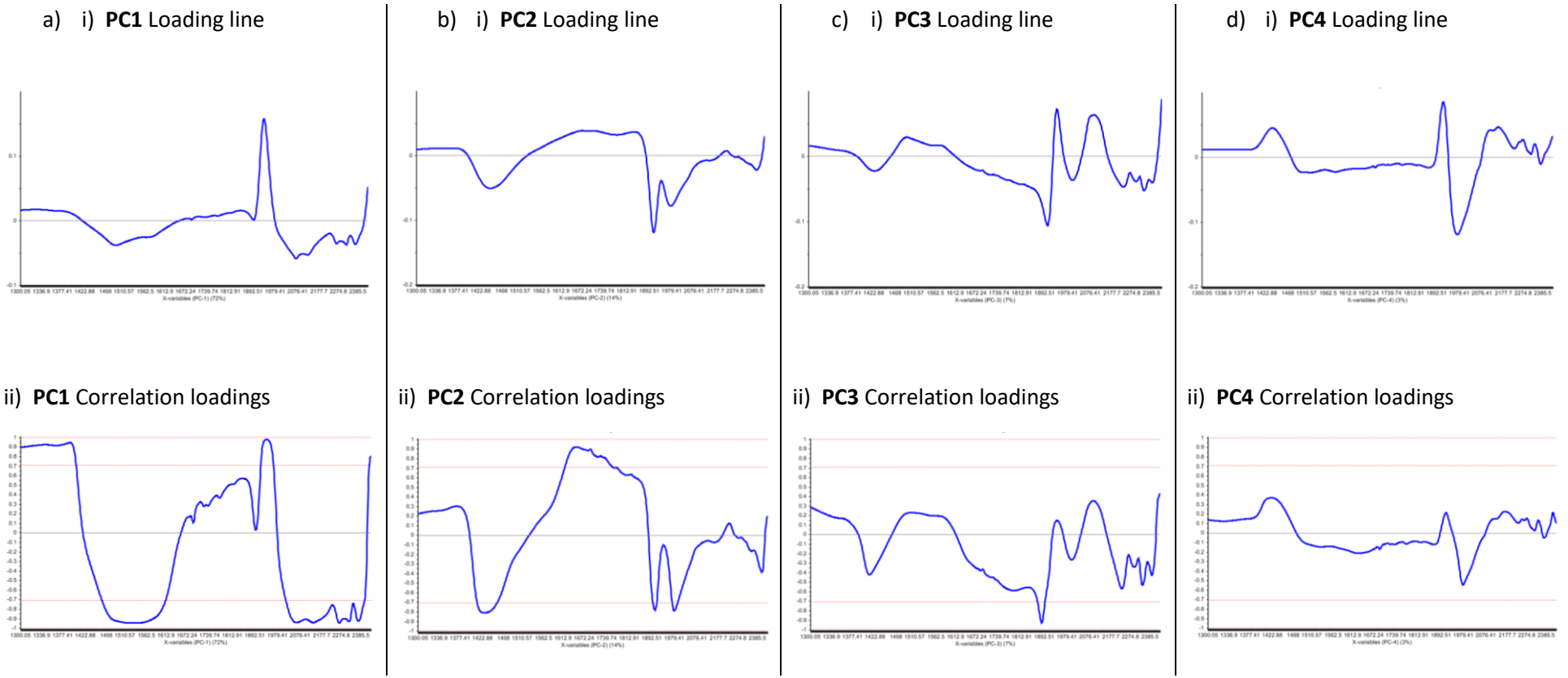

Figure A10 PCA a) i) loadings line and ii) correlation loadings line plot for **PC1 (72%),** b) i) loadings line and ii) correlation loadings line plot for **PC2 (14%),** c) i) loadings line and ii) correlation loadings line plot for **PC3 (7%),** d) i) loadings line and ii) correlation loadings line plot for **PC4 (3%)** of A_{All} data (SNV and detrend (2^{nd} order polynomial)).

Storage Trial: *Loadings line and correlation loadings line plots of 2nd derivative SG (3rd order polynomial, 15 smoothing points) pre-processed data*

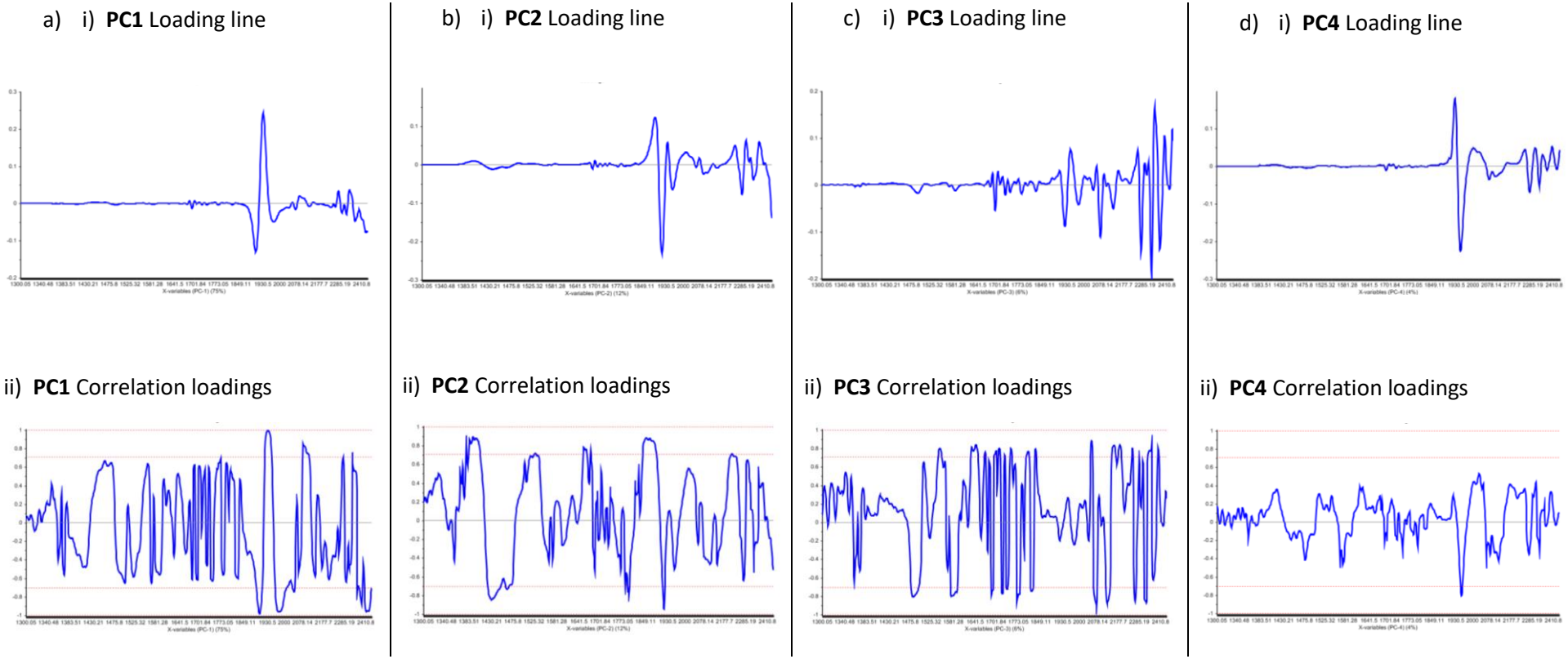

Figure A11 PCA a) i) loadings line and ii) correlation loadings line plot for **PC1 (75%),** b) i) loadings line and ii) correlation loadings line plot for **PC2 (12%),** c) i) loadings line and ii) correlation loadings line plot for **PC3 (6%),** d) i) loadings line and ii) correlation loadings line plot for **PC4 (4%)** of A_{All} data (2nd derivative SG (3rd order polynomial, 15 smoothing points)).